論文 / 著書情報
Article / Book Information

題目(和文)	
Title(English)	SOLID FUEL PRODUCTION FROM PAPER SLUDGE EMPLOYING HYDROTHERMAL TREATMENT AND ITS CO-COMBUSTION PERFORMANCE WITH COAL
著者(和文)	アリープラサートチナタン
Author(English)	Chinnathan Areeprasert
出典(和文)	学位:博士（工学）, 学位授与機関:東京工業大学, 報告番号:甲第9939号, 授与年月日:2015年6月30日, 学位の種別:課程博士, 審査員:吉川　邦夫,竹下　健二,高橋　史武,時松　宏治,梶谷　史朗
Citation(English)	Degree:, Conferring organization: Tokyo Institute of Technology, Report number:甲第9939号, Conferred date:2015/6/30, Degree Type:Course doctor, Examiner:,,,,
学位種別(和文)	博士論文
Type(English)	Doctoral Thesis

SOLID FUEL PRODUCTION FROM PAPER SLUDGE EMPLOYING HYDROTHERMAL TREATMENT AND ITS CO-COMBUSTION PERFORMANCE WITH COAL

Doctoral Dissertation

Chinnathan Areeprasert

Department of Environmental Science and Technology

Interdisciplinary Graduate School of Science and Engineering

Tokyo Institute of Technology

June 2015

Acknowledgement

The author gratefully acknowledges:

1. My mum, dad, and sister who always provide endless supports for *everything* in my life.
2. Professor Kunio Yoshikawa, as the advisor for giving me one of the best opportunities in my life and essential guidance and suggestion throughout this research.
3. Associate Professor Fumitake Takahashi, as the co-advisor, for valuable advice.
4. Assistant Professor Kiyoshi Tsuji for support during the experiment in Japan.
5. Mrs. Eriko Ohno for administrative work during my study.
6. The Faculty of Engineering, Kasetsart University, as the scholarship provider during the study.
7. Associate Professor Thanya Kiatiwat, Associate Professor Chawalit Kittichaikarn, Assistant Professor Wichai Sivakosit, and the administrative staff of the Department of Mechanical Engineering, Faculty of Engineering, Kasetsart University, for administrative supports.
8. Dr. Kriengkrai Suksankraisorn and Mr. Korakoch Petchdee, a collaborative research group from the Siam Cement Public Company Limited (SCG), for funding (Chapter 2) and supporting throughout this study.
9. Dr. Pandji Prawisudha, Dr. Zhao Peitao, Dr. Anchan Paethanom, for support on Chapter 2.
10. Mr. Prut Chanyavanich, Dr. Shen Yafei, and Dr. Bayu Prabowo, for assistance on Chapter 3 and 4.
11. Associate Professor Fabrizio Scala[1], Dr. Antonio Coppola[2], Dr. Massimo Urciuolo[2], and Dr. Ricardo Chirone[2], a collaborative research group from [1]Università degli Studi di Napoli Federico II and [2]Istituto di Ricerche sulla Combustione – CNR, for remarkably support and supervision on Chapter 5 and 6.
12. Friends and colleagues for our close friendship, especially thanks to Mr. Ma Dachao for great friendship and support throughout this study.

Comments, suggestions, and criticisms concerning some errors would be greatly appreciated as they will contribute to further improvement of this research.

Chinnathan Areeprasert

Contents

Chapter 1

General introduction

Abstract: This chapter provides background information on this research. It begins with an introduction of pulp and paper industry including general paper making process and its energy utilization. Then, problematic waste in pulp and paper industry, paper sludge, is introduced along with general disposal practices. Next, co-combustion of biomass and waste with conventional fossil fuels such as coal is reviewed as it could be one part of the solutions to deal with the paper sludge. More importantly, essential applications of subcritical water is described and the hydrothermal treatment technology is emphasized offering the method to convert high moisture waste into alternative fuel. The combination of these two technologies have, eventually, become the objective of this research, which focuses on alternative solid fuel production from paper sludge by hydrothermal treatment and co-combustion performance of the treated paper sludge with coal. Finally, the outline of this study and scope of work are presented as well.

1.1 Pulp and paper industry

1.1.1 Introduction to pulp and paper industry

Pulp and paper industry plays very important roles on people and societies all around the world. The products from this industry, including books, newspapers, magazines, office papers, issue papers, and tissue products, and so on, are related to our daily life. Examples of the products from pulp and paper industry are shown in Figure 1-1 The net consumption of paper and paperboard is shown in Figure 1-2. The pulp and paper industry is essential; however, it has many impacts on both human and environment. With improper action in the business, this industry can generate many problems such as violation of land and forest, devastating local livelihood through deforestation, water contamination to people near paper mills, and health threatening pollutions.

Figure 1-1 Examples of products from paper industry (Source: Solenis Solutions Switzerland GmbH).

Pulp and paper mills could be nonintegrated or integrated operations. The former imports pulp to the mill from other pulp makers and only operates the downstream process, i.e., paper production process. The nonintegrated mills significantly reduces a requirement on the use of land, energy, and water. Thus, this type of mill can be located closer to large work force populations as well as their customers. The integrated mill is ones that produce both pulp and paper. This brings the benefit of sharing common auxiliary systems as steam, electricity, and wastewater treatment within pulp and paper production plants. Moreover, cost for transportation is also reduced. A paper production mill can be a single paper machine or several machines that can produce a single grade of paper or a various type of papers. In spite of the different types or size of the machine and final products, the fundamental papermaking process remains the same.

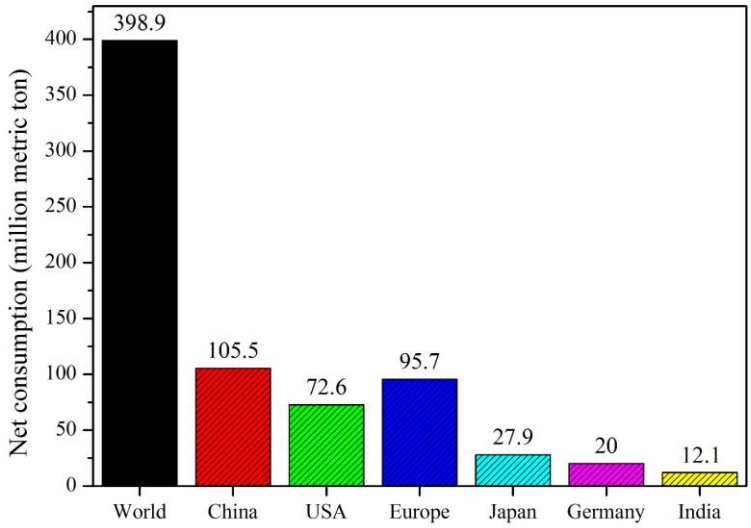

Figure 1-2 Paper & paperboard net consumption in million metric ton in 2012 (Source: www.paperonweb.com)

1.1.2 Pulp and paper making process

Figure 1-3 shows the paper production process. The modern paper production process involves wood preparation process from trees, recycled paper, or agricultural residues. They may be in several different forms depending on the origin of the raw material. Several examples are short logs of round wood with the bark, chips from a sawmill, pre-chipped debarked wood, or waste sawdust. In the case that raw round wood is used, debarking process where the fresh wood is tumbled by large steel drums is necessary. The debarked wood are then chipped in a chipper or grinder for the chemical or mechanical pulping process for fiber separation, respectively.

Several pulping technologies can be diverged during the fiber separation process. In the mechanical pulping process, the fiber separation is relatively simple. The prepared chips are crushed by grinding

wheels where the washing process is continuously operated. Then, the fines pulp is screened, thickened, and stored for the paper making process.

In the chemical pulping, the prepared chips are fed into a large pressure cooker as a digester. The white liquor is added during the digestion process and the fed chips are cooked with steam at specific temperatures and duration to separate the fibers and partially dissolved lignin and other extractives. After the digestion, the cooked pulp, the brown stock, is discharged into a non-pressurized pressure vessel where the steam and volatile materials are released. The brown stock containing the recovered fibers is further washed, screened, and cleaned to remove contaminants. Then, it is ready for further processing. For the fate of the white liquor added during the digestion process as a chemical, it turned dark brown as a result of the dissolved lignin. The combination of the chemicals and dissolved lignin at this phase is called black liquor. The black liquor, then, goes to the chemical recovery plant where the lignin is burned for energy recovery and the chemicals are recovered, purified, reconstituted, and, finally, reused in the digester.

The combination of the mechanical and the chemical pulping can be done by feeding the prepared chips to rapid rotating disk grinders. Then, the grinded chips are pretreated by steam or steam/chemical to obtain thermomechanical pulp (TMP) or chemi-thermomechanical pulp (CTMP), respectively. After a second stage refining, the pulp is screened, cleaned, and ready for further processes.

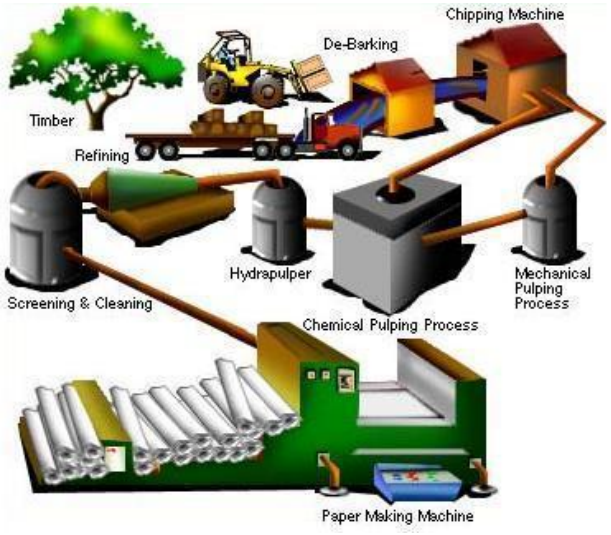

Figure 1-3 Paper production process (Source: Form Factory (Malaysia) Sdn Bhd.)

After the raw pulp is obtained, the bleaching process is necessary since the brown pulp contains some amount of lignin and other discoloration. The product from this process has lighter in color or becomes white depending on the final product preference. The bleaching process can be done by multiple stages employing chlorination and oxidation. The lignin left in the raw pulp is, again, solubilized leaving cellulose as a major product. A number of bleaching agents may be used and are applied in a stepwise

fashion within a bleaching sequence. The bleaching agents are used sequentially. Chlorine gas, chlorine dioxide, sodium hypochlorite, hydrogen peroxide, and oxygen are the examples of the bleaching agents to dissolve lignin. Between bleaching treatments, the dissolved lignin is extracted from the surface of the fibers by a strong alkali, e.g., sodium hydroxide. The cost of the bleaching agents, desired products condition such as brightness, and environmental guidelines and regulations are key factors regarding bleaching process designation.

After that, the pulp is ran through a paper making machine to obtain a large roll of paper before it will be further converted to final products such as office papers, packaging boxes, or tissue papers. The production process could be diverged from the previous explanation depending on each manufacturing company.

1.1.3 Energy utilization in pulp and paper industry

The pulp and paper production is one of the most energy intensive industries. It was estimated that the energy from steam is around 81% of the total energy consumption in the pulp and paper industry [1]. Besides the pulp and paper industry, other steam intensive processes are also found in the food processing industry (57%), the chemicals industry (42%), and the petroleum refining industry (23%) [1]. In pulp and paper industry, the paper mill boilers generate steam not only for cooking the woodchips in the pulping process but also for drying the paper and generating electricity internally used in the paper mill. Generally, energy production in the mill is derived from biomass mostly bark and wood by-product as fuel. For example, shares of energy sources in total energy consumption in the member countries of the confederation of European Paper Industry (CEPI, 2007) is mainly biomass including black liquor as high as 50 percent. Utilization of waste biomass generated from the mill is still limited around one percent and the rest is relying on conventional fossil fuels such as gas, oil, and coal.

1.2 Paper sludge

Paper sludge is generated from two sources: the main and the secondary clarifiers [2,3]. The main clarifier, where precipitated particles are collected, produces high fiber concentration sludge, which is called primary sludge. It consists of wood fibers: cellulose, hemicellulose, and lignin [4]. Moreover, specific substances for paper making process, such as kaolin and calcium carbonate, were also found in the primary sludge [5]. For the secondary sludge, it is produced from the secondary clarifier and the wastewater treatment facility and contains fewer amounts of solid particles. The characteristics of the paper sludge depend on raw materials, techniques employed, water treatment processes, and designed property of paper products in each manufacturer [6]. Figure 1-4 illustrates the paper sludge after the mechanical belt pressing which has the moisture content around 75–80 percent.

Nowadays, landfilling is one of the most common practices for paper sludge disposal [3,7,8]. However, it brings about lots of severe problems to society, such as groundwater contamination caused by leachate [3]. Another common way to destroy the paper sludge is incineration. The incineration plants can eliminate waste by burning and recovering the heat for other purposes such as to generate electricity. The substantial volumetric reduction is satisfied and it can break down hazardous bacteria or microorganism, which can be found in medical waste. To maintain a good combustion performance, the incinerator needs the primary fuel such as coal, oil, or gas. The main reason is that water content in paper sludge is very high; therefore, it cannot be burnt solely or used directly as fuel. Other drawbacks that make the incineration inadvisable, especially in developing countries, are high cost not only for the capital investment but also for the operational cost.

Figure 1-4 Paper sludge (Courtesy of Siam Kraft Industry Co., Ltd)

Many approaches have been developed to manage the paper sludge. Thermochemical conversion technology, for example, gasification, is an interesting method. By converting solid waste into gaseous fuel, the waste can be eliminated with low air pollutants. Syngas after cleaning can be further utilized in a gas engine for electrical power generation. However, a main disadvantage is that tar and other inorganic compounds in the syngas have to be eliminated before utilization. Practically, usable fuel for the downdraft gasifier usually should have the moisture content less than 25 percent. This is because the thermal efficiency will be reduced due to the heat is used to evaporate the water inside the fuel; therefore, high moisture waste is also problematic for this process. Supercritical water gasification (SWG), which is commonly known as a utilization of water above 374 °C and 22 MPa as a medium, which has a low dielectric constant, low viscosity, and high diffusivity. Additionally, mass transport rate of this process is very high since a complete miscibility of the organic compound and gases leading to an ultimately high destruction rate [9]. The SWG was able to generate valuable gases, such as hydrogen and methane, from the pulp and paper sludge [10]. It showed a satisfying energy recovery and was able to convert organic materials into useful chemicals; however, due to its severe operational

condition and corrosion problem, the SWG might be impractical in the industry especialy in developing countries [11-13].

1.3 Co-combustion of biomass and waste with coal

As mentioned earlier, large amount of steam is used in the paper factory. Steam generation unit such as fluidized bed boiler is generally utilized in this industry. Fuel supplied to the boiler can be conventional fossil fuels and biomass residues generated from the pulp and paper production process. This combination of fuel supplying technique is called as co-combustion or co-firing. Co-combustion of biomass and waste with coal has been studied by many researchers both experimental- and modeling-approaches [14-20]. Sami et al. summarized the co-firing of several types of biomass, e.g., agricultural residues, refuse-derived fuel, and animal waste, with coal [14]. According to that study, it was concluded co-firing these fuels showed the possibility to diminish NO_x and SO_x emission from the original pulverized-coal burning power stations [14] in spite of the different characteristics of biomass and coal as well as some technical problems such as fouling issues. In a large-scale coal-fired CHP power plant, sawdust has been introduced to be burned with coal [15]. Savolainen stated that the co-firing of the sawdust with coal was successful in term of the emission reduction and no negative effects on the boiler, electrostatic precipitator, and flue-gas desulfurization performances were observed. However, it was reported that the drying capacity of the mills was not adequate when increasing the amount of the sawdust due to its high moisture content (50–65 wt.%) [15]. Flame stability of biomass co-firing with coal in an industrial-scale combustion facility has been investigated by Lu et al. [16]. It was concluded that adding the biomass less than one-fifth for co-firing with coal could limit adverse influences on the flame stability; however, with a higher amount of biomass, the additional portion did affect the flame front due to the variation of the physical and chemical properties [16]. The study of co-firing applications of the paper sludge with either a subbituminous coal [19] or a semi-anthracite coal [20] showed some benefits in view of energy recovery and environmental friendliness. According to the literature, the amount of biomass/waste to be co-fired with coal is dependent on the characteristic of each fuel such as physical and chemical components as well as the water content.

1.4 Waste treatment and upgrading

A subcritical water condition (SWC) is the one where water exits in the state below and near its critical point (374 ˚C and 22.1 MPa) , and it has interesting properties such as catalytic behavior for organic compounds due to the drastically higher amount of ionic products compared to water at the ambient condition [21]. SWC causes degradation of substances as well as creates various reactions, for instance, hydrolysis, dehydration, decarboxylation, condensation, and aromatization. The application of extraction characteristic starts when water is heated to the temperatures higher than its ambient boiling

temperature [22]. The extraction occurs to ionic and polar species at a low temperature while, at higher temperatures (near the critical temperature), nonpolar substances could be dissolved and extracted [21,22]. According to Brunner, biomass components such as starch, sugars, cellulose, hemicellulose, and lignin can be processed by SWC [22]. This brings opportunities to the utilization of SWC for biomass feedstock transformation into other valuable materials. The application of SWC could be simply categorized based on its operating conditions, i.e., the temperature, the pressure, and the holding time, and the motivation on the final products. The examples of the applications of SWC regarding waste treatment and conversion could be reported as follows

1.4.1 Waste Autoclave

Waste autoclaving is a combination of thermal and mechanical treatment. The former is using the steam as the pressure and the heat source, which is usually known as 'pressure cooker' method. The mechanical processing is done by a rotating part to mix the waste inside the pressure vessel. The common types of waste for this treatment are, for example, bio-hazardous wastes and medical wastes. As a result of the mechanical heat treatment, paper and fiber can be disintegrated, plastics can be softened, and hazardous matter can be sterilized and the waste volume can be reduced. Another important factor of waste autoclave is the processing time that can optimize the decontamination of the waste.

1.4.2 Hydrothermal carbonization

Hydrothermal carbonization (HTC) is used to convert organic materials into carbonaceous solid product by using moderate water temperature (180–350 ˚C) and pressure (2–10MPa) [23,24]. The product from HTC is char that has a higher heating value as well as sterilized biological substances [24,25]. The holding time of HTC is generally long and it could be in the range of 2–12 h [24,26]. However, a shorter holding time at a relatively higher pressure carbonization condition has also been tested [27]. According to He et al., they were concluded that HTC could convert sewage sludge into char to be used as a solid fuel in view of the fuel characteristics and the combustion performance [24]. In addition, the HTC process was applied to municipal solid waste streams [28] as well as biomass/agricultural residues [29,30]. Based on the study by Oliveira et al., using corn silage and dough residues as feedstock for HTC could produce biochar that had better quality and similar characteristics with brown coal [30].

1.4.3 Hydrothermal liquefaction

Hydrothermal liquefaction (HTL) is focused on liquid products, i.e., heavy oils and water-soluble oils. The temperature condition in HTL is relatively high and could be ranged from 250–380 ˚C approaching a supercritical water condition [31,32]. The yields of the liquid products from HTL could be in-between 20–60% depending on the operating conditions as well as the use of solvents or catalysts during the process [33]. HTL of the secondary pulp/paper powder for energy recovery was studied [34]. It was

suggested that HTL in the presence of H_2 of the secondary pulp/paper sludge with $Ca(OH)_2$ catalyst could be an effective way for energy recovery via liquid oil production. From an investigation of Zhang et al., bio-crude oil has been produced from the paper sludge and waste newspaper by HTL [31]. The produced heavy oils from HTL from a combination of samples at 300 ˚C for 20 minutes gave significantly higher energy content product.

1.4.4 Hydrothermal treatment

Hydrothermal treatment (HTT) has been investigated by several researchers in recent years [35-37]. This innovative treatment process can convert waste to value-added resources such as coal-like solid fuel or organic fertilizer [36,38]. Namioka et al. [35] applied HTT to produce solid fuel and studied the effect of HTT on sewage sludge dewaterability. When increasing the HTT temperature, more moisture could be reduced by the same dewatering condition. Sakaguchi et al. [39] upgraded high moisture content brown coal by HTT and reported that fuel property of hydrothermally treated brown coal was improved due to the increase in the heating value during HTT. In a 3-m^3 demonstration plant, HTT has been proven to reduce organic chlorine and improve natural drying performance of the Japanese municipal solid waste to produce safe and clean solid fuel [36,40].

1.5 Research objective

Since the paper sludge is very problematic and difficult to dispose, this research is devoted to find the systematic and practical solution. The appropriate way to deal with the paper sludge is the Waste-to-Energy technology. There are various technologies that are applicable to convert waste into energy both thermochemical and biochemical conversion [41,42]. Several technologies have been mentioned in the previous section.

Co-combustion of sludge with coal can be implemented in-house in conventional coal-fired power plants without significant modifications and major investments [43,44]. It can reduce the coal demand as well as exploit the waste efficiently through energy recovery. Moreover, the transportation of the paper sludge whose main composition is water is inappropriate and uneconomical. Therefore, the in-house co-combustion with coal could be the practical and feasible solution. However, bad fuel characteristics of paper sludge could unfavorably affect co-combustion application in many ways. For example, high water content does not only limit the amount of paper sludge for co-combustion with coal but also increases the flue gas volume after water evaporation leading to some problematic issues. Therefore, the effective and feasible pretreatment technology is necessary before the co-firing application. According to the previous successful studies on HTT, this technology could be successfully implemented to treat paper sludge before using as an alternative solid fuel in co-combustion application.

In sum, the main objective of this research is to promote Waste-to-Energy technology in the pulp and paper industry by using the hydrothermal treatment to upgrade paper sludge followed by the co-combustion of the hydrothermally treated paper sludge with coal. An illustration of the proposed system is shown in Figure 1-5. The feasibility of the hydrothermal treatment process was also focused as well as the performance of the combustion/co-combustion test for the raw paper sludge and the hydrothermally treated paper sludge with different types of coal.

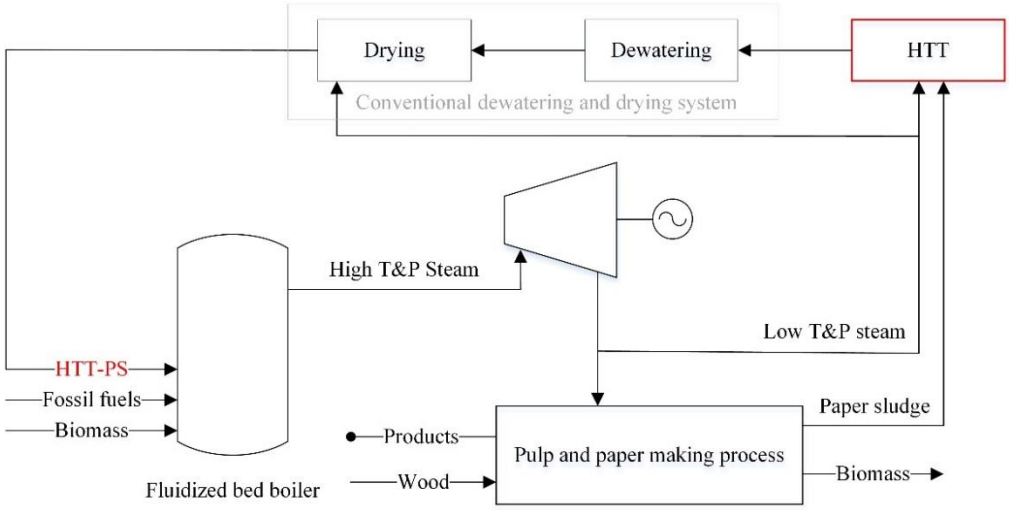

Figure 1-5 Integration of hydrothermal treatment for paper sludge and its co-combustion with coal in a conventional pulp and paper making process

1.6 Outline and scope

To realize the objective of this study, the outline of this research is proposed and illustrated in Figure 1-6. A series of experiments, both lab-scale and pilot-scale hydrothermal treatment (HTT), fundamental combustion, basic co-combustion, and practical co-combustion plus its detail phenomena clarification, have been conducted. The equipment has been selected according to the scheme of each study. Five main chapters in this thesis are devoted to main contents of this research. They are in Chapters 2–6. Chapter 1 and 7 are the introduction and conclusion with recommendation of this research, respectively. The content of this work is presented as follows:

Chapter 1: *Introduction*

It is the current chapter discussing about the background of this research. Firstly, the introduction of the pulp and paper industry is described and the general information of the problematic waste from the industry, the paper sludge, is provided. Then, the research objective is stated. Finally, the outline and scope of this study are presented.

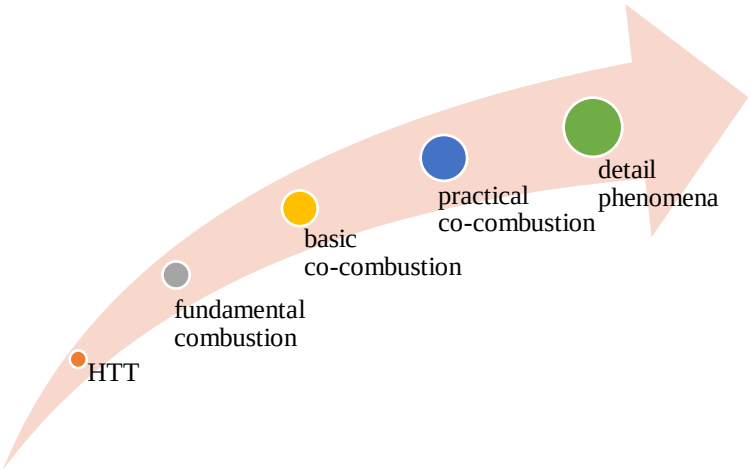

Figure 1-6 Outline of this research

Chapter 2: *Lab-scale and pilot-scale investigation on hydrothermal treatment of paper sludge for solid fuel production*

This chapter aims to investigate alternative solid fuel production from paper sludge employing the hydrothermal treatment (HTT) in a lab-scale facility for implementation of the pilot-scale plant. The paper sludge was subjected to HTT under subcritical hydrothermal conditions. In the lab-scale experiment, the temperature conditions were 180, 200, 220, and 240 °C at the pressure around 1.8–2.4 MPa, while it was 197 °C at 1.9 MPa in the pilot plant as the optimum condition. The holding time was 30 minutes in both cases. The hydrothermally produced solid fuel was evaluated in regards to its fuel properties, dewatering and drying performances, and mass distribution. Furthermore, the energy balance of the process was studied. Results showed that the higher heating value of the pretreated paper sludge was slightly improved by HTT. By mechanical dewatering, only 4.1% of moisture in the raw paper sludge can be removed while the 200 °C hydrothermally treated paper sludge showed 19.5% moisture reduction. According to the energy balance of the pilot plant, the recovered energy was significantly higher than the energy input, showing the feasibility of employing HTT to produce alternative solid fuel from paper sludge.

Chapter 3: *Combustion characteristics and kinetics study of hydrothermally treated paper sludge by thermogravimetric analysis*

In this chapter, an investigation on combustion characteristics of the hydrothermally treated paper sludge was performed as a fundamental combustion study. As shown in Chapter 2, the paper sludge was treated at the temperature range of 180–240 °C under pressurized conditions with a holding time of 30 minutes by a lab-scale apparatus. The optimized temperature (197 °C at 1.9 MPa) was used to

treat the paper sludge in a pilot plant with the same holding time. The combustion behavior of the products and the reference materials, including cellulose, hemicellulose, and lignin, were studied by the thermogravimetric analysis. The major decomposition of paper sludge was devoted to cellulose. The ignition temperature was originally low around 257–271 °C. The burnout temperature was approximately 679–695 °C. From the two-stage kinetics study, it was revealed that the activation energy of the treated paper sludge was lower than the original material indicating a higher reactivity and they were in the range of 113–147 kJ/mol.

Chapter 4: *Co-combustion of hydrothermally treated paper sludge with subbituminous coal in a fixed bed combustor*

After the fundamental combustion study in Chapter 3, the basic co-combustion test was conducted in this chapter. In this study, the co-combustion of the hydrothermally treated paper sludge with subbituminous coal was investigated. The solid fuel was produced from paper sludge by the hydrothermal pilot plant at the temperature of 197 °C and the pressure of 1.9 MPa for 30 minutes. NO emissions were tested by a batch-type fixed bed combustor. The result showed that the NO emissions could be reduced around 26–31% and, therefore, the mixture of coal and hydrothermally treated paper sludge (HTT-PS) yielded lower NO emission compared to the mixture of coal and raw paper sludge. NO conversion of the HTT-PS was lower than the original paper sludge. Finally, the slagging and fouling indices were calculated. The fouling and slagging tendencies of HTT-PS were improved.

Chapter 5: *Fluidized bed co-combustion of hydrothermally treated paper sludge with two coals of different rank*

In this chapter, the practical co-combustion test was conducted. Fluidized bed co-combustion of raw paper sludge (Raw-PS) and hydrothermally treated paper sludge (HTT-PS) with either low (Lo-Coal) or high reactivity coal (Hi-Coal) was investigated. The paper sludge was treated in a pilot-scale hydrothermal reactor at 197 °C and 1.9 MPa for 30 minutes. The procedure is the same as in Chapter 2. South African bituminous and Thai subbituminous coals were selected as representative of Lo-Coal and Hi-Coal, respectively. A 110-mm bubbling fluidized bed combustor was used in this study. During the steady combustion tests, the nominal temperature was 850 °C, the fluidization velocity was 0.5 m/s, and the excess air was varied as 20%, 40%, and 60%. Co-combustion tests were conducted by feeding the sludge at the mixing ratio of 30% and 50% (mass basis) with coal. The focus of this study was on NO_x emission and unburned carbon performance. Results showed that at 30% mixing ratio using HTT-PS instead of Raw-PS could reduce NO_x emission by 3–6% and 9–17% in the case of Lo-Coal and Hi-Coal, respectively, and the loss of unburned carbon could be decreased by 15–18% and 36–53% for Lo-

Coal and Hi-Coal, respectively. On the whole, the hydrothermally treated paper sludge showed better performance and would be a better choice compared to the original raw paper sludge.

Chapter 6: *Effect of hydrothermal treatment on primary fragmentation and attrition phenomena during fluidized bed combustion of paper sludge*

In Chapter 6, the effect of HTT on fluidized bed combustion of paper sludge focusing on essential particle comminution phenomena, i.e., the primary fragmentation and the char particle attrition, were investigated. This chapter explains the important findings in Chapter 5, i.e., the reduction of unburned carbon by HTT. The systematic combination of experimental techniques were carried out to test raw paper sludge (Raw-PS), hydrothermally treated papers sludge (HTT-PS), and subbituminous coal (Sub-C). The results showed that all three samples extensively underwent the primary fragmentation. From the char particle attrition, the Sub-C intensely experienced particle rounding off and, after that, became very strong against mechanical abrasive attrition followed by HTT-PS and Raw-PS. It was clearly observed from the oxidative attrition test that Sub-C exhibited postcombustion of fines and resulted in significantly lower amount of the elutriation rate whereas Raw-PS and HTT-PS went through a combustion-assisted attrition leading to higher amount of generated fines. In both cases, HTT-PS showed lower amount of fine particles than the original material indicating better combustion performance. Furthermore, CO_2 profile from the oxidative attrition test implied that the combustion of HTT-PS completed significantly earlier than the other fuels showing its superior burnout performance.

Chapter 7: *Conclusions*

The main findings from each chapter are re-summarized in this chapter. The experimental results are linked together between each study to articulate and explain the important mechanism. Finally, the recommendation for future work or implementation of this research is suggested.

References

[1] Saidur R, Abdelaziz EA, Demirbas A, Hossain MS, Mekhilef S. A review on biomass as a fuel for boilers. Renew Sust Energ Rev. 2011;15:2262-89.

[2] Martins FM, Martins JM, Ferracin LC, da Cunha CJ. Mineral phases of green liquor dregs, slaker grits, lime mud and wood ash of a Kraft pulp and paper mill. J Hazard Mater. 2007;147:610-7.

[3] Mahmood T, Elliott A. A review of secondary sludge reduction technologies for the pulp and paper industry. Water Res. 2006;40:2093-112.

[4] Bayr S, Rintala J. Thermophilic anaerobic digestion of pulp and paper mill primary sludge and co-digestion of primary and secondary sludge. Water Res. 2012;46:4713-20.

[5] Alda Od, Jesús AG. Feasibility of recycling pulp and paper mill sludge in the paper and board industries. Resour Conserv Recy. 2008;52:965-72.

[6] Monte MC, Fuente E, Blanco A, Negro C. Waste management from pulp and paper production in the European Union. Waste Manag. 2009;29:293-308.

[7] Méndez A, Fidalgo JM, Guerrero F, Gascó G. Characterization and pyrolysis behaviour of different paper mill waste materials. J Anal Appl Pyrol. 2009;86:66-73.

[8] Wajima T, Rakovan JF. Removal behavior of phosphate from aqueous solution by calcined paper sludge. Colloid Surface A. 2013;435:132-8.

[9] Dutournié P, Mercadier J. Supercritical waste hydrothermal treatment modelisation of non-stationary phenomena in a reactor. The Journal of Supercritical Fluids. 2004;32:153-60.

[10] Zhang L, Xu CC, Champagne P. Energy recovery from secondary pulp/paper-mill sludge and sewage sludge with supercritical water treatment. Bioresour Technol. 2010;101:2713-21.

[11] Toor SS, Rosendahl L, Rudolf A. Hydrothermal liquefaction of biomass: A review of subcritical water technologies. Energy. 2011;36:2328-42.

[12] Chandra R, Takeuchi H, Hasegawa T. Hydrothermal pretreatment of rice straw biomass: A potential and promising method for enhanced methane production. Appl Energy. 2012;94:129-40.

[13] Kritzer P, Dinjus E. An assessment of supercritical water oxidation (SCWO) existing problems, possible solutions and new reactor concepts. Chem Eng J. 2001;83:207-14.

[14] Sami M, Annamalai K, Wooldridge M. Co-firing of coal and biomass fuel blends. Prog Energ Combust. 2001;27:171-214.

[15] Savolainen K. Co-firing of biomass in coal-fired utility boilers. Appl Energy. 2003;74:369-81.

[16] Lu G, Yan Y, Cornwell S, Whitehouse M, Riley G. Impact of co-firing coal and biomass on flame characteristics and stability. Fuel. 2008;87:1133-40.

[17] Backreedy RI, Fletcher LM, Jones JM, Ma L, Pourkashanian M, Williams A. Co-firing pulverised coal and biomass: a modeling approach. P Combust Inst. 2005;30:2955-64.

[18] Williams A, Pourkashanian M, Jones JM. Combustion of pulverised coal and biomass. Prog Energ Combust. 2001;27:587-610.

[19] Vamvuka D, Salpigidou N, Kastanaki E, Sfakiotakis S. Possibility of using paper sludge in co-firing applications. Fuel. 2009;88:637-43.

[20] Yanfen L, Xiaoqian M. Thermogravimetric analysis of the co-combustion of coal and paper mill sludge. Appl Energy. 2010;87:3526-32.

[21] Kruse A, Dinjus E. Hot compressed water as reaction medium and reactant. J Supercrit Fluids. 2007;39:362-80.

[22] Brunner G. Near critical and supercritical water. Part I. Hydrolytic and hydrothermal processes. J Supercrit Fluids. 2009;47:373-81.

[23] Mumme J, Eckervogt L, Pielert J, Diakite M, Rupp F, Kern J. Hydrothermal carbonization of anaerobically digested maize silage. Bioresour Technol. 2011;102:9255-60.

[24] He C, Giannis A, Wang J-Y. Conversion of sewage sludge to clean solid fuel using hydrothermal carbonization: Hydrochar fuel characteristics and combustion behavior. Appl Energy. 2013;111:257-66.

[25] Park S-J, Bae J-S, Lee D-W, Ra HW, Hong J-C, Choi Y-C. Effects of Hydrothermally Pretreated Sewage Sludge on the Stability and Dispersibilty of Slurry Fuel Using Pulverized Coal. Energ Fuel. 2011;25:3934-9.

[26] Sevilla M, Fuertes AB. The production of carbon materials by hydrothermal carbonization of cellulose. Carbon. 2009;47:2281-9.

[27] Parshetti GK, Liu Z, Jain A, Srinivasan MP, Balasubramanian R. Hydrothermal carbonization of sewage sludge for energy production with coal. Fuel. 2013;111:201-10.

[28] Berge ND, Ro KS, Mao J, Flora JR, Chappell MA, Bae S. Hydrothermal carbonization of municipal waste streams. Environ Sci Technol. 2011;45:5696-703.

[29] Wiedner K, Rumpel C, Steiner C, Pozzi A, Maas R, Glaser B. Chemical evaluation of chars produced by thermochemical conversion (gasification, pyrolysis and hydrothermal carbonization) of agro-industrial biomass on a commercial scale. Biomass Bioenerg. 2013;59:264-78.

[30] Oliveira I, Blohse D, Ramke HG. Hydrothermal carbonization of agricultural residues. Bioresour Technol. 2013;142:138-46.

[31] Zhang L, Champagne P, Xu C. Bio-crude production from secondary pulp/paper-mill sludge and waste newspaper via co-liquefaction in hot-compressed water. Energy. 2011;36:2142-50.

[32] Xu C, Lancaster J. Conversion of secondary pulp/paper sludge powder to liquid oil products for energy recovery by direct liquefaction in hot-compressed water. Water Res. 2008;42:1571-82.

[33] Xu C, Etcheverry T. Hydro-liquefaction of woody biomass in sub- and super-critical ethanol with iron-based catalysts. Fuel. 2008;87:335-45.

[34] Xu C, Lancaster J. Conversion of secondary pulp/paper sludge powder to liquid oil products for energy recovery by direct liquefaction in hot-compressed water. Water Res. 2008;42:1571-82.

[35] Namioka T, Morohashi Y, Yamane R, Yoshikawa K. Hydrothermal treatment of dewatered sewage sludge cake for solid fuel production. J Environ Eng. 2009;4:68-77.

[36] Prawisudha P, Namioka T, Yoshikawa K. Coal alternative fuel production from municipal solid wastes employing hydrothermal treatment. Appl Energy. 2012;90:298-304.

[37] Muthuraman M, Namioka T, Yoshikawa K. A comparative study on co-combustion performance of municipal solid waste and Indonesian coal with high ash Indian coal: A thermogravimetric analysis. Fuel Process Technol. 2010;91:550-8.

[38] Nakhshiniev B, Gonzales HB, Yoshikawa K. Hydrothermal treatment of date palm lignocellulose residue for organic fertilizer conversion: effect on cell wall and aerobic degradation rate. Compost Sci Util. 2012;20:245-53.

[39] Sakaguchi M, Laursen K, Nakagawa H, Miura K. Hydrothermal upgrading of Loy Yang Brown coal — Effect of upgrading conditions on the characteristics of the products. Fuel Process Technol. 2008;89:391-6.

[40] Indrawan B, Prawisudha P, Yoshikawa K. Chlorine-free solid fuel production from municipal solid waste. J Jpn Inst Energ. 2011;90:1171-82.

[41] Tabasová A, Kropáč J, Kermes V, Nemet A, Stehlík P. Waste-to-energy technologies: Impact on environment. Energy. 2012;44:146-55.

[42] McKendry P. Energy production from biomass (part 2): conversion technologies. Bioresour Technol. 2002;83:47-54.

[43] Tsai M-Y, Wu K-T, Huang C-C, Lee H-T. Co-firing of paper mill sludge and coal in an industrial circulating fluidized bed boiler. Waste Manag. 2002;22:439-42.

[44] Zhao C, Sun X, Chen X, Gu L, Li Y, Yuan K. Investigation on co-combustion characteristic of paper mill waste and coal in circulating fluidized bed. Proceedings of the 18th International Conference on Fluidized Bed Combustion. Toronto, Canada2005. p. 631-7.

Chapter 2

Lab-scale and pilot-scale investigation on hydrothermal treatment of paper sludge for solid fuel production

Abstract: This chapter aims to investigate alternative solid fuel production from paper sludge employing the hydrothermal treatment (HTT) in a lab-scale facility for implementation of the pilot-scale plant. The paper sludge was subjected to HTT under subcritical hydrothermal conditions. In the lab-scale experiment, the temperature conditions were 180, 200, 220, and 240 °C at the pressure around 1.8–2.4 MPa, while it was 197 °C at 1.9 MPa in the pilot plant as the optimum condition. The holding time was 30 minutes in both cases. The hydrothermally produced solid fuel was evaluated in regards to its fuel properties, dewatering and drying performances, and mass distribution. Furthermore, the energy balance of the process was studied. Results showed that the higher heating value of the pretreated paper sludge was slightly improved by HTT. By mechanical dewatering, only 4.1% of moisture in the raw paper sludge can be removed while the 200 °C hydrothermally treated paper sludge showed 19.5% moisture reduction. According to the energy balance of the pilot plant, the recovered energy was significantly higher than the energy input, showing the feasibility of employing HTT to produce alternative solid fuel from paper sludge.

2.1 Background

As mentioned in Chapter 1, paper sludge comes from the primary clarifier and it mainly consists of discarded woody fibers [1,2]. Another portion of the paper sludge comes from the wastewater treatment facility and it is called as the secondary sludge, which has a very high water content [1]. This leads to the difficulties in managing as well as reduce performance of the combustor when it is used as boiler fuel. As the objective of this research is to use paper sludge as the alternative fuel in co-combustion application, the hydrothermal treatment (HTT) was firstly used to upgrade the paper sludge.

To realize this goal, the lab-scale test of the alternative solid fuel production from paper sludge employing HTT was done. The HTT condition, i.e., the temperature and its corresponding pressure, was optimized by both the product and process analyses. The holding time was fixed to simplify the evaluation since it has relatively less effect compared to the temperature and pressure. The product after HTT has to have a comparable or even better quality in view of solid fuel. For example, the dewaterability and energy content have to be improved. At the same time, the HTT condition has to be feasible from the aspect of the energy output/input ratio. By considering both product and process, the optimized condition of HTT could be achieved.

In the pilot-scale demonstration, the optimized temperature condition determined based on the lab-scale experiment was adopted. The holding time was varied to observe its effect. The evaluation has been

done with the similar procedure with the lab-scale test, and both product and process analyses are in focus. The mass and energy balances were analyzed. These calculations are more realistic compared to the one from the lab-scale experiment since it mostly derived from the experimental data. Therefore, the data from the mass and energy balance could be utilized for scaling-up. Furthermore, the mechanism of the effect of HTT on paper sludge has been investigated. The content in this chapter is considered as a fundamental step to achieve the integrated Waste-to-Energy solution for paper sludge in the pulp and paper industry.

2.2 Materials and methods

2.2.1 Raw material

The raw paper sludge (Raw-PS), which was provided by the Siam Kraft Industry Company Limited, Thailand, is the mixture of the primary and secondary sludge. The preliminary dewatered paper sludge shown in Figure 2-1 was the raw material for both lab-scale and pilot-scale experiments.

Figure 2-1 Paper sludge (left: lab-scale; right: pilot-scale)

2.2.2 Lab-scale experiment

2.2.2.1 Lab-scale hydrothermal treatment

In the laboratory, Raw-PS was treated in a batch-type electric heater autoclave machine (MMJ-500, OM Lab-Tech Co., Ltd., Japan) illustrated in Figure 2-2. The experimental system consists of a reactor, an electric heater, and a condenser with a water-cooling bath. The size of the vertical reactor is 500 mL. At the beginning, pure water (Wako Pure Chemical Industries, Ltd. Japan) was mixed with the paper sludge with the mass ratio of 1:1 to simulate the HTT condition. The prepared sample was poured into the reactor assembled with a stirrer. It was kept rotating during the experiment to assure the uniformity of the product. Before heating up, argon gas was introduced to create an oxygen free environment. The paper sludge was subjected to four temperatures variation, 180, 200, 220, and 240 ˚C with a holding

time of 30 minutes. After the treatment, the pressure inside the reactor was released by discharging the steam through the condenser. Shortly after the pressure was reduced to atmospheric condition, the product was thoroughly removed from the reactor as well as the condensate left in the condenser and its piping for calculating the mass balance. Each experiment was performed three times to assure the repeatability. Table 2-1 summarizes all the operating conditions in this work.

2.2.2.2 Lab-scale dewatering and drying

The mechanical dewatering and thermal drying were integrated into the proposed alternative solid fuel production process. The hydrothermally treated paper sludge (HTT-PS) was subjected to the dewatering test after HTT. It was conducted by a mechanical pressing device illustrated in Figure 2-3. The machine consists of a piston, a cylinder, and an orifice plate. HTT-PS was filled in the cylinder then it was pressurized at a pressure of 0.6 MPa for 15 minutes. Nitrogen gas was used as a pressure source. During the experiment, the seal and filter cloth were able to minimize errors. Subsequently, the dewatered solid was immediately taken into a convective force-drying process by an air blow dryer machine illustrated in Figure 2-4 for the drying test. The machine generates air flow by a centrifugal air compressor assembled with an electric heater to increase the air temperature. The dewatered sludge was put on the ASP-4100 electronic balance (As One Corp., Japan) integrated with the data logger. Due to the sensitivity of the electronic balance, the drying apparatus was calibrated before testing to minimize errors. The temperature condition of the drying experiment was controlled at 32 ˚C with an average velocity of 1.2 m/s. After the sample weight was constant for 1 h, the experiment was terminated. The dewatering and drying conditions are also shown in Table 2-1.

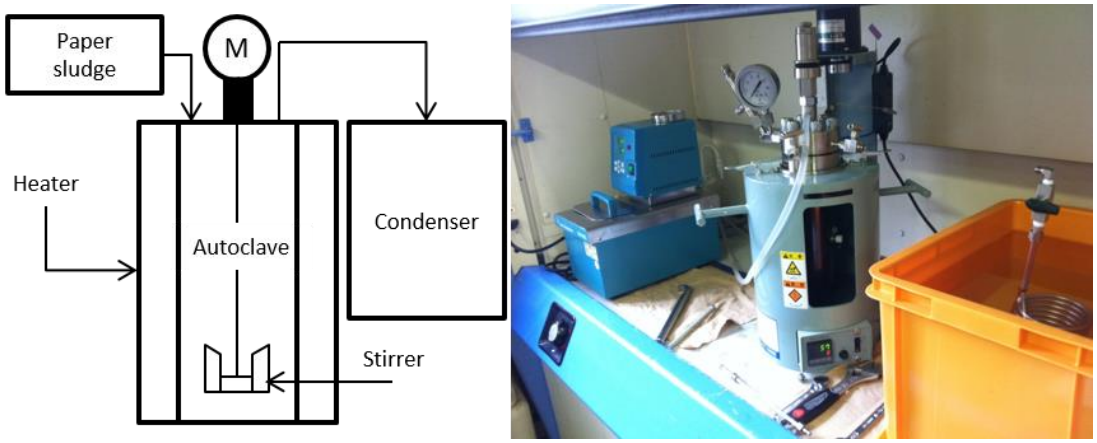

Figure 2-2 Autoclave machine

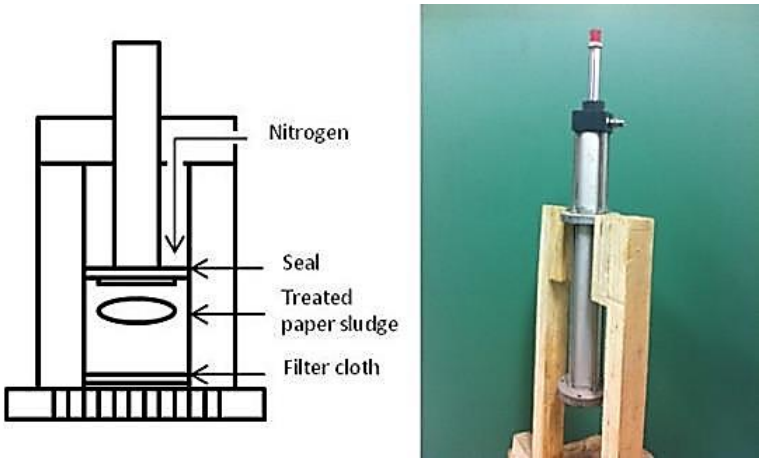

Figure 2-3 Mechanical pressing device

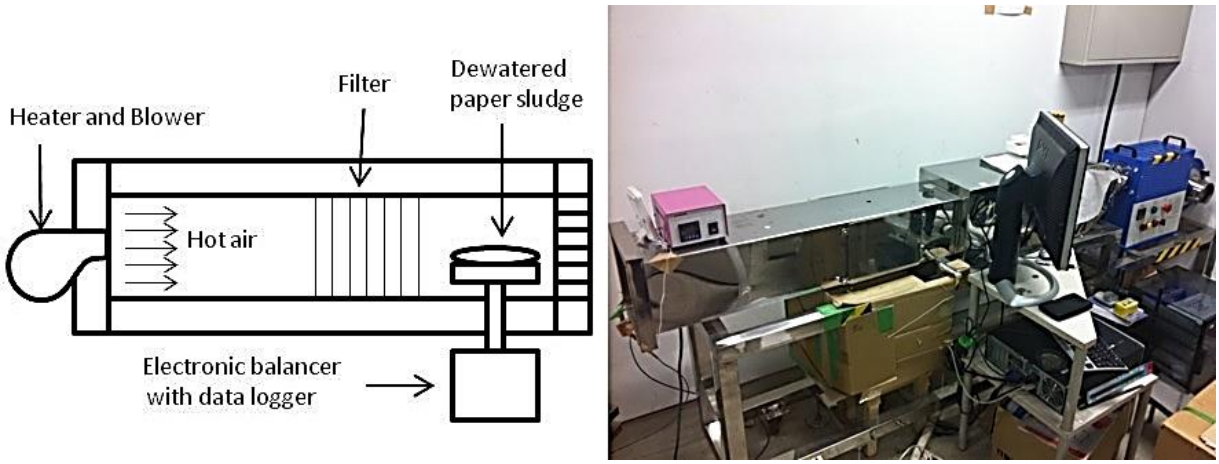

Figure 2-4 Air blow drying machine

2.2.3 Pilot-scale experiment

2.2.3.1 Pilot-scale hydrothermal treatment

For the pilot-scale HTT, the reactor is a 1-m^3 cylindrical batch-type assembled with an automatic stirrer illustrated in Figure 2-5. Approximately 351 kg of Raw-PS were supplied to the reactor in each experiment. Similar to the lab-scale procedure, the sample was initially kept mixing by a stirrer with a rotational velocity of 20 rpm. Then, the treatment condition was achieved by injecting a saturated steam generated by a fire-tube boiler fueled by liquefied petroleum gas (LPG). The operating condition was 1.9 MPa with an average temperature of 197 ˚C. When the temperature reached the desired state, the treatment process was instantly kept holding for 15 and 30 minuters. After the reaction was finished, the steam was flushed out to reduce the pressure inside the reactor. Finally, the products were extracted from the reactor directly by drain valves after the pressure fell down to 0.5 MPa. The pilot-scale HTT experimental condition is summarized in Table 2-1.

Figure 2-5 Hydrothermal pilot plant (Courtesy of SCG)

2.2.3.2 Pilot-scale dewatering and drying

The dewatering test of the pilot-scale experiment was performed by a 1.5-kW centrifugal decanter as shown in Figure 2-6. After HTT-PS was taken out from the reactor, it was filled into a three-layer textile-made bag, which has 650-micron mesh in each layer, to prevent the loss of the sample. Before starting the dewatering test, two bags, which have the same amount of samples, were tested together across from each other in order to balance the centrifugal machine during the operation. The rotational speed was 960 rpm and the dewatering time was 5 minutes. It should be mentioned that the pressure exerting on the sample was calculated from the division of centrifugal force to the circular area of the sludge cake after centrifuging. After the dewatering test, the sludge cake was immediately taken out. To perform the natural drying test, the sludge cake was first manually crushed then it was filled in a 30×30 cm plate and placed indoors with an average temperature of 32 ˚C. The 24-h natural drying of both samples were done under the same conditions. All the operating conditions mentioned above are also summarized in Table 2-1.

2.2.4 Sample analysis

Raw-PS and HTT-PS were analyzed in view of the physical appearance as well as the chemical composition. The appearance of the paper sludge was compared between before and after HTT and the drying process. In the laboratory, Raw-PS and HTT-PS were dried at 105 ˚C in an electric oven and pulverized before the analysis. The proximate and ultimate analysis were carried out as the dry basis with the Shimadzu 50 TGA/DTA analyzer and PerkinElmer 2400 Series II CHN organic elemental analyzer. The higher heating value (HHV, dry basis) was determined by the Shimadzu CA-4PJ bomb calorimeter. In case of the pilot-scale samples, the proximate analysis was conducted by the Leco's TGA701 Thermogravimetric Analyzer using the ASTM D7582 Standard Test Methods for Proximate Analysis of Coal and Coke by Macro Thermogravimetric Analysis. Leco's TruSpec CHNS/O was used to perform the ultimate analysis according to the ASTM D3176 Standard Practice for Ultimate

Analysis of Coal and Coke and the HHV was measured by the Leco's AC600 Bomb Calorimeter using the ASTM D5865 Standard Test Method for Gross Calorific Value of Coal and Coke.

Scanning electron microscopy (SEM) was performed by the JSM-6610LA scanning electron microscope (JEOL Co., Ltd. Japan) to study the surface morphology of the samples. Furthermore, the Fourier transform infrared spectrometry (FTIR) was done by the JIR-SPX200 FT-IR spectrometer (JEOL Co., Ltd. Japan) to investigate the mechanism of HTT. The fine particle samples were mixed with KBr and pelletized. Then, it was scanned from 400 to 4000 cm^{-1} with the resolution of 4 cm^{-1}.

Figure 2-6 1.5 kW centrifugal decanter (Courtesy of SCG)

Table 2-1 Summary of experimental condition

Parameters	Laboratory	Pilot
Hydrothermal treatment (HTT)		
Sludge mass	60±0.2 g	351±1 kg
Pressure (MPa)	1.8-2.4	1.9±0.05
Temperature (˚C)	180, 200, 220, 240	197±3
Holding period (min)	30	15, 30
Dewatering experiment		
Dewatering method	Pressing	Centrifuging
Dewatering pressure(MPa)	0.6	0.5
Dewatering time (min)	15	5
Drying experiment		
Drying mechanism	Thermal	Natural
Air temperature (˚C)	32±0.4	32±3
Air velocity (m/s)	1.2	N/A

2.2.5 Process analysis

2.2.5.1 Lab-scale process analysis

The analysis of lab-scale solid fuel production process was conducted to know the mass balance and estimated energy consumption and energy recovery. The mass balance plays very important role because all of the products after the treatment have different characteristics, amount, and value. They have to be appropriately utilized in order to add the value to the system. The amount of the products were determined interactively between each experiment within the control volume as follows:

1. Input and output of the small-scale autoclave facility for HTT,
2. Input and output of the mechanical pressing device for the dewatering experiment,
3. Input and output of the air blow dryer machine for the drying experiment.

In the laboratory, the mass balance equation was based on the following equations:

$$m_{sludge} + m_{moisture} + m_{added\ water} = m_{HTT\ sludge} + m_{blow-off\ gas} \quad (2\text{-}1)$$

where m_{sludge} = mass of dried Raw-PS supplied to the autoclave machine, $m_{moisture}$ = mass of moisture in Raw-PS supplied to the autoclave machine , $m_{added\ water}$ = mass of the additional water supplied to the autoclave machine, $m_{HTT\ sludge}$ = mass of HTT-PS products after the treatment including the condensed steam, and $m_{blow-off\ gas}$ = blow-off gas output of the condenser (calculated by the difference),

$$m_{HTT\ sludge} = m_{de\ solid} + m_{de\ liquid} \quad (2\text{-}2)$$

where $m_{HTT\ sludge}$ = mass of HTT-PS supplied for the mechanical pressing device, $m_{de\ solid}$ = mass of the dewatered solid after dewatering, $m_{de\ liquid}$ = mass of the dewatered liquid after dewatering,

$$m_{de\ solid} = m_{dried\ solid} + m_{evap\ moisture} \quad (2\text{-}3)$$

where $m_{de\ solid}$ = the dewatered solid part of HTT-PS supplied to the air blow dryer, $m_{dried\ solid}$ = mass of the dried HTT-PS product from the air blow dryer which was considered as totally dried, $m_{evap\ moisture}$ = evaporated moisture during drying.

The energy consumption and the energy recovery were discussed for assuring the possibility of the solid fuel production process from paper sludge. Combining the theoretical assumptions and experimental data, the net energy consumption for treating the paper sludge in each condition has been determined. Additionally, to evaluate the feasibility of the process, the ratio of the energy output/input can be approximately estimated by Equation 2-4 [1].

$$\text{Energy Output/Input Ratio} = \frac{(\text{HHV of Product}) \times (\text{Dried Mass})}{(\text{Energy Input})} \quad (2\text{-}4)$$

where HHV (dry basis) is the higher heating value of HTT-PS, the dried mass is the dried HTT-PS after the drying experiment, and the energy input was calculated by Equation 2-5.

$$\text{Energy Input} = \left[m_{sludge} c_p (T_T - T_{rm})\right] + \left[m_{water}\left(h_{g,T} - h_{l,T_{rm}}\right)\right] \quad (2\text{-}5)$$

where m_{sludge} is the dried mass of Raw-PS, c_p is the specific heat of Raw-PS, T_T is the specific temperature condition for each experiment, T_{rm} is the room temperature, $h_{g,T}$ is an enthalpy of the saturated vapor at the specific temperature, $h_{l,T_{rm}}$ is the enthalpy of the saturated liquid at the room temperature, and m_{water} is the water in Raw-PS.

The calculation for the lab-scale experiment has been done under the following assumptions:

1. The water was heated from 25 ˚C to the saturated vapor water state in each specific temperature.
2. The energy consumption of the electrical stirrer and other electrical utilities were neglected.
3. The energy utilized in the dewatering experiment has been neglected.
4. The energy used for water evaporation was estimated by multiplying the amount of moisture evaporated in the drying experiment with a latent heat for evaporation of water (2.26 MJ/kg),
5. The specific heat of sludge was assumed to be 1.7 kJ/kg·K.

2.2.5.2 Pilot-scale process analysis

In order to understand the process characteristic and ensure economic feasibility of the pilot-scale alternative solid fuel production process, the process analysis as the mass and energy balances have to be discussed.

As mentioned in the lab-scale experiment, the mass balance is essential especially in the larger scale experiment. In the pilot-scale mass balance, both mass input and output to the reactor and other facilities during the whole treatment process were determined as follows:

1. Input and output of the pilot-scale hydrothermal plant for HTT
2. Input and output of the centrifugal decanter machine for the dewatering experiment
3. Input and output of the indoor 24 h natural drying experiment
4. Additional mass balance for the dry basis product

The mass balance equation can be obtained as follows:

$$m_{sludge} + m_{steam} = m_{slurry} + m_{liquid} + m_{blow-off\,gas} \quad (2\text{-}6)$$

where m_{sludge} = wet basis Raw-PS mass supplied to the reactor, m_{steam} = mass of steam supplied to the reactor, m_{slurry} = slurry part of the product as the output of HTT, m_{liquid} = liquid part of the product

as the output of HTT, and $m_{blow-off\ gas}$ = blow-off gas to the condenser as condensed steam as the output of HTT (calculated by the difference).

$$m_{slurry} = m_{de\ solid} + m_{de\ liq} \quad (2\text{-}7)$$

where m_{slurry}= slurry part of the product supplied to the centrifugal decanter, $m_{de\ solid}$ = dewatered solid product as the output of the dewatering experiment, $m_{de\ liq}$= dewatered liquid product as the output of the dewatering experiment.

$$m_{de\ solid} = m_{nad\ solid} + m_{nad\ evap\ liq} \quad (2\text{-}8)$$

where $m_{de\ solid}$= dewatered solid product supplied for the natural drying experiment, $m_{nad\ solid}$ = naturally dried solid mass as the output of the natural drying experiment, $m_{nad\ evap\ liq}$= naturally evaporable moisture during the naturaly drying experiment.

$$m_{nad\ solid} = m_{tot\ dried\ solid} + m_{evap\ liq} \quad (2\text{-}9)$$

where $m_{nad\ solid}$ = mass after the natural drying experiment, $m_{tot\ dried\ solid}$= dry basis of the final product, $m_{evap\ liq}$ = the rest of the evaporable moisture. It should be noted that the 24 h natural drying experiment cannot reduce the moisture of the sample to zero; thus the total dried mass (dry basis of HTT-PS) was determined in the analysis center. And, the total moisture, needed to be evaporated after the dewatering experiment, was the accumulation of $m_{nad\ evap\ liq}$ and $m_{evap\ liq}$.

Energy balance is indispensable because it implies the possibility of the alternative solid fuel production process. It was calculated based on the information, measurement data, and assumption. The previous study by Namioka [3] discussed about the energy consumption of the solid fuel production from sewage sludge compared with the conventional drying process. It was said that the energy consumption of the proposed system was two-thirds of the drying process. Based on the study on the energy balance of HTT by Dr. Pandji Prawisudha [4], two phases energy consumption in HTT were suggested: (i) steam injection and (ii) holding period. In each phase, the energy utilized in the process was categorized into three groups: (1) energy from steam, (2) electrical energy from motor attached with the reactor, and (3) energy from other electrical utilities. This valuable investigation was utilized as the core concept of the energy balance study.

In this study, further extension of the energy balance has been proposed as *the Integrated Total Energy Balance of Alternative Solid Fuel Production from High Moisture Waste Employing Hydrothermal Treatment*. The integration of the dewatering and drying experiments' energy consumption were presented; thus, the energy analysis of the complete solid fuel production process from sludge could be estimated.

The energy output/input ratio was utilized similar to the laboratory-scale experiment. When this value is higher than one, it means that the system generates excessive amount of energy, which implies its sustainability. On the other hand, if the value is lower than one, it indicates that the system needs other energy sources to operate and maintain the process. Thus, the energy output/input ratio could evaluate the feasibility. It was determined from the following equation:

$$\text{Energy Output/Input Ratio} = \frac{(\text{Energy Output})}{(\text{Energy Input})} \quad (2\text{-}10)$$

The energy output from the system was calculated by the recovered energy from the dried mass of the final product, which is the multiplication of the higher heating value, and the dried mass of the product as shown in Equation 2-11. And, the total energy input to the solid fuel production process is the accumulation of the energy used in HTT (steam injection and holding period), the dewatering process, and the drying process as presented in Equation 2-12.

$$[\text{Energy Output}] = [\text{HHV of sludge}] \times [\text{Dried mass of sludge}] \quad (2\text{-}11)$$

$$[\text{Energy Input}] = \begin{bmatrix}\text{HTT}\\ \text{Steam injection}\end{bmatrix} + \begin{bmatrix}\text{HTT}\\ \text{Holding period}\end{bmatrix} + \begin{bmatrix}\text{Dewatering}\\ \text{process}\end{bmatrix} + \begin{bmatrix}\text{Drying}\\ \text{Process}\end{bmatrix} \quad (2\text{-}12)$$

Next, the total energy from steam was calculated by Equation 2-13. The steam was generated by the fire-tube boiler using the liquefied petroleum gas (LPG) as fuel. The efficiency of the boiler was approximately 89% and LPG, which has the HV of 26.78 MJ/liter, was provided by the PTTNGV Co., Ltd. It should be noted that the energy from LPG was easily derived from a multiplication of an amount of LPG used and its heating value as the input energy to the boiler. After multiplying the raw energy in LPG and the efficiency of the boiler, the total energy from steam was obtained. The third term in the Equation 2-13 is the energy of the steam at a specific pressure and temperature, which equals to the total energy from steam. The specific temperature of the steam at the boiler can be determined from this equation giving the occurring thermodynamic process of the steam in the boiler. The atmospheric temperature was 22 ˚C and the total water consumption was presented in the previous mass balance section as the total steam consumption. The operating pressure of the boiler was 2.1 MPa.

$$\begin{bmatrix}\text{Total energy}\\ \text{from steam}\end{bmatrix} = [m_{\text{fuel,total}} \cdot HV_{\text{fuel}}] \times [\eta_{\text{boiler}}] = m_{\text{water,tot}}\left(h_{(P,T)} - h_{T_0}\right) \quad (2\text{-}13)$$

Equation 2.14 shows the energy utilized in the steam injection phase, which were (1) energy from steam, (2) electrical energy from stirrer's motor for keeping the sample mixed, and (3) electrical energy from boiler utilities including water pump, controller, and burner.

$$\begin{bmatrix}\text{HTT}\\ \text{Steam injection}\end{bmatrix} = \begin{bmatrix}\text{Energy from}\\ \text{steam @ inj.}\end{bmatrix} + \begin{bmatrix}\text{Energy from}\\ \text{motor @ inj.}\end{bmatrix} + \begin{bmatrix}\text{Energy from}\\ \text{utilities @ inj.}\end{bmatrix} \quad (2\text{-}14)$$

The energy from steam during the injection process was determined by Equation 2-15, where $m_{water,inj.}$ is the mass of the water fed to the boiler during the steam injection process, $h_{(P,T)}$ is the enthalpy of the water at the specific pressure and temperature derived from Equation 2-13 and h_{T_0} is the enthalpy of the water at atmospheric temperature.

$$\begin{bmatrix}\text{Energy from}\\ \text{steam @ inj.}\end{bmatrix} = m_{water,inj.}\left(h_{(P,T)} - h_{T_0}\right) \quad (2\text{-}15)$$

The electrical energy from the motor of the stirrer could be estimated by Equation 2-16 as taking the integration of power usage of the motor over operating time during the steam injection process, where, $P_{m,inj}$ is the electrical power of the motor used during the steam injection phase which equals to the electrical current measuring at the control monitor of the motor ($I_{m,inj}$) multiplied by the supplied voltage at the plant (380 volt) and the power factor (0.8). Since the integration needs the function approximately derived from the original curve, the calculation was done precisely by accumulating the area under the power and time curve as presented in Equation 2-16. The same approach was applied to Equation 2-17 for the calculation of energy from utilities during the steam injection process, where $P_{u,inj}$ is the electrical power of the utilities during the steam injection phase, $I_{u,inj}$ is the electrical current of the utilities used in the steam injection phase.

$$\begin{bmatrix}\text{Energy from}\\ \text{motor @ inj.}\end{bmatrix} = \text{Area of } P_{m,inj} - \text{t curve} \sim \int_{t_1}^{t_2} P_{m,inj} \cdot dt;\ P_{m,inj} = I_{m,inj} V \cos \emptyset \quad (2\text{-}16)$$

$$\begin{bmatrix}\text{Energy from}\\ \text{utilities @ inj.}\end{bmatrix} = \text{Area of } P_{u,inj} - \text{t curve} \sim \int_{t_1}^{t_2} P_{u,inj} \cdot dt;\ P_{u,inj} = I_{u,inj} V \cos \emptyset \quad (2\text{-}17)$$

The energy consumption of the holding period during HTT was determined by Equation 2-18. It can be separated into three groups similar to the steam injection phase. The energy from steam during the holding period was calculated by Equation 2-19, where $m_{water,hld.}$ is the water consumption of the boiler during the holding period, and it was used to compensate the heat loss. The energy from electrical utilities was from the motor of the stirrer and the boiler utilities. The calculation methods presented in Equation 2-20 and 2-21 are the same as the steam injection phase, where $P_{m,hld}$ is the electrical power of the stirrer's motor, $I_{m,hld}$ is the electrical current of the motor used in the holding period, $P_{u,hld.}$ is the electrical power of the utilities, and $I_{u,hld.}$ is the electrical current of the utilities used in the holding period.

$$\begin{bmatrix}\text{HT}\\ \text{Holding period}\end{bmatrix} = \begin{bmatrix}\text{Energy from}\\ \text{steam @ hld.}\end{bmatrix} + \begin{bmatrix}\text{Energy from}\\ \text{motor @ hld.}\end{bmatrix} + \begin{bmatrix}\text{Energy from}\\ \text{utilities @ hld.}\end{bmatrix} \quad (2\text{-}18)$$

$$\begin{bmatrix}\text{Energy from}\\ \text{steam @ hld.}\end{bmatrix} = m_{water,hld.}\left(h_{(P,T)} - h_{T_0}\right) \quad (2\text{-}19)$$

$$\begin{bmatrix}\text{Energy from}\\ \text{motor @ hld.}\end{bmatrix} = \text{Area of } P_{m,hld}t \text{ curve} \sim \int_{t_1}^{t_2} P_{m,hld} \cdot dt;\ P_{m,hld} = I_{m,hld} V \cos \emptyset \quad (2\text{-}20)$$

$$\begin{bmatrix}\text{Energy from}\\ \text{utilities @ hld.}\end{bmatrix} = \text{Area of } P_{u,hld} - t \text{ curve} \sim \int_{t_1}^{t_2} P_{u,hld} \cdot dt;\ P_{u,hld} = I_{u,hld} V \cos \emptyset \quad (2\text{-}21)$$

Eventually, the energy consumption of the dewatering and drying experiments are calculated by Equation 2-22 and 2-23, respectively. The centrifugal decanter was operated by a 1.5 kW motor transferring the centrifugal force by belts. The maximum speed was utilized; thus, electrical energy used in the dewatering process was the multiplication of $P_{m,centrif.}$ (maximum power of 1.5 kW) and the operating time to dewater all of the treated paper sludge after HTT. For the natural drying process, it was determined by multiplying the evaporated mass of the water during the drying test (after the dewatering process) with the latent heat of evaporation (2.26 MJ/kg).

$$\begin{bmatrix}\text{Dewatering}\\ \text{process}\end{bmatrix} = \begin{bmatrix}\text{Electrical energy}\\ \text{from motor}\end{bmatrix} = \left[P_{m,centrif.} \cdot t\right] \quad (2\text{-}22)$$

$$\begin{bmatrix}\text{Drying}\\ \text{process}\end{bmatrix} = \begin{bmatrix}\text{Solar energy}\\ \text{for evaporation}\end{bmatrix} = m_{water} \cdot L \quad (2\text{-}23)$$

2.3 Results and discussion

2.3.1 Appearance

Figure 2-7 shows the comparison of the products appearance after HTT by varying the treatment temperature and drying (24 h oven drying at 105 ˚C). The paper sludge become dark grey slurry-like after subjected to HTT. Moreover, the size of the product was clearly smaller and the color was much darker for the higher treatment temperature. When treated at 240 ˚C, considerably higher amount of liquid was obtained compared to other lower temperature conditions. This is because the fiber structure, mainly composed of cellulose and hemi-cellulose [5], was destroyed and decomposed during HTT as a result of heat and pressure. According to the literature, wood components begin to decompose at the temperature around 160–200 ˚C for hemicellulose and 240-350 ˚C for cellulose [6]. The mechanism of essential decomposition at the temperature below 200 ˚C was suggested as depolymerization of cellulose [7]. Hence, the appearance of HTT-PS clearly showed the effects of HTT on the decomposition of paper sludge which depends on the severity of the treatment condition. In other words, when the temperature was increased, more destructive effects were occurred to the structure of the paper sludge.

From the appearance of the dry product, shrinkage was clearly observed in Raw-PS due to the loss of moisture during the drying process. Thus, it physically indicated that Raw-PS contained more moisture compared to the others. Initially, Raw-PS has very bad odor, it seemed to be better after HTT because

the sterilization of microbes in Raw-PS probably suppressed the production of bad smell gas such as hydrogen sulfide [8].

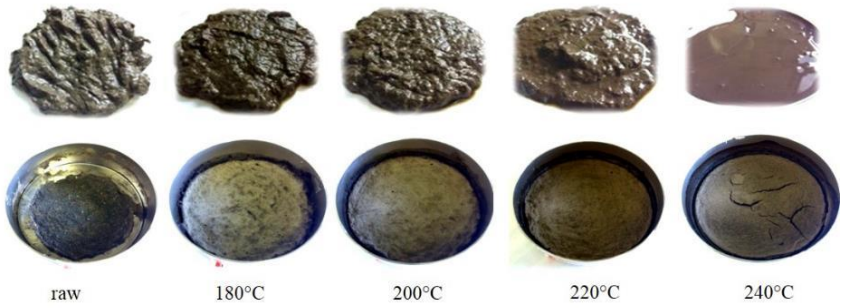

Figure 2-7 Appearance of the raw and hydrothermally treated paper sludge

For the pilot-scale product, the comparison of Raw-PS and HTT-PS are presented in Figure 2-8. HTT-PS had slurry-like characteristic and it has grey color while Raw-PS looks more solid-like. The appearance of HTT-PS from both 15 and 30 min holding time were very similar. It can be observed that HTT-PS contained higher moisture content and this could be due to the condensation of the steam and a chemical reaction that yields water such as dehydration reaction. The liquid can be observed in the product storage tanks and HTT-PS seemed to be smaller and stuck together like mud.

Figure 2-8 Paper sludge before (left) and after hydrothermal treatment (right)

However, after the dewatering process, the color of HTT-PS was obviously darker and browner when compared to Raw-PS. The sludge cakes after the dewatering and drying were shown in Figure 2-9. The odor was much better. Since the appearance of HTT-PS with 15 and 30 min holding time has no significant difference, it implied that the holding time had less effects on the appearance compared to the pressure and temperature. The holding time could play role in the appearance when it was significantly longer; however, it means the higher process time and energy consumption.

Additionally, SEM micrographs were used to study fibrous morphology of the paper sludge as shown in Figure 2-10. A large fibrous material can be observed in the raw paper sludge illustrated in Figure 2-10a. For the paper sludge treated at the temperature of 180 ˚C (Figure 2-10b) and 200 ˚C (Figure 2-10c), the big fibrous particle was vanished while the long chain fibrous material was still observable. Figure 2-10d and 2-10e illustrate that most of the fibrous material was degraded when it was treated at higher treatment temperature especially at 240 ˚C. The SEM image of the pilot-scale product presented in Figure 2-10f also shows the same characteristic with the lab-scale product. Thus, the SEM analysis suitably articulated the destructive effect of HTT as explained above.

Figure 2-9 Hydrothermally treated paper sludge after dewatering test (left) and naturally dried (right)

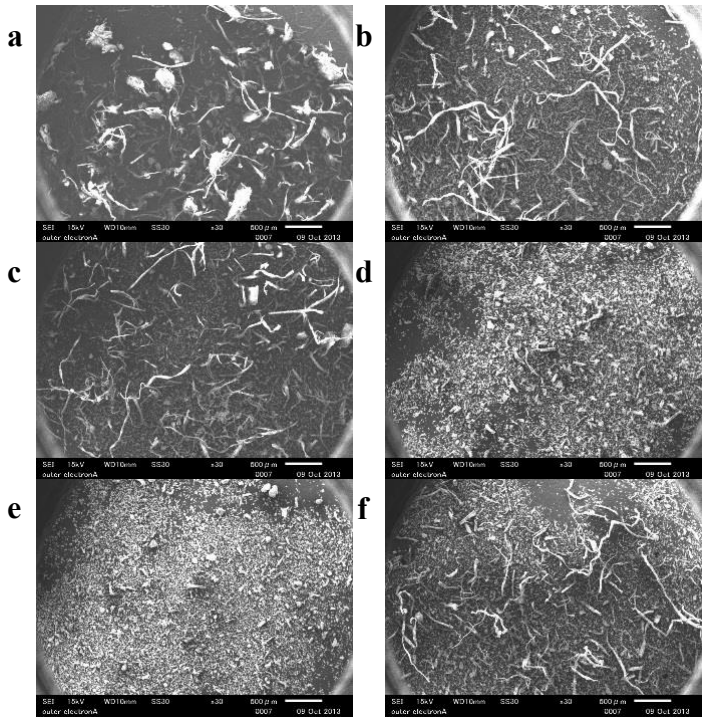

Figure 2-10 SEM images, a: Raw; b: 180 ˚C; c: 200 ˚C; d: 220 ˚C; e: 240 ˚C; f: 197 ˚C

2.3.2 Dewatering and drying performances

In this study, the water removal process consists of dewatering and drying. The moisture content in solid fuel greatly affects the combustion performance such as fuel consumption and combustion efficiency. The availability of moisture could benefit for the combustion process; however, when higher than 30%, it significantly decreased the burning rate and ignition front propagation [9]. Thus, the effect of HTT on the dewatering and drying performances was studied. Initially, the moisture content of Raw-PS was 76.0% (lab) and 76.4% (pilot), which was tremendously difficult to be dewatered. Figure 2-11 shows the graphical dewatering performance of the paper sludge before and after HTT. The moisture content in Raw-PS was reduced from 76.0% to 72.9% after the dewatering process; while it was decreased to 65.3% for HTT-PS at 180 ˚C. When the treatment temperature increased to 200 and 220 ˚C, the moisture content was reduced to 61.2% and 60.4% after the mechanical dewatering process. Moreover, it can be as low as 54.5% when it was treated with 240 ˚C HTT temperature. After the mechanical dewatering, the moisture reduction rate of Raw-PS was 4.1% whereas HTT-PS showed, at least, 23%. It is more than five times higher than that of the raw paper sludge. Therefore, we can say that the dewatering performance was significantly improved after HTT.

Figure 2-11 also illustrates the forced convective drying results. The weight loss of the sample attributed to the evaporation of the moisture inside the sample. With HTT, the moisture reduction rate was higher as can be observed by comparing the slope of the curve. HTT-PS was approximately reduced to 15%, which is low enough for utilization in a commercial boiler. On the other hand, Raw-PS still has a moisture content more than 25%.

For the pilot-scale experiment, both Raw-PS and HTT-PS were subjected to the dewatering test by the centrifugal decanter, which generates the pressure approximately 0.5 MPa to the samples. Figure 2-11 presents the graphical result of the dewatering and drying performances. The moisture content of Raw-PS was initially 76.4% and it was decreased to 72.3% after dewatering showing 5.4% moisture reduction rate. After HTT, the moisture content was increased from 76.4% to 83.9% and 83.6% with 15 and 30 min holding time, respectively. Then, after the centrifugal dewatering, it was reduced to 61.5% and 61.8% for the 15 and 30 min holding time, respectively, presenting the reduction of 26.0%. The dewatering performance was significantly improved since HTT paper sludge showed approximately, at least, five times higher than that of Raw-PS. After 1 h natural drying, the moisture content of Raw-PS, which has 72.3% moisture left after dewatering, was decreased to 69.6%, reducing 3.7%. In case of HTT-PS, the moisture content was reduced from 61.8% to around 57.0%, performing 7.8% reduction. The drying performance of HTT-PS was doubled indicating that HTT has a positive benefit to the drying process. The results from both lab-scale and pilot-scale experiments show that the paper sludge has better dewatering and drying performances after subjected to HTT. This is because cell structures of sludge have been crushed and bound water was released [4]. Generally, the moisture in the sludge contains free water, surface water, interstitial water, and bound water. At ~105 ˚C, the free

and surface water can be evaporated whereas the interstitial and bound water need the higher temperature up to 400 ˚C to evaporate [10]. Thus, Raw-PS has the difficulties in the water removal process due to the interstitial and bound water was still contained in the cell boundary. By employing HTT, the interstitial and bound water could be dewatered and evaporated easily.

The remanent moisture in the dewatered product was about 61.0% for both lab-scale (200 ˚C) and pilot-scale (197 ˚C) experiments. However, the results of the drying performance were quite different. From the pilot-scale result, the moisture left in the 24 h naturally dried product was approximately 52% while the lab-scale dried products contained about 15.0% moisture content within 10 h. The drying performance of the lab-scale product was significantly better because the drying condition were different. The drying condition in the laboratory was the convective force drying while it was the natural drying in the pilot-scale experiment. Moreover, significantly small amount of sample was used in the lab-scale test. Obviously, small amount of sample that was dried by heated air with a well-circulated atmosphere can provide a better drying condition.

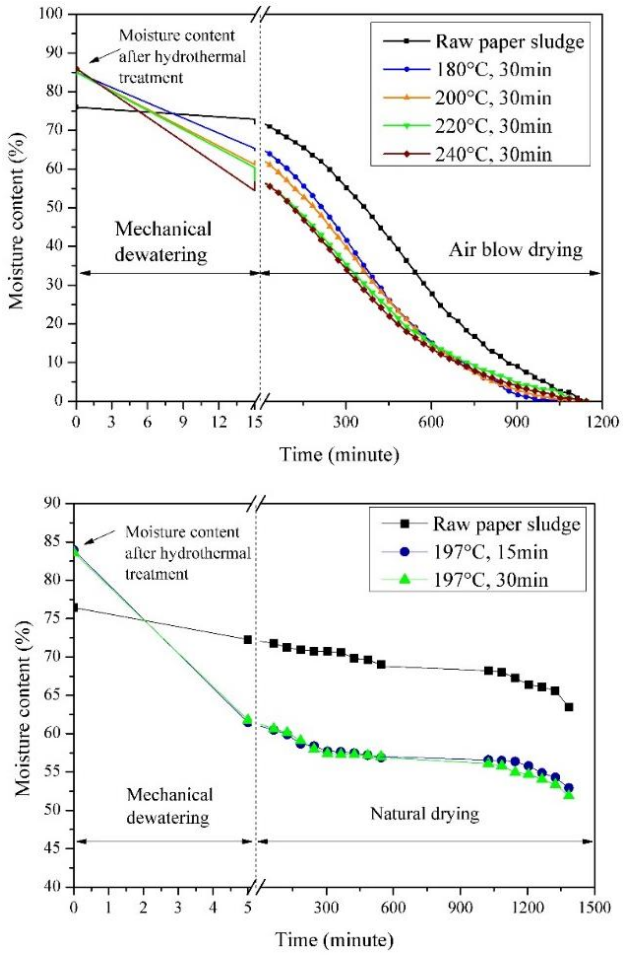

Figure 2-11 Moisture in paper sludge during the dewatering and drying test

2.3.3 Fuel property

Proximate analysis of Raw-PS and HTT-PS is summarized in Table 2-2. It was clearly shown that volatile matter (VM) was relatively decreased after HTT while fixed carbon (FC) and ash were relatively increased. Raw-PS has 62.1% VM and it was slightly decreased to 60.1%, 57.8%, 56.5%, and 56.5% after treated with 180, 200, 220, and 240 ˚C HTT, respectively. The FC increased from 3.9% to 4.5%, 5.0%, 6.5%, and 7.7% while the ash content increased from 34.1% to 35.4%, 37.2%, 37.0%, and 35.8% with the increase of the temperature from 180 ˚C to 240 ˚C, respectively. The loss of VM could be attributed to the hydrolysis of the polysaccharide into glucose [11,12]. In an oxygen free environment, the polysaccharide can be decomposed into CO_2 and water with the temperature of 180–250 ˚C [12] and the high temperature condition (240 ˚C) also enhances the polymerization reaction.

Ultimate analysis result is summarized in Table 2-2. The carbon content of Raw-PS was 31.3% and it was 31.7%, 30.8%, 32.4%, and 35.6% at the 180, 200, 220, and 240 ˚C HTT condition, respectively. The carbon content was increased when HTT temperature increases. Hydrogen was decreased from 4.6% before the treatment to 4.2%, 3.9%, 3.9%, and 4.2% while nitrogen was also decreased from 2.2% to 2.0%, 1.7%, 1.4%, and 2.0% as increasing the treatment temperature, respectively. The reduction in the weight ratio of oxygen can be observed and this contributed to the higher energy content in the product. The oxygen content was 27.8% for Raw-PS and 180 ˚C HTT and decreased to 26.4%, 25.4%, and 24.5% for the 200, 220, and 240 ˚C treatment condition, respectively. Table 2-2 also shows the higher heating value (HHV) that was gradually increased after HTT. The HHV of HTT-PS was around 13.4–13.6 MJ/kg while Raw-PS's HHV was only 12.7 MJ/kg. This is because the ratio of the FC, which has much higher energy content compared to the VM, was increased resulting in the improvement of the HHV. In other words, the energy density of HTT-PS was slightly increased.

For pilot-scale experiment, the proximate analysis, ultimate analysis, and heating value were analyzed are presented in Table 2-2. For paper sludge, the results of the 15 and 30 min HTT conditions were not significantly different. The proximate analysis showed that VM was decreased whereas the ash and FC were increased. VM was decreased from 62.1% to 59.9% and 59.4% for the 15 and 30 min holding time HTT, respectively. The ash was increased from 27.0% to 29.8% and 30.5% and the FC was slightly decreased from 10.9% to 10.3% and 10.1% after 15 and 30 min holding time HTT, respectively.

The ultimate analysis shows that the carbon content was similar in the case of Raw-PS and HTT-PS 15 min. However, it was slightly increased for the 30 min HTT. Hydrogen contained in Raw-PS was 4.3% and it was around 4.2–5% in the case of HTT-PS. The nitrogen in Raw-PS was 3.9% and it was in-between 3.1–4.6% after HTT with the holding time of 15 and 30 minutes. As the nitrogen content was decreased after HTT, it shows the possibility of NO_x emission reduction during the combustion process. Sulfur content was around 0.5–0.6% in both Raw-PS and HTT-PS. The oxygen content was 29.5% for

Raw-PS and gradually decreased to 25.4% and 26.5% by HTT 15 and 30 min, respectively. For the higher heating value (HHV) and lower heating value (LHV), Raw-PS has HHV and LHV of 14.1 MJ/kg and 11.1 MJ/kg, respectively. HHV and LHV of the 15 min HTT-PS were 13.6 MJ/kg and 12.5 MJ/kg, respectively. It was observed that HHV was slightly lower (3.6% reduction) than Raw-PS while LHV was higher (12.2% increasing). For the longer holding treatment period, 30 minutes, both HHV and LHV were increased. HHV was increased from 14.1 MJ/kg to 14.9 MJ/kg, which was 5.5% enhancement while LHV rose from 11.1 MJ/kg to 11.6 MJ/kg accounting 4.2% increase. From the viewpoint of the energy content in the sample, HTT with 30 min holding time was more effective than the shorter holding time as both of HHV and LHV were improved. From the fuel properties, it can be concluded that HTT-PS has comparable or even higher fuel properties.

Table 2-2 Fuel properties

Items/conditions	Lab-scale (˚C)					Pilot-scale (˚C)		
	Raw	180	200	220	240	Raw	197/15 min	197/30 min
				Proximate analysis (%)				
Initial moisture	76.0	-	-	-	-	76.4	-	-
Ash	34.1	35.4	37.2	37.0	35.8	27.0	29.8	30.5
Volatile matter	62.1	60.1	57.8	56.5	56.5	62.1	59.9	59.4
Fixed carbon	3.9	4.5	5.0	6.5	7.7	10.9	10.3	10.1
				Ultimate analysis (%)				
Carbon	31.3	31.7	30.8	32.4	35.6	34.8	34.6	35.2
Hydrogen	4.6	4.2	3.9	3.9	4.2	4.3	5.1	4.2
Nitrogen	2.2	2.0	1.7	1.4	2.0	4.0	4.6	3.1
Sulfur	-	-	-	-	-	0.6	0.5	0.6
Oxygen*	27.8	27.8	26.4	25.3	22.4	29.3	25.4	26.5
				Atomic ratio				
H/C	1.76	1.59	1.52	1.44	1.42	1.48	1.77	1.43
O/C	0.67	0.66	0.64	0.59	0.47	0.64	0.55	0.56
				Heating value (MJ/kg)				
HHV	12.7	13.4	13.4	13.4	13.6	14.1	13.6	14.7

* calculated by difference

2.3.4 Mass balance

Raw-PS and distilled water mixing ratio was one to one. The mass balance of 200˚C HTT condition is shown in Figure 2-12. Approximately 60 g of Raw-PS was utilized in each experiment. HTT-PS was increased from 60.1 to 91.0 g because of the additional water used for mocking up the hydrothermal condition. The dewatered liquid was around 55.8 g while the totally dried solid part was only 13.7 g and it is equal to 11.8% of the total mass input to the system.

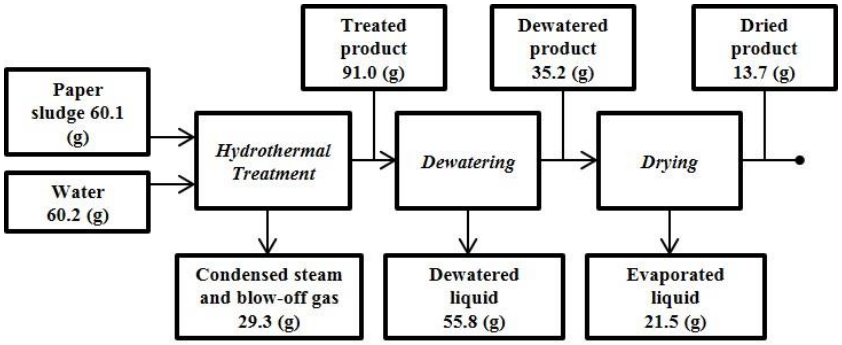

Figure 2-12 Laboratory-scale mass balance of the 200 ˚C, 30 min hydrothermal condition

Table 2-3 presents all of the experiments' mass balance by taking the mass of Raw-PS input to the reactor as the datum (100%). After Raw-PS was dewatered, the mass of the dewatered solid was 88.6% and the dewatered liquid was 11.4%. Large amount of moisture, 64.6%, has to be evaporated during the drying experiment. After HTT, HTT-PS product was significantly increased and it was decreased when the temperature was higher. The condensate and blow-off gas were also calculated. The former was collected during the experiment while the latter was determined by the difference. Then, the treated product was subjected to the dewatering test. The large amount of dewatered liquid was obtained. After the drying test was finished, the final product was decreased as HTT temperature was increased. The higher treatment temperature means more severe condition was applied; thus, the sample was decomposed or disintegrated leading to lower mass recovery after the drying. Furthermore, the evaporated moisture during the drying test indicates that the lower amount of moisture was left (after dewatering) and need to be removed by drying. In other words, the low amount of evaporated moisture showed the better dewatering performance.

Table 2-3 Mass balance in the solid fuel production process

condition	Hydrothermal treatment (%)				Dewatering (%)		Drying (%)	
(˚C, 30 min)	Sludge input	Steam input	Treated product	Condensate blow-off gas	Dewatered product	Dewatered liq.	Dried product	Evap. moisture
Raw	100	0	100	0	88.6	11.4	24.0	64.6
180	100	100	159.1	41.4	68.9	90.2	23.9	45.0
200	100	100	151.4	48.7	58.5	92.9	22.7	35.8
220	100	100	146.2	53.5	53.9	92.3	21.9	32.0
240	100	100	143.1	57.0	44.1	99.0	20.1	24.0

Figure 2-13 illustrates the mass distribution for each treatment condition. As mentioned above, the sludge input has been taken to be the datum (100%). The treated product was decreased whereas the condensate and blow-off gas were increased when the paper sludge was subjected to a higher temperature condition. Comparing between the treated product column and the dewatered product column, there were the significant reduction due to the moisture has been squeezed out. As a result, the dewatered liquid has large amount as seen in the dewatered liquid column. When increasing the

temperature, the group of dewatered product showed the decreasing trend while it was slightly increased in the dewatered liquid's group. In the last two column, they are the mass balance during the drying experiment. The dried recovered mass was reduced due to higher severity of the treatment.

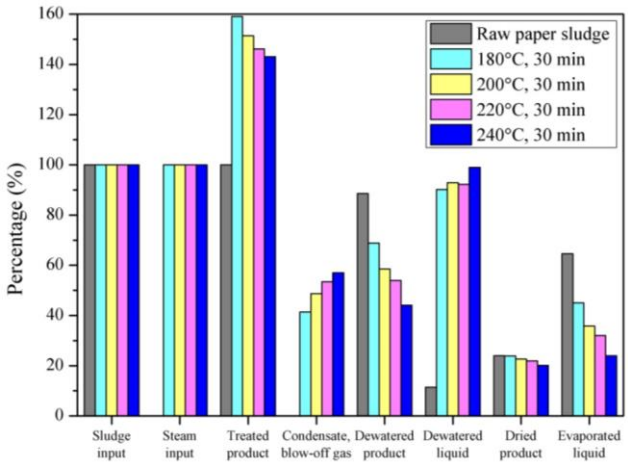

Figure 2-13 Mass distribution for the solid fuel production process

Figure 2-13 and 2-14 show pilot-scale mass balance of the 15 and 30 min HTT. The sludge input was fixed at approximately 350 kg. The steam consumption of the 15 and 30 min holding time HTT was 136 and 138 kg, respectively. The value was not significantly different which implied that the longer holding time has less effect on the steam consumption since 2 kg more steam was used when increasing the holding time. As using the raw material as the datum (100%), the mass of steam consumption was 38.8% and 39.3% in case of 15 and 30 min holding time, respectively. It should be noted that the condensate was calculated by the difference and it was approximately 37.0% in both cases. The total product from HTT was the accumulation of HTT-PS and the treated liquid part is called wastewater. It was 352.6 kg which was 100.7% of the raw input. Although HTT-PS and the treated liquid part are the total product from the reactor, they were separated into two categories in order to differentiate their characteristic and utilization. From the pilot-experiment, the treated liquid part or wastewater from the reactor was increased from 25.6% to 29.9% when increasing the holding time; thus, when the longer holding period of HTT was used, the more treated liquid part from the reactor would be obtained. The treated products from the 15 and 30 min holding time condition were 75.4% and 73.0% which have no significant difference.

HTT-PS was subjected to the dewatering test by the centrifugal decanter, then the dewatered liquid, which was also the wastewater, was taken out. The dewatered product was 32.0% and 31.3% in the case of the 15 and 30 min treatment time. It was decreased when the holding time was longer. The shorter holding time yielded higher amount of HTT-PS and the dewatered product after the dewatering test; however, the difference was not so obvious. Additionally, the dewatered liquid was 43.4% and

decreased to 41.7% when increasing the holding period. After 24 h natural drying, 20.4 kg and 22.5 kg of the moisture were evaporated and the naturally dried products were 91.9 kg and 87.3 kg for HTT with 15 and 30 min holding times. The evaporated moisture during the natural drying was 5.8% and 6.4%, respectively. Finally, the dry base HTT-PS can be recovered as 43.3 kg or 12.4% and 42.0 kg or 12.0% for the 15 and 30 min treatment time, respectively. The recovered mass will be further utilized as solid fuel. Raw-PS has the solid content of 23.6% which means that after alternative solid fuel production process, the mass recovery rate was approximately 50.0%.

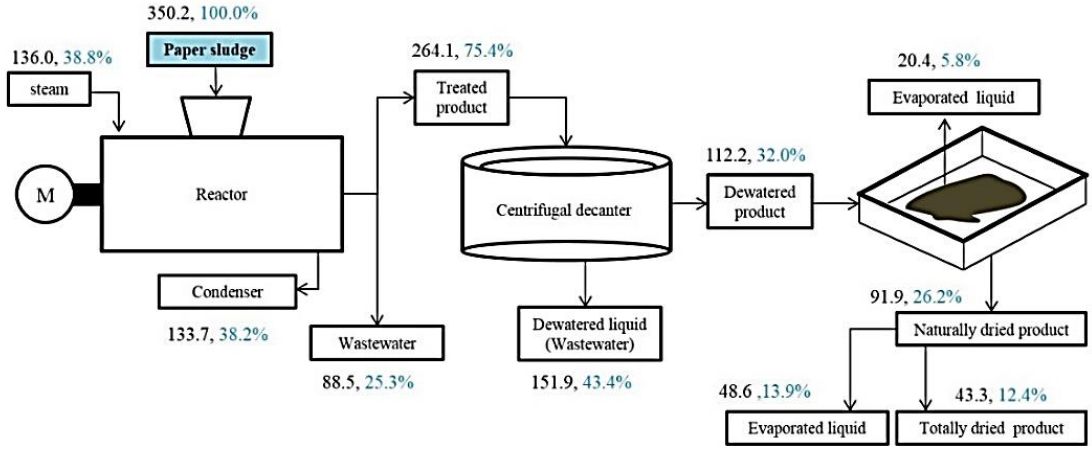

Figure 2-14 Mass balance for the pilot-scale hydrothermal treatment with 15 min holding time (unit: kg)

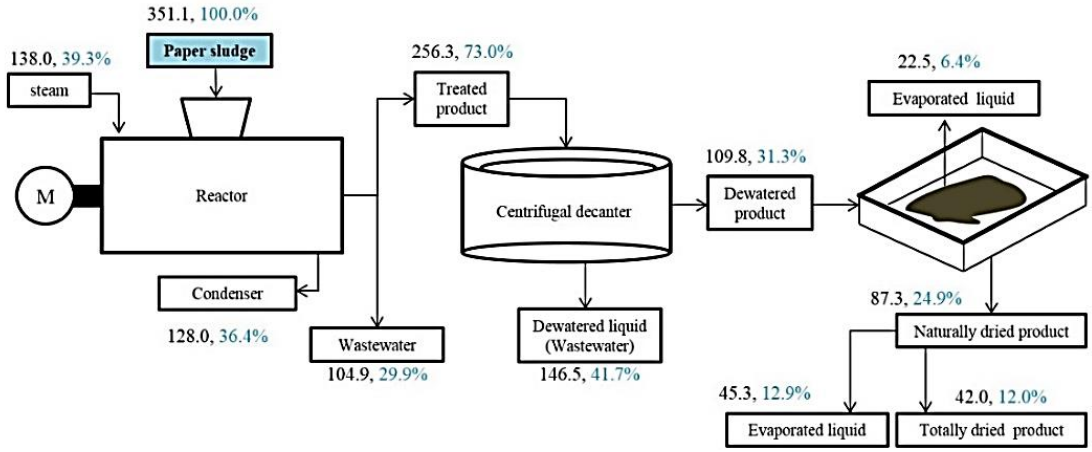

Figure 2-15 Mass balance for the pilot-scale hydrothermal treatment with 30 min holding time (unit: kg)

2.3.5 Estimated energy consumption and energy recovery

The energy used to heat up all of the water and the solid content in the paper sludge to the target temperature was defined as the energy input. The recovered energy from the final product was the multiplication of the higher heating value of HTT-PS and its dried mass. The calculation result of the lab-scale is presented in Table 2-4 as the percentage of the total energy input (100% as the datum).

As shown in Table 2-4, there was no significant difference between the energy output compared for all of the treatment temperatures; however, the 200 ˚C result showed the highest energy output as well as the energy output/input ratio. Taking 79.6% of the total energy input, the 240˚C HTT demonstrated the best dewatering and drying performances. Despite of that, the energy required for HTT was the highest leading to the lowest energy output/input ratio. The lowest required energy for the main energy consumption process was obtained under the 180˚C treatment condition while the required energy for dewatering and drying was the highest. This implied that the larger moisture content was left after the dewatering process, which means low dewaterability compared to other conditions. Although, the energy used for HTT was the lowest, the energy output/input ratio was not optimized. The 200 ˚C HTT has the best energy output/input ratio, which was 4% higher than the total energy input. Its energy used in HTT was 72.3% of the total energy input and the required energy for the dewatering and drying tests was 27.7% of the total energy input.

Table 2-4 Estimated energy produced and utilized

Condition (˚C,30 min)	Energy output (%)	Energy Input (%)		Energy Output/Input Ratio
		Hydrothermal treatment	Dewatering and drying	
180	102.0	67.3	32.7	1.02
200	104.0	72.3	27.7	1.04
220	103.0	74.6	25.4	1.03
240	101.0	79.6	20.4	1.01

2.3.6 Energy balance from the pilot-scale demonstration plant

The energy balance of the alternative solid fuel production from paper sludge presented in Figure 2-16 utilized the dried base mass of Raw-PS as the datum (100%). At the boiler, the energy from LPG was 23.8% and 24.1% in the case of HTT with 15 and 30 min holding times. The energy from the steam and the recovered energy from HTT-PS was 21.2% and 50.5% for 15 min HTT and 21.4% and 53.1% for 30 min HTT, respectively. It was clearly observed that the recovered energy was higher than the required energy from LPG, approximately 50.0% in both cases. It means that the pilot plant can be sustained by the energy from HTT-PS. Moreover, the electrical consumption by the stirrer, boiler utilities, and centrifugal decanter was very low as 0.6%, 0.1%, and 1.2% for the 15 min holding time and 0.9%, 0.2%, and 1.2% for the 30 min holding time. The heat loss from the reactor was 1.7% for the 15 min holding time and approximately doubled to 3.6% when increasing the holding time.

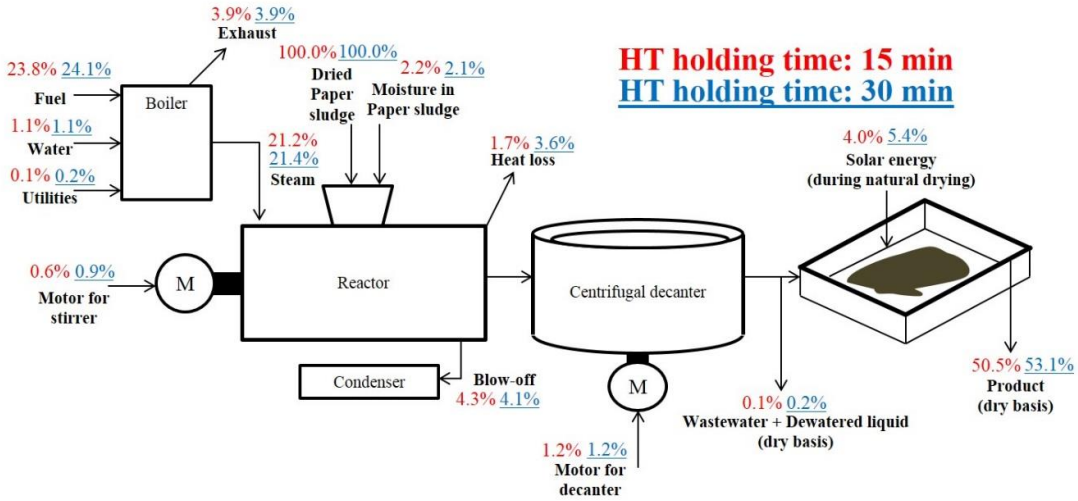

Figure 2-16 Total energy balance (in thermal basis) of the alternative solid fuel production from paper sludge

The energy used in the natural drying experiment was significantly high compared to the electrical energy consumption of the centrifugal decanter. The energy contained in blow-off gas (steam flushing to release the pressure in the reactor) was approximately 4.0% in both conditions. By varying the holding period, the energy balance were not significantly different in view of the energy consumption. On the other hand, it can be suggested that the steam consumption depends on the steam injection phase but not on the holding phase. The energy consumption in the system was dependent on the type of the raw material and the HTT condition. Higher moisture content leads to higher energy consumption. Since the product's fuel properties were better in the case of 30 min HTT and the steam consumption was not significantly different, the 30 min holding period hydrothermal treatment could be the appropriate condition regardless of small difference on time consumption.

2.3.7 Mechanism of HTT effect on paper sludge

2.3.7.1 Van Krevelen diagram

Table 2-2 shows the decrease of H/C and O/C atomic ratios, which can be visualized by Van Krevenlen diagram shown in Figure 2-17. The carbonization process of the paper sludge after HTT was presented along with the atomic ratio of coal: anthracite, bituminous, subbituminous, and lignite. The atomic ratio moving from upper right to lower left illustrates the advancement of the carbonization process. It was clearly observed that the dehydration and decarboxylation reactions played important roles in the carbonization process of paper sludge. When increasing the HTT temperature, the degree of carbonization was intensified. The 240 ˚C HTT-PS was nearly approached the region of lignite, which was considered as a low rank coal. Although the atomic ratios of the pilot-scale samples were different, the carbonization process had the same characteristic with the lab-scale result.

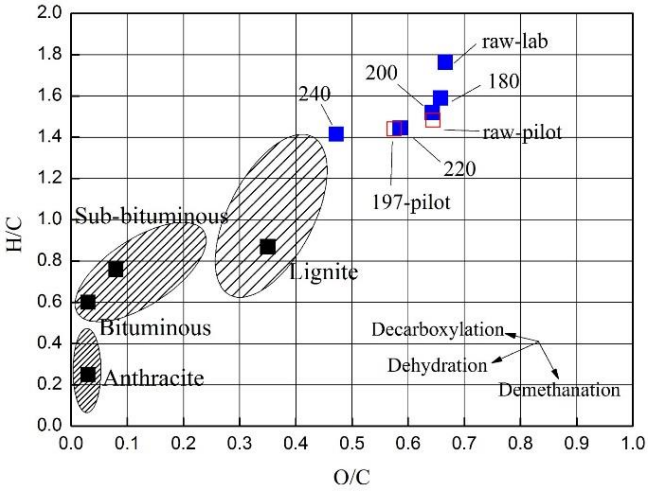

Figure 2-17 Van Krevelen diagram of raw and treated paper sludge compared with coals

2.3.7.2 Fourier transformed infrared spectroscopy (FTIR) analysis

Figure 2-18 shows FTIR spectra of Raw-PS and HTT-PS as the variation of the HTT temperature. It should be noted that the peak around 2300 to 2400 cm^{-1} was attributed to uncontrollable CO_2 in the measurement environment. The characteristic of the peak could be explained as follows:

1. The two weak bands at 3697 and 3620 cm^{-1} implied the kaolinite were common additional substance for improving paper quality [13-15]. With the increase of the HTT temperature, those two peaks had no remarkable difference.

2. The broad band between 3600 and 3200 cm^{-1} was attributed to the characteristic band of cellulose that was the composition in the paper sludge. Particularly, the rounded tip band appeared in this region was a vibration of hydroxyl functional group, −OH stretching. Moreover, HTT seemed to have no effect on the −OH band in cellulose since the reduction of peak intensity was not observed. However, compared to the cellulose [16,17], it was clearly shown that the peak of the paper sludge became less intense. The former might be ascribed to the source of paper sludge, which is derived from woody material that had already subjected to the pretreatment process by either thermo-mechanical or thermo-chemical processes, commonly known as the pulping process [18,19].

3. The band around 2800 to 3000 cm^{-1} was observed and it was assigned to a vibration of aliphatic $-CH_x$ stretching and there were two peaks at 2922 and 2852 cm^{-1}. They could be attributed to a vibration of asymmetric C−H stretching in cellulose [20].

4. In this region, there were two identical peaks at 1645 and 1430 cm^{-1} and one tiny band at 1540 cm^{-1}. The peak at 1645 cm^{-1} was originated by C=N stretching vibration of amides [20]. The absorption

peak of the paper sludge after HTT became weak as it was rounded especially when treated with the high temperature. Thus, it could be suggested that amides were hydrolyzed through the hydrolysis reaction during HTT. The band around 1430 cm^{-1} were attributed to $-CH_x$ aliphatic compound such as $-CH_2$ and $-CH_3$ [17]. For the treated paper sludge, the intensified band around 1430 cm^{-1} implied that the aliphatic compounds or non-aromatic compounds were obtained after HTT treatment. Finally, the tiny band around 1540 cm^{-1} was assigned to C=O asymmetric stretching in carboxylic group [21,22]. It was eliminated in case of the hydrothermally treated paper sludge indicating an occurrence of decarboxylation reaction.

5. The peaks, 1160, 1112, and 1030 cm^{-1}, were appeared in the paper sludge and they became more intense in case of HTT paper sludge. It could be attributed to C−O−C asymmetric stretching in aliphatic ether or C−O−C stretching in ether because of the dehydration reaction of alcohol. When the treatment temperature was higher than 200 ˚C, the peaks had no obvious difference. Additionally, the peak at 1030 cm^{-1} might be attributed to Si−O stretching vibration indicating the presence of SiO_2 in the sludge [22,23].

6. In the last region, the small peak at 875 cm^{-1} might be devoted to $CaCO_3$ as another additional substance originated from the paper production process [17].

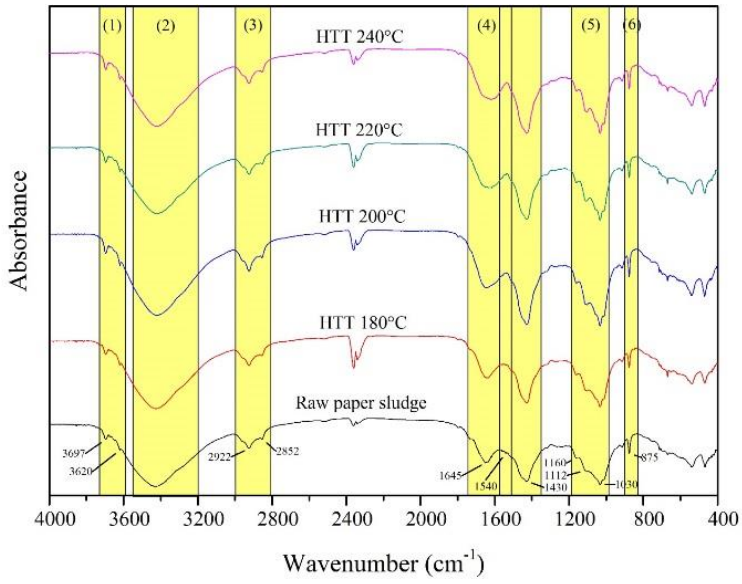

Figure 2-18 FTIR spectra of raw and hydrothermally treated paper sludge obtained from the lab-scale experiment

2.4 Conclusion

In this chapter, we investigated the alternative solid fuel production from paper sludge employing the hydrothermal treatment (HTT) in the lab-scale facility for implementation of the pilot-scale plant has been done. The paper sludge was subjected to HTT under subcritical hydrothermal conditions. In the lab-scale experiment, the temperature conditions were 180, 200, 220, and 240 ˚C at the pressure around 1.8–2.4 MPa, while it was 197 ˚C at 1.9 MPa in the pilot plant as the optimum condition. The holding time was 30 minutes in the lab-scale and 15 and 30 minutes in the pilot-scale experiment. The summary of the main findings can be made as follows:

1. HTT-PS became darker, slurry-like with less bad odor. The moisture content in the product was initially higher. The appearance of the products became more liquid-like when increasing the treatment temperature.

2. The dewatering performance of HTT-PS was significantly improved, at least five times better than Raw-PS. This finding was similar in both the lab-scale and the pilot-scale tests. Moreover, the drying performance of HTT-PS was also improved compared to Raw-PS.

3. The fuel property of HTT-PS was comparable or even higher compared to Raw-PS. The higher heating value of HTT-PS was slightly increased.

4. From the pilot-scale mass balance, the amount of steam used in HTT was approximately 40% of Raw-PS mass input and it has no significant difference between the 15 and 30 min HTT condition. The amount of HTT-PS after the dewatering test was approximately one-third and the treated liquid part was approximately 40.0% of the Raw-PS input. Thus, the mass balance showed some benefits in view of bulk volume reduction.

5. In the viewpoint of the energy consumption, high HTT temperature condition enhanced required energy that could not appropriate for industrial process. The 200 ˚C HTT showed the satisfied improvement of the fuel property, dewatering and drying performances, and mass recovery after the whole treatment process. Therefore, the optimized condition of the paper sludge from the laboratory-scale experiment was 200 ˚C HTT condition.

6. From the pilot-scale energy balance, the main energy consumption process was the steam injection phase during HTT while the electrical energy consumption was very small. The energy recovered in the dry HTT-PS was approximately 50.0% more than the energy consumption of the boiler. This indicates the possibility to produce the alternative solid fuel from paper sludge by employing the hydrothermal treatment.

Based on the summary of the results listed above, it can be concluded that HTT was not only able to produce the alternative solid fuel from paper sludge but also feasible for commercialization.

References

[1] Xu C, Lancaster J. Conversion of secondary pulp/paper sludge powder to liquid oil products for energy recovery by direct liquefaction in hot-compressed water. Water Res. 2008;42:1571-82.

[2] Hamzeh Y, Ashori A, Mirzaei B. Effects of Waste Paper Sludge on the Physico-Mechanical Properties of High Density Polyethylene/Wood Flour Composites. J Polym Environ. 2010;19:120-4.

[3] Namioka T, Morohashi Y, Yamane R, Yoshikawa K. Hydrothermal treatment of dewatered sewage sludge cake for solid fuel production. J Environ Eng. 2009;4:68-77.

[4] Prawisudha P, Namioka T, Yoshikawa K. Coal alternative fuel production from municipal solid wastes employing hydrothermal treatment. Appl Energy. 2012;90:298-304.

[5] Marche T, Schnitzer M, Dinel H, Paré T, Champagne P, Schulten HR, et al. Chemical changes during composting of a paper mill sludge–hardwood sawdust mixture. Geoderma. 2003;116:345-56.

[6] Park S-W, Jang C-H, Baek K-R, Yang J-K. Torrefaction and low-temperature carbonization of woody biomass: Evaluation of fuel characteristics of the products. Energy. 2012;45:676-85.

[7] van der Stelt MJC, Gerhauser H, Kiel JHA, Ptasinski KJ. Biomass upgrading by torrefaction for the production of biofuels: A review. Biomass Bioenergy. 2011.

[8] Namioka T, Morohashi Y, Yoshikawa K. Mechanisms of malodor reduction in dewatered sewage sludge by means of the hydrothermal torrefaction. J Environ Eng. 2011;6:119-30.

[9] Zhao W, Li Z, Zhao G, Zhang F, Zhu Q. Effect of air preheating and fuel moisture on combustion characteristics of corn straw in a fixed bed. Energ Convers Manage. 2008;49:3560-5.

[10] Ohm TI, Chae JS, Kim JE, Kim HK, Moon SH. A study on the dewatering of industrial waste sludge by fry-drying technology. J Hazard Mater. 2009;168:445-50.

[11] Torii N, Okai A, Shibuki K, Aida TM, Watanabe M, Ishihara M, et al. Production of d-glucose from pseudo paper sludge with hydrothermal treatment. Biomass Bioenerg. 2010;34:844-50.

[12] Lu L, Namioka T, Yoshikawa K. Effects of hydrothermal treatment on characteristics and combustion behaviors of municipal solid wastes. Appl Energy. 2011;88:3659-64.

[13] Bundy WM, Ishley JN. Kaolin in paper filling and coating. Appl Clay Sci. 1991;5:397-420.

[14] Prasad MS, Reid KJ, Murray HH. Kaolin: processing, properties and applications. Appl Clay Sci. 1991;6:87-119.

[15] Mgbemena CO, Ibekwe NO, Sukumar R, Menon ARR. Characterization of kaolin intercalates of oleochemicals derived from rubber seed (Hevea brasiliensis) and tea seed (Camelia sinensis) oils. J King Saud Univ Sci. 2013;25:149-55.

[16] Yang H, Yan R, Chen H, Lee DH, Zheng C. Characteristics of hemicellulose, cellulose and lignin pyrolysis. Fuel. 2007;86:1781-8.

[17] Méndez A, Fidalgo JM, Guerrero F, Gascó G. Characterization and pyrolysis behaviour of different paper mill waste materials. J Anal Appl Pyrol. 2009;86:66-73.

[18] Harinath E, Biegler LT, Dumont GA. Predictive optimal control for thermo-mechanical pulping processes with multi-stage low consistency refining. J Process Control. 2013;23:1001-11.

[19] Feria MJ, Garcia JC, Diaz MJ, Fernandez M, Lopez F. Biorefinery process for production of paper and oligomers from Leucaena leucocephala K360 with or without prior autohydrolysis. Bioresour Technol. 2012;126:64-70.

[20] Lin Y, Wang D, Wang T. Ethanol production from pulp & paper sludge and monosodium glutamate waste liquor by simultaneous saccharification and fermentation in batch condition. Chem Eng J. 2012;191:31-7.

[21] Li M, Li W, Liu S. Hydrothermal synthesis, characterization, and KOH activation of carbon spheres from glucose. Carbohydr Res. 2011;346:999-1004.

[22] He C, Giannis A, Wang J-Y. Conversion of sewage sludge to clean solid fuel using hydrothermal carbonization: Hydrochar fuel characteristics and combustion behavior. Appl Energy. 2013;111:257-66.

[23] Yuan J-H, Xu R-K, Zhang H. The forms of alkalis in the biochar produced from crop residues at different temperatures. Bioresour Technol. 2011;102:3488-97.

Chapter 3

Combustion characteristics and kinetics study of hydrothermally treated paper sludge by thermogravimetric analysis

Abstract: In this chapter, an investigation on combustion characteristics of the hydrothermally treated paper sludge was performed as a fundamental combustion study. As shown in Chapter 2, the paper sludge was treated at the temperature range of 180–240 °C under pressurized conditions with a holding time of 30 minutes by a lab-scale apparatus. The optimized temperature (197 °C at 1.9 MPa) was used to treat the paper sludge in a pilot plant with the same holding time. The combustion behavior of the products and the reference materials, including cellulose, hemicellulose, and lignin, were studied by the thermogravimetric analysis. The major decomposition of paper sludge was devoted to cellulose. The ignition temperature was originally low around 257–271 °C. The burnout temperature was approximately 501–523 °C. From the two-stage kinetics study, it was revealed that the activation energy of the treated paper sludge was lower than the original material indicating a higher reactivity and they were in the range of 113–147 kJ/mol.

3.1 Background

In Chapter 2, the hydrothermal treatment (HTT) was successfully used to produce solid fuel from paper sludge and showed its feasibility. Next, to realize the goal of this research, the fundamental combustion of the hydrothermally treated paper sludge (HTT-PS) has to be performed in comparison with the raw paper sludge (Raw-PS). The objective of this chapter is to understand the effect of HTT on paper sludge combustion fundamentally. Therefore, the comparative study on combustion characteristics of Raw-PS and HTT-PS was performed by the thermogravimetric analysis (TGA) and kinetics study.

An investigation of biomass/waste combustion has been extensively done by using TGA [1-4]. For instance, Yanfen and Xiaoqian investigated co-combustion of coal and paper mill sludge by using TGA and found that the experiments could help explaining and predicting the behavior of coal and paper sludge mixture in practical application [1]. Furthermore, Lu et al. studied the combustion behavior of the hydrothermally treated municipal solid waste (MSW) and found that the combustion characteristics of the Japanese and Chinese MSW were controlled by main constituents of rice and cellulose, respectively [2]. Moreover, characteristic parameters, such as the ignition and the burnout temperature, are essential for a handling process and co-firing application. According to Xu et al., the ignition temperature is a critical parameter concerning fire hazard and self-explosion during the utilization process of biochar [3]. A solid fuel that has a lower burnout temperature implies better burnout performance since it needs less time and lower temperature to complete the combustion process [4]. These two important parameters can be predicted by using the TGA. The kinetics study on the original

biomass/waste have been also greatly investigated [5-7]; however, the effects of HTT on the kinetic parameters, i.e., the activation energy and the pre-exponential factor, have been rarely studied. Thus, the effect of HTT on combustion characteristics and the kinetic parameters of paper sludge has to be studied before further implementation of HTT-PS in co-combustion application.

3.2 Materials and methods

3.2.1 Raw and hydrothermally treated paper sludge

Raw paper sludge (Raw-PS) provided by the Siam Kraft Industry Co., Ltd., Thailand, was subjected to a subcritical hydrothermal treatment in both the lab-scale and the pilot-scale processes as described in Chapter 2. In the lab-scale, the raw paper sludge (Raw-PS-Lab) was treated by an electrically heated autoclave machine (MMJ-500, OM Lab-Tech Co., Ltd., Japan). The treatment temperature was 180, 200, 220, and 240 ˚C under the pressure in the range of 1.8–2.4 MPa with the holding time of 30 minutes. After HTT, the pressure was released and the product was thoroughly extracted from the reactor, mechanically dewatered, and convectively dried. In this study, the paper sludge that was hydrothermally treated at 180, 200, 220, and 240 ˚C were named as HTT-PS-180˚C, HTT-PS-200˚C, HTT-PS-220˚C, and HTT-PS-240˚C, respectively.

In the pilot-scale experiment, 1-m^3 cylindrical batch-type hydrothermal reactor was utilized to treat raw paper sludge (Raw-PS-Pilot) at the temperature of 197 ˚C and the pressure of 1.9 MPa with the holding time of 30 minutes. After the treatment was finished, the 197 ˚C hydrothermally treated paper sludge (HTT-PS-197˚C) was removed, centrifugally dewatered, and naturally dried. The proximate analysis, the ultimate analysis, and the higher heating value (HHV) of the samples were analyzed on a dry basis as shown in Table 3-1.

Table 3-1 Fuel analysis.

Sample (˚C)	Proximate analysis (%)			Ultimate analysis (%)					HHV
	FC	VM	Ash	C	H	N	S	O	(MJ/kg)
Raw-PS-Lab	3.7	62.2	34.1	33.4	4.3	2.2	0.4	25.6	13.6
HTT-PS-180	4.5	60.1	35.4	33.5	4.0	2.2	0.3	24.6	13.7
HTT-PS-200	5.3	57.7	37.0	34.6	4.0	1.9	0.3	22.2	14.4
HTT-PS-220	6.6	56.6	36.8	34.4	3.8	2.1	0.2	22.7	14.5
HTT-PS-240	7.9	56.4	35.7	34.6	3.6	2.1	0.2	23.8	14.7
Raw-PS-Pilot	4.7	61.9	33.4	31.7	3.8	2.7	0.4	28.0	13.2
HTT-PS-197	4.8	58.5	36.7	31.9	3.4	2.1	0.3	25.6	13.7

FC: fixed carbon; VM: volatile matter; C: carbon; H: hydrogen; N: nitrogen; S: sulfur; O: oxygen calculated by difference; HHV: higher heating value.

3.2.2 Thermogravimetric analysis

Thermogravimetric analysis (TGA) of Raw-PS and HTT-PS were performed by the simultaneous Shimadzu D50 TGA/DTA analyzer illustrated in Figure 3-1. The samples were dried in an electric oven at 105 ˚C for 12 h to minimize the effect of the inherent moisture before starting the experiment. Approximately 10 mg of sample was loaded into an Al_2O_3 ceramic crucible with the particle size less than 250 µm. Air was constantly supplied at 150 ml/min and the test was done under the atmospheric pressure. The sample was heated from the room temperature to 850 ˚C at the heating rate of 5 ˚C/min to minimize the heat transfer limitation. The sample weight loss was continuously recorded as the function of time and temperature.

Since the main compositions of the paper sludge are cellulose, hemicellulose, and lignin, the comparative study of the paper sludge and the lignocellulosic materials could be performed. A general lignocellulosic characterization of paper sludge can be found by several researchers [8-10]. For instance, based on the investigation from Yamashita et al., half of the composition in the paper sludge is carbohydrate which is the mixture of cellulose and hemicellulose while approximately 15% belongs to lignin [9]. To further investigate the combustion characteristics of paper sludge and the effect of HTT, the reference materials, i.e., standard cellulose, xylan as hemicellulose, and lignin were subjected to the TGA test at the same condition for the comparative study.

From the weight loss (TG) and the rate of weight loss (DTG) profiles, after the inherent moisture was removed, the temperature at which the weight loss started was defined as the volatile release temperature (T_v). The maximum weight loss temperatures (T_1, T_2, and T_3) were noted when the DTG curve shows multiple peaks. The temperature that the weight loss was stabilized was denoted as the burnout temperature (T_b) regardless of the combustion of calcium carbonate. The ignition temperature (T_i) was graphically determined based on the temperature at which the DTG curve showed its peak and the corresponding slope to the intersection with respect to the TG profile as well explained by Li et al. [11]. Preliminary tests were carried out to confirm suitable parameters and each experiment was done at least twice. Several repetitions were performed when some variability occurred.

Figure 3-1 Shimadzu D50 TGA/DTA analyzer

3.2.3 Kinetics study

3.2.3.1 Model-fitting

More information on the effect of HTT on the paper sludge combustion behavior can be obtained by studying the kinetic parameters, the apparent activation energy (E) and the pre-exponential factor (A), based on the non-isothermal thermogravimetric data. Since oxygen generates various phenomena, combustion process is very complex [12] such as gas-phase reactions of volatiles released at low temperatures and oxygen and char combustion [13]. The kinetics in two separate reactions: A (solid) → B (char) + C1 (gas); B (char) → C2 (gas) + D (ash). Thus, the thermal decomposition of Raw-PS and HTT-PS during the combustion process can be described as

$$d\alpha/dt = k(T)f(\alpha) \quad (3\text{-}1)$$

where f(α) is a model of the reaction regarding the solid-state reaction [14,15]; α is the extent of the conversion or the decomposed fraction of the sample at time t which is expressed as

$$\alpha = (m_i - m_t)/(m_i - m_f) \quad (3\text{-}2)$$

where m_i is the initial mass of the sample, m_t is the mass of the sample at time t, and m_f is the final mass of the sample obtained from thermogravimetric data. The temperature dependent rate constant k(T) is generally expressed through the Arrhenius equation

$$k(T) = A\exp(-E/RT) \quad (3\text{-}3)$$

where A is the pre-exponential factor, E is the apparent activation energy, and R is the universal gas constant (8.314 J/mol·K). A mathematical term of the constant heating rate β is described as

$$\beta = dT/dt \quad (3\text{-}4)$$

Then, Equation 3-3 and 3-4 were substituted to Equation 3-1, rearranged in the general form, and integrated; which gives

$$g(\alpha) = \int_0^{\alpha} d\alpha/f(\alpha) = (A/\beta)\int_{T_0}^{T} \exp(-E/RT)\,dT = (AE/\beta R)p(x) \quad (3\text{-}5)$$

where g(α) is called as an integral of the reaction model.

Table 3-2 presents the reaction models applied in this study. The first-order chemical reaction model (O1) is the most frequently used for investigating the thermal degradation of biomass under both inert and oxidative conditions. In addition to the famous first-order reaction model, the second-order (O2) and the third-order reaction (O3) models were also utilized. If the heterogeneous solid-state reaction follows the reaction order model, the reaction rate is determined by the chemical reaction. For the

geometrical contraction model, when the reaction occurs rapidly on the surface of the particle, the reaction is controlled by the results of an interface reaction that progressed toward the center of the particle [16]. C1 and C2 are three-dimensional contraction models that consider the cylindrical and the spherical particle, respectively. For the diffusion models, the model where the concentration gradient is restricted to only one way mass transport is called as the one-dimensional diffusion model (D1) [17]. The two-dimensional model (D2) and the three-dimensional model (D3) are used for the cylindrical and the spherical diffusion mechanism, respectively. These two models are applied when all three mass transfer directions are important. The former is used when the diffusion occurs radially as the particle is assumed to be cylindrical while the latter is based on the spherical particle assumption [17]. The D4, Ginstilin-Brounshtein model, is another type of a three-dimensional diffusion model where the reaction starts on the spherical particle surface [18].

Table 3-2 The reaction models and the expression of integral of reaction models used in this study.

Reaction model	g(α)
Reaction-order model	
First-order reaction (O1)	$-\ln(1-\alpha)$
Second-order reaction (O2)	$[1/(1-\alpha)]-1$
Third-order reaction (O3)	$(1/2)[(1-\alpha)^{-2}-1]$
Geometrical contraction model	
Contracting cylinder (C1)	$1-(1-\alpha)^{1/2}$
Contracting sphere (C2)	$1-(1-\alpha)^{1/3}$
Diffusion model	
One-dimensional diffusion (D1)	$-\alpha^2$
Two-dimensional diffusion (D2)	$(1-\alpha)\ln(1-\alpha)+\alpha$
Three-dimensional diffusion (D3)	$[1-(1-\alpha)^{1/3}]^2$
Ginstlin-Brounshtein (D4)	$1-(2/3)\alpha-(1-\alpha)^{2/3}$

To calculate the kinetic parameters, the temperature integral term in Equation 3-5 was estimated by the Coats-Redfern approximation [19]:

$$p(x) \cong (\exp(-x))/x \tag{3-6}$$

Then substituting this to Equation 3-5, taking natural logarithms and rearranging; yields

$$\ln(g(\alpha)/T^2) = \ln(AR/\beta E)\,(1-2RT/E) - (E/RT) \tag{3-7}$$

Since $(RT/E) \ll 1$, the term $(1-2RT/E)$ was approximately equal to unity $(1-2RT/E \approx 1)$. Hence,

$$\ln(g(\alpha)/T^2) = \ln(AR/\beta E) - (E/R)(1/T) \tag{3-8}$$

Plotting $\ln(g(\alpha)/T^2)$ vs. $(1/T)$ will give a straight line whose slope equals to $-E/R$. Therefore, the E and A can be determined by the slope and the intercept, respectively.

3.2.3.2 Isoconversional method (model-free)

As the model-fitting method could produce uncertain values of the Arrhenius parameters [15] as its calculation based on a single heating rate assumption that might not be sufficient. Therefore, in this study, the isoconversion method was also applied to confirm reliability of the results calculated by the model-fitting method. The idea of the isoconversion method is based on the assumption that the reaction rate at constant extent of conversion is only a function of temperature and the determination of kinetic parameters is done without prior information of reaction mechanism in term of reaction model f(α) [20,21]. To perform kinetics calculation by isoconversional method, Vyazovkin et al. recommended that the non-isothermal experiments have to be done by at least three heating rates and it was suggested that the heating rate has to be low to diminish the deviation of the sample temperature from the furnace temperature [20]. Thus, in this study, the three heating rates, 5, 15, and 25 ˚C/min, were used.

The Kissinger-Akahira-Sunose method (KAS) was utilized in this study. The KAS method was representative of the isoconversional method which offers a significant improvement in the accuracy of the activation energy value [20]. The temperature integral term in Equation 3-5 can also be approximated by the Coats-Redfern approximation as in the model-fitting method. Then, by substituting Equation 3-6 to 3-5, taking natural logarithms, and rearranging; gives

$$\ln(\beta/T^2) = \ln(AR/Eg(\alpha)) - (E/R)(1/T) \quad (3\text{-}9)$$

At a constant conversion, plotting $\ln(\beta/T^2)$ vs.$(1/T)$ obtained from different heating rates yields a straight line whose slope provides E as a function of the conversion.

3.3 Results and discussion

3.3.1 Effect of HTT on combustion behavior

3.3.1.1 TG/DTG profiles of Raw-PS and HTT-PS

Figure 3-2 shows the TG/DTG profiles of lab-scale samples. The inherent moisture was observed in all of the samples because tiny particles seemed to absorb moisture easily. Regardless of the inherent moisture evaporation, the thermal decomposition of Raw-PS and HTT-PS were divided into three stages. At the first stage, from 100 to 200 ˚C, approximately 3% of weight loss was detected. It could be attributed to the decomposition of low stability organic compounds (LSOC) presented in the secondary sludge [22]. These findings were also observed in the TG/DTG profiles of the pilot-scale samples as shown in Figure 3-3.

As the weight was sharply decreased, it was determined as the second stage, 200–550 ˚C. It contributed to the major decomposition of both Raw-PS and HTT-PS. From the TG profiles in Figure 3-2, the weight loss during the second stage represented 87.4, 86.1, 86.3, 84.8, and 83.5% of the total

combustible part for Raw-PS-Lab, and HTT-PS-180˚C, HTT-PS-200˚C, HTT-PS-220˚C, and HTT-PS-240˚C, respectively. In the case of the pilot-scale samples, its second stage occupied 82.8% and 82.3% of the total combustible part for Raw-PS-Pilot and HTT-PS-197˚C, respectively. The rapid devolatization, where the first maximum peak of DTG profile was observed, was located between 200 and 350 ˚C and it was approximately accounted for 56% of the total combustible part. Moreover, it was found that the TG profiles of all samples were adjacent until 320 ˚C, then, the curve of HTT-PS started to diverge from that of the raw material. When increasing the HTT temperature, it was clearly shown that the divergence began faster as illustrated in the TG profile of HTT-PS-240˚C. This evidence indicated that the weight loss of HTT-PS began decelerating before that of Raw-PS since it has lower amount of the combustible part. Then, the second peak of the DTG profile was observed in case of Raw-PS. However, it was eliminated after HTT; this implied that some compositions had been removed during HTT. The determination of the substances that was attributed to the second peak would be described by comparing the DTG profiles of the paper sludge with the reference materials presented in the next subsection. For the third stage where the third peak in the DTG profiles was found, it was devoted to the decomposition of minerals, i.e., calcium carbonate [1,23,24]. After the sample was burnt out, it was observed that the incombustible part of HTT-PS was higher than that of Raw-PS.

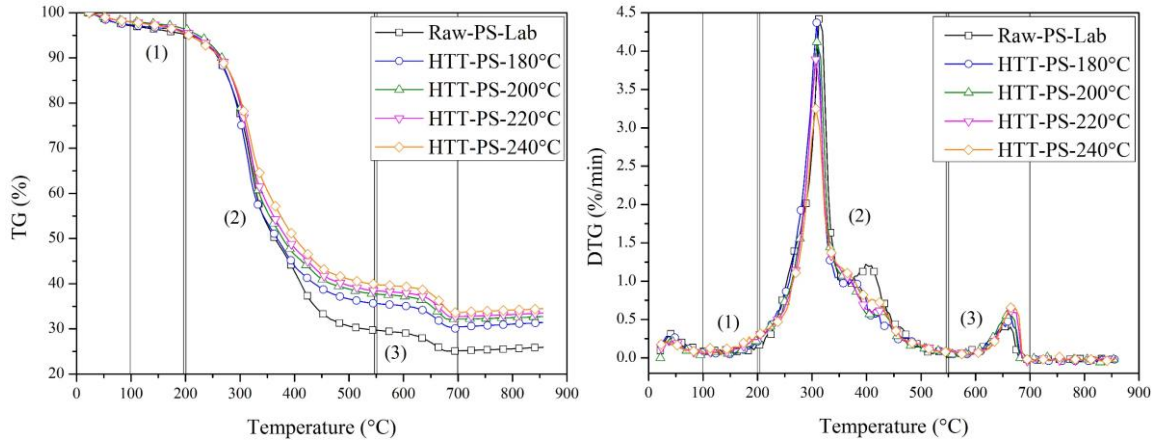

Figure 3-2 TG/DTG profiles of the lab-scale raw and hydrothermally treated paper sludge.

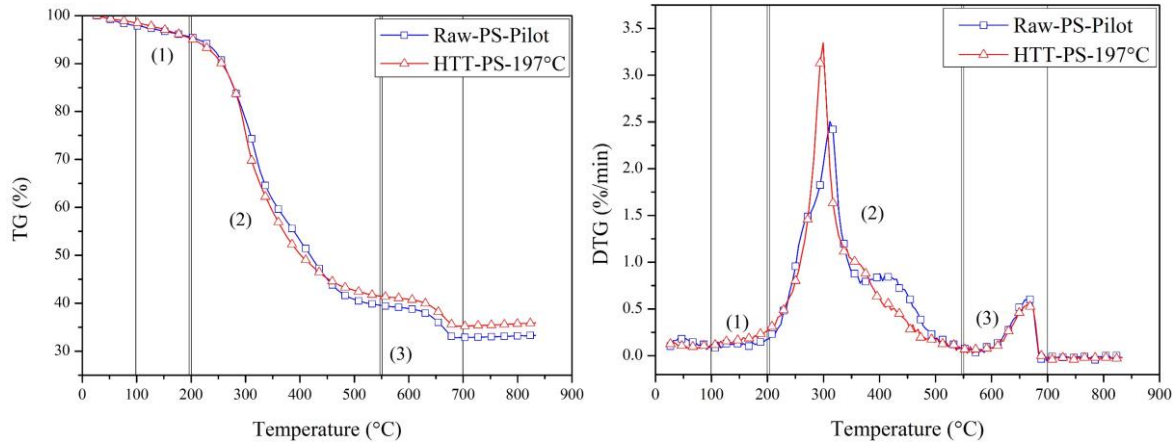

Figure 3-3 TG/DTG profiles of the pilot-scale raw and hydrothermally treated paper sludge.

3.3.1.2 TG/DTG profiles of Raw-PS and HTT-PS compared to reference materials

Figure 3-4 and 3-5 present the TG/DTG profiles of the reference materials. From the TG curve, cellulose rapidly decomposed from 277 to 342 ˚C, which was accounted to 79% of the original weight. The maximum weight loss rate obtained from the DTG profile was 19.1 %/min at 312.5 ˚C. Then, cellulose had a slower decomposition rate and a small second peak was observed in the DTG profile. At 527 ˚C, the weight loss was stabilized. The thermal degradation of hemicellulose started at 177 ˚C, which was earlier than cellulose due to its weaker structure. Hemicellulose is a polysaccharide and it consists of a random, amorphous structure, which is weak while the structure of cellulose is a long linear chain of polysaccharide without branches, which is very strong [25]. The weight loss of hemicellulose was greatly extended throughout the TG curve. The rapid weight loss was found in the range of 197 to 321 ˚C and the maximum DTG peak was observed at 271 ˚C with the weight loss rate of 3.8 %/min. The final decomposition of hemicellulose was at 805 ˚C. Lignin, which has a comparatively complex structure and aromatic rings, had wide devolatilization from 192 to 764˚C and its weight loss rate was very slow due to low reactivity characteristic [26]. However, above 764 ˚C, a large amount of lignin was decomposed and the maximum DTG peak was observed at 808 ˚C with the weight loss rate of 23.2 %/min. The results of the reference materials' combustion behaviors were in agreement with other researchers [25,26].

The TG/DTG profiles of Raw-PS and HTT-PS were compared to the profiles of reference materials as illustrated in Figures 3-4 and 3-5 for lab- and pilot-scale, respectively. It was clearly shown that hemicellulose began to decompose before the paper sludge. The maximum weight loss rate (DTG peak) of hemicellulose was located in the region that Raw-PS and HTT-PS started decomposition. For lignin, the TG/DTG profiles were also overlapped with the profiles of Raw-PS and HTT-PS. It has the slow decomposition at the beginning of the devolatilization. Thus, at the beginning, the decomposition of hemicellulose and lignin could be responsible for the weight loss of Raw-PS and HTT-PS.

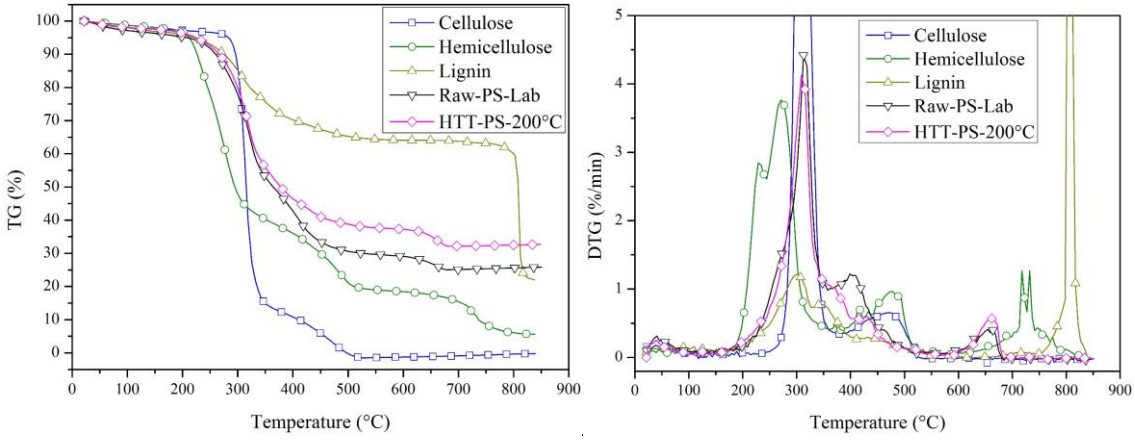

Figure 3-4 TG/DTG profiles of lab-scale raw and 200 ˚C hydrothermally treated paper sludge compared to reference materials, cellulose, xylan as hemicellulose, and lignin.

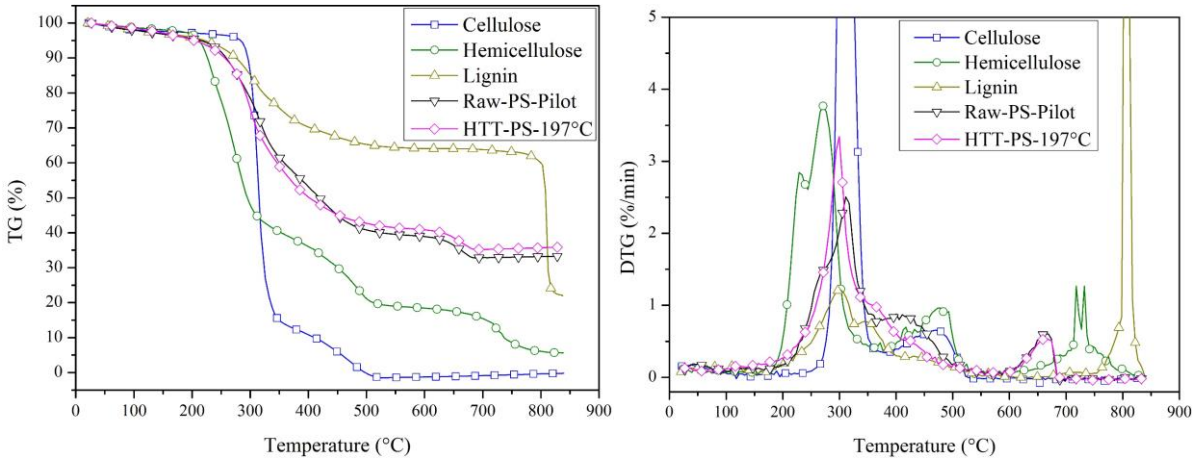

Figure 3-5 TG/DTG profiles of pilot-scale raw and 197 ˚C hydrothermally treated paper sludge compared to reference materials, cellulose, xylan as hemicellulose, and lignin (TG: weight loss and DTG: rate of weight loss).

During the rapid devolatilization process, the weight loss rate of both Raw-PS-Lab and HTT-PS-200˚C were sharply increased and the DTG profiles had the same characteristic with that of cellulose. Although the maximum weight loss rate of cellulose was significantly higher than that of the paper sludge, the corresponding temperatures at their peaks were located in the same region. Since the paper sludge is a byproduct of the pulping process, it contained some of discarded, processed cellulose and mingled with other minerals [27]. Therefore, the concentration of cellulose in the paper sludge was definitely less than the standard cellulose and this contributed to the lower peak. Lignin also showed a higher weight loss rate in this region; however, it was comparatively slow. In more detail, the DTG peak of Raw-PS-Pilot located near the hemicellulose's DTG profile. This implied that the pilot-scale samples contained more hemicellulose than those from the lab. Around 350 ˚C, the DTG curves of both Raw-PS-Lab and Raw-PS-Pilot diverged from cellulose and showed their second peaks. As there was an area that has no correlation between the second peaks of Raw-PS and the reference materials, it inferred that there were other non-lignocellulosic materials contaminated with the paper sludge. These non-fibrous contaminants might come from a fiber recovery process including the wastewater recycling process such as wood handling or chemical recovery system [27] or the wastewater treatment process. As the secondary (biological) sludge was mixed with the primary (pulp) sludge, it could be suggested that the non-fibrous material was the organic polymers or dead bacteria from the secondary sludge because these components had their thermal decomposition in this region (300–450 ˚C) [28,29]. Since the non-woody contaminants and some of hemicellulose were decomposed by HTT, HTT-PS-197˚C showed a higher DTG peak compared to Raw-PS-Pilot. The decomposition of hemicellulose was also found in the application of HTT as a pretreatment for organic fertilizer production from date palm [30]. On the other hand, it was found that the DTG maximum peak of HTT-PS-200˚C was lower than Raw-PS-Lab even though the fraction of non-woody contamination was destroyed. This might be attributed to the

effectiveness of the lab-scale experiment that was not only eliminated the non-woody parts but also decomposed some of cellulose in the paper sludge since the relatively small amount of samples were subjected to the treatment. The decomposition of cellulose that resulted in the lower maximum DTG peak was also observed from HTT-PS-240˚C due to the high temperature condition previously shown in Figure 3-2. By comparing with the reference materials, it could be said that cellulose dominated the major decomposition of Raw-PS and HTT-PS while hemicellulose and lignin controlled to some extent.

At a higher temperature, the decomposition of cellulose and hemicellulose and the major weight loss of lignin were observed; however, they had no relationship with the peaks of the paper sludge samples. In summary, the devolatilization of both paper sludge before and after HTT was firstly triggered by the combustion of hemicellulose and lignin while the majority of the weight loss was attributed to the decomposition of cellulose. Therefore, the lignocellulosic constituents played important roles in the combustion characteristics of the paper sludge.

3.3.1.3 Characteristic parameters in combustion

Table 3-3 presents the essential temperature parameters in the combustion process. It should be noted that these parameters are derived from the TGA test at one specific heating rate. The volatile release temperature (T_v) of Raw-PS-Lab was 199 ˚C while it was reduced to 190, 177, 170, and 154 ˚C for HTT-PS-180˚C, HTT-PS-200˚C, HTT-PS-220˚C, and HTT-PS-240˚C, respectively. For the pilot-scale sample, the T_v of Raw-PS-Pilot was 198 ˚C and it was decreased to 177 ˚C for HTT-PS-197˚C. During the operation, the reduction of T_v due to HTT might bother combustion system because the devolatilization could occur prior to the designed condition, particularly a feeding system that directly contact with solid fuel and located near a furnace.

The ignition temperature (T_i) is an essential parameter in a solid fuel burning system. It plays important role in the combustion process because of the influence on the flame stability, evolution of emission and pollutants, and the flame extinction; thus, T_i is substantially important for boiler designing and operation [31]. The ignition temperatures vary broadly in the literature and should be used only as estimation. It is dependent on many factors such as the heating rate, the partial pressure of oxygen, and the humidity. T_i of Raw-PS and HTT-PS are presented in Table 3-3. The original T_i of Raw-PS-Lab was 271 ˚C which is low when compared to coal whose T_i is considerably higher [32]. T_i of the lab-scale samples were slightly decreased to 270, 268, 267, and 262 ˚C in case of HTT-PS-180˚C, HTT-PS-200˚C, HTT-PS-220˚C, and HTT-PS-240˚C, respectively. For the pilot-scale sample, however, T_i was increased from 257 to 259 ˚C. This could be explained that the pilot-scale sample contained higher amount of hemicellulose, as mentioned in the previous subsection, that started burning at relatively lower temperature and it was degraded during HTT leading to the increase of T_i. When the carbonization process occurred during HTT, the O/C and the H/C atomic ratios were reduced and became like a low

rank coal such as lignite [33]. Thus, T_i could be higher and approached that of coal after HTT. However, T_i was not solely affected by the reduction of the atomic ratios. Other parameters also have influences. The physical characteristics, such as the fiber structure, the pore size, and the uniformity, affect T_i. This finding was also observed from the hydrothermal upgrading of brown coal by Sakaguchi et al. [34]. From the lab-scale samples, it was found that the characteristics of T_i were dominated by the physical structures. As T_i was relatively low, HTT-PS could help igniting the combustion process when co-fired with high-grade coal that has a lower reactivity, i.e., anthracite. However, the risk of flame hazard during storing, handling and conveying is enhanced because of higher reactivity of HTT-PS. The tendency to self-ignition is due to a large fraction of volatile matter, which is mainly the oxygen functional group. Additionally, the very fine particle of HTT-PS could initiate a dust explosion, rapid combustion of dust particles in the air, which could be followed by a disastrous secondary explosion by other nearby fuels.

The first peak of the DTG profile from Raw-PS-Lab was occurred at 312.6 (T_1). After HTT, T_1 was slightly shifted to lower temperature region as it was slightly decreased to 309, 309, 307, and 307 ˚C for HTT-PS-180˚C, HTT-PS-200˚C, HTT-PS-220˚C, and HTT-PS-240˚C, respectively. For the pilot-scale samples, T_1 was reduced from the original value of 311 to 299 ˚C for HTT-PS-197˚C. It means that HTT-PS needs shorter time to achieve the maximum decomposition rate. The rate of weight loss throughout the DTG profile of all samples exhibit their maximum values at the first peak. The DTG maximum value of Raw-PS-Lab was 4.4 %/min while it was decreased to 4.4, 4.1, 3.9, and 3.3 %/min in case of HTT-PS-180˚C, HTT-PS-200˚C, HTT-PS-220˚C and HTT-PS-240˚C, respectively. However, due to the low amount of fibrous materials and high contaminants in Raw-PS-Pilot, the weight loss rate was lower than HTT-PS-197˚C.

Table 3-3 Essential characteristic parameters.

Sample (˚C)	T_v (˚C)	T_i (˚C)	T_1(˚C)	DTG_1 (%/min)	T_2 (˚C)	DTG_2 (%/min)	T_3 (˚C)	DTG_3 (%/min)	T_b (˚C)
Raw-PS-Lab	199	271	313	4.4	399	1.2	654	0.4	518
HTT-PS-180	190	270	309	4.4	N/A	N/A	665	0.5	519
HTT-PS-200	177	268	309	4.1	N/A	N/A	666	0.6	501
HTT-PS-220	169	267	307	3.9	N/A	N/A	665	0.6	504
HTT-PS-240	154	262	307	3.3	N/A	N/A	670	0.7	514
Raw-PS-Pilot	198	257	311	2.5	400	0.9	664	0.60	522
HTT-PS-197	177	259	299	3.3	N/A	N/A	664	0.6	523

T_v: the volatile release temperature; T_i: the ignition temperature; T_1: the temperature at the first peak of maximum weight loss rate; DTG_1: the maximum weight loss rate at the first peak; T_2: the temperature at the second peak of the weight loss rate; DTG_2: the weight loss rate at the second peak; T_3: the temperature at the third peak of the weight loss rate; DTG_3: the weight loss rate at the third peak; T_b: the burnout temperature; N/A: no peak available.

For the second DTG peak, it was only found in Raw-PS. The temperature at the second peak (T_2) of Raw-PS-Lab and Raw-PS-Pilot was 399 and 400 ˚C, respectively. After HTT, these peaks were eliminated. After the stabilization of the second peak, the third peak of Raw-PS-Lab and Raw-PS-Pilot occurred at 654 and 664 ˚C, respectively. The temperatures at the third peak were slightly shifted to higher in both lab-scale and pilot-scale HTT-PS. It has already mentioned that the decomposition occurred at this stage was due to the other minerals, such as calcium carbonate whose peak can be observed in this region [35]. The burnout temperature (T_b) was noted regardless of the decomposition of calcium carbonate and other minerals.

3.3.2 Kinetics study

3.3.2.1 Effect of HTT on kinetic parameters

Generally, the reaction-order models and the diffusion mechanisms are utilized to investigate the combustion kinetics of biomass [17,33,36]. As mentioned earlier, the combustion behavior of the paper sludge exhibited three stages with different characteristics. In the kinetics study, the data contributed to the major weight loss, the second stage, was focused. In the second stage, it can be observed that the DTG profiles of Raw-PS showed two peaks whereas HTT-PS had a peak and shoulder; therefore, at least two independent reactions are necessary to evaluate the thermal decomposition of the samples. Then, Equation 3-8 was separately applied to each range where different reactions occurred. The extent of the conversion (α) was also recalculated as well. In this study, the commonly used reaction models in the combustion kinetics listed in Table 3-2 were tested. The models that gave the highest correlation coefficient could be the representative mechanism in each range. In addition, it should be noted that the thermal decomposition of the additional substances (third stage), such as calcium carbonate, was beyond the scope of this study. This is because the thermal decomposition of calcium carbonate is very sensitive to carbon dioxide that presents in this combustion environment leading to the difficulty in the investigation [23,37]. The inherent moisture evaporation and LSOC decomposition (first stage) were also negligible.

The evaluation temperature range presented in Table 3-4 was selected from the second stage DTG profile as illustrated in Figures 3-2 and 3-3. Range 1 was from the temperature that the weight loss rate was higher than 0.2 %/min to the end of the first peak of Raw-PS. At that point, Range 2 was started and it was terminated when the DTG value was lower than 0.2 %/min. Table 4 shows the models that yielded the highest r-squared value as the representative of the correlation coefficient which are the first-order reaction (O1), the second-order reaction (O2), and the three-dimensional diffusion (D3). The apparent activation energy (E), the pre-exponential factor (A), and the r-squared are also shown in Table 3-4. Moreover, the plotting results of those models that gave the highest correlation coefficient is presented in Figure 3-6. Since cellulose plays major role in Raw-PS and HTT-PS decomposition, it

should be noted that the E value of the standard cellulose could range in-between 110–198 kJ/mol depending on the thermal decomposition processes [38].

From Table 3-4, in the first range, both O1 and D3 models showed high r-squared value. Although the E value derived from O1 was lower than the value calculated from D3, both of them showed the decreasing trends due to the effect of HTT. For O1, the E value was reduced from the original value of 92 to 88, 77, 72, and 63 kJ/mol when increases the HTT temperature from 180–240˚C. It was also decreased from 78 to 65 kJ/mol for Raw-PS-Pilot and HTT-PS-197˚C, respectively. When using the D3 model, the E value was reduced from 173 to 168, 147, 138 and 122 kJ/mol for the lab-scale samples treated at the HTT temperature of 180, 200, 220 and 240 ˚C, respectively. For the E value of the pilot-scale samples, it was also decreased from the original value of 149 to 125 kJ/mol. The lower value of the activation energy implied that the sample became easier to engage in thermal decomposition. This could be articulated by the evidence on the significant reduction of volatile release temperature. When increasing the HTT temperature, the A value was decreased as can be observed in both the lab-scale and the pilot-scale results indicating the effect of HTT that reduced the frequency of molecule collision during the reaction; thus, the combustion intensity in this range could be dwindled.

For the second range, it was observed that the r-squared of O2 was the highest. Thus, O2 was the best representative mechanism in this range and the E and A values are also presented in Table 3-4. Figure 3-6 illustrates the E value in the second range that was higher than that of the first range and it was decreased from the original value of 178 to 156 kJ/mol for HTT-PS-180˚C. However, the E value increased to 184, 185, and 206 kJ/mol when treated at 200, 220, and 240 ˚C, respectively. Similarly, it increased from 156 to 194 kJ/mol in the case of the pilot-scale samples. The A value also showed the same trend with that of the E value. In the second range, it could be explained that at a low HTT temperature, the effect of HTT was just reducing volatile matter (VM) at the beginning resulting in the lower E value because of less amount of easy-to-be-ignited substances. However, at a higher HTT temperature, i.e. higher than 180˚C in this study, the pretreatment played a major role on char formation as the carbonization progress [39]. Thus, more energy is necessary to activate the reaction in this second range for char combustion [36]. Moreover, Figure 3-7 illustrates the E value of each range and the weighted average E value of each first range and the second range. It should be noted that the mathematical average of the activation energy in this study was calculated solely for illustrating the effect of HTT on the activation energy; thus, those values are not fundamental thermodynamics constant. This practice has previously performed for the purpose of ranking the activities of coals by Cumming [40]. The weighted average activation energy of HTT-PS in both lab-scale and pilot-scale was lower than the raw materials and it was reduced when increasing the HTT temperature. This implied that the first range played more important role since the decomposition was comparatively higher and the energy used to initiate the combustion process was reduced because of HTT.

Table 3-4 Kinetic parameters calculated by the first- and second-order reaction models and the three-dimensional diffusion model.

Sample (˚C)	Range 1 (R1)				Range 2 (R2)			
	T(˚C)	E (kJ/mol)	A (min^{-1})	R^2	T (˚C)	E (kJ/mol)	A (min^{-1})	R^2
first-order reaction (O1)								
Raw-PS-Lab	212-358	92	1.1E+09	0.9967	-	-	-	-
HTT-PS-180	198-351	88	7.3E+08	0.9931	-	-	-	-
HTT-PS-200	192-373	77	4.1E+07	0.9944	-	-	-	-
HTT-PS-220	185-374	72	1.4E+07	0.9917	-	-	-	-
HTT-PS-240	176-378	63	1.7E+06	0.9876	-	-	-	-
Raw-PS-Pilot	204-363	78	7.2E+07	0.9966	-	-	-	-
HTT-PS-197	175-381	65	3.0E+06	0.9944	-	-	-	-
second-order reaction (O2)								
Raw-PS-Lab	-	-	-	-	358-485	178	5.9E+14	0.9987
HTT-PS-180	-	-	-	-	351-485	156	1.9E+13	0.9866
HTT-PS-200	-	-	-	-	373-475	184	1.5E+15	0.9853
HTT-PS-220	-	-	-	-	374-480	185	1.5E+15	0.9899
HTT-PS-240	-	-	-	-	378-480	206	6.2E+16	0.9935
Raw-PS-Pilot	-	-	-	-	363-495	156	6.8E+12	0.9958
HTT-PS-197	-	-	-	-	381-479	194	5.7E+15	0.9904
three-dimensional diffusion (D3)								
Raw-PS-Lab	212-358	173	2.3E+15	0.9979	-	-	-	-
HTT-PS-180	198-351	168	1.2E+15	0.9982	-	-	-	-
HTT-PS-200	192-373	147	7.4E+12	0.9959	-	-	-	-
HTT-PS-220	185-374	138	1.2E+12	0.9945	-	-	-	-
HTT-PS-240	176-378	122	3.4E+10	0.9928	-	-	-	-
Raw-PS-Pilot	204-363	149	1.7E+13	0.9909	-	-	-	-
HTT-PS-197	175-381	125	7.7E+10	0.9935	-	-	-	-

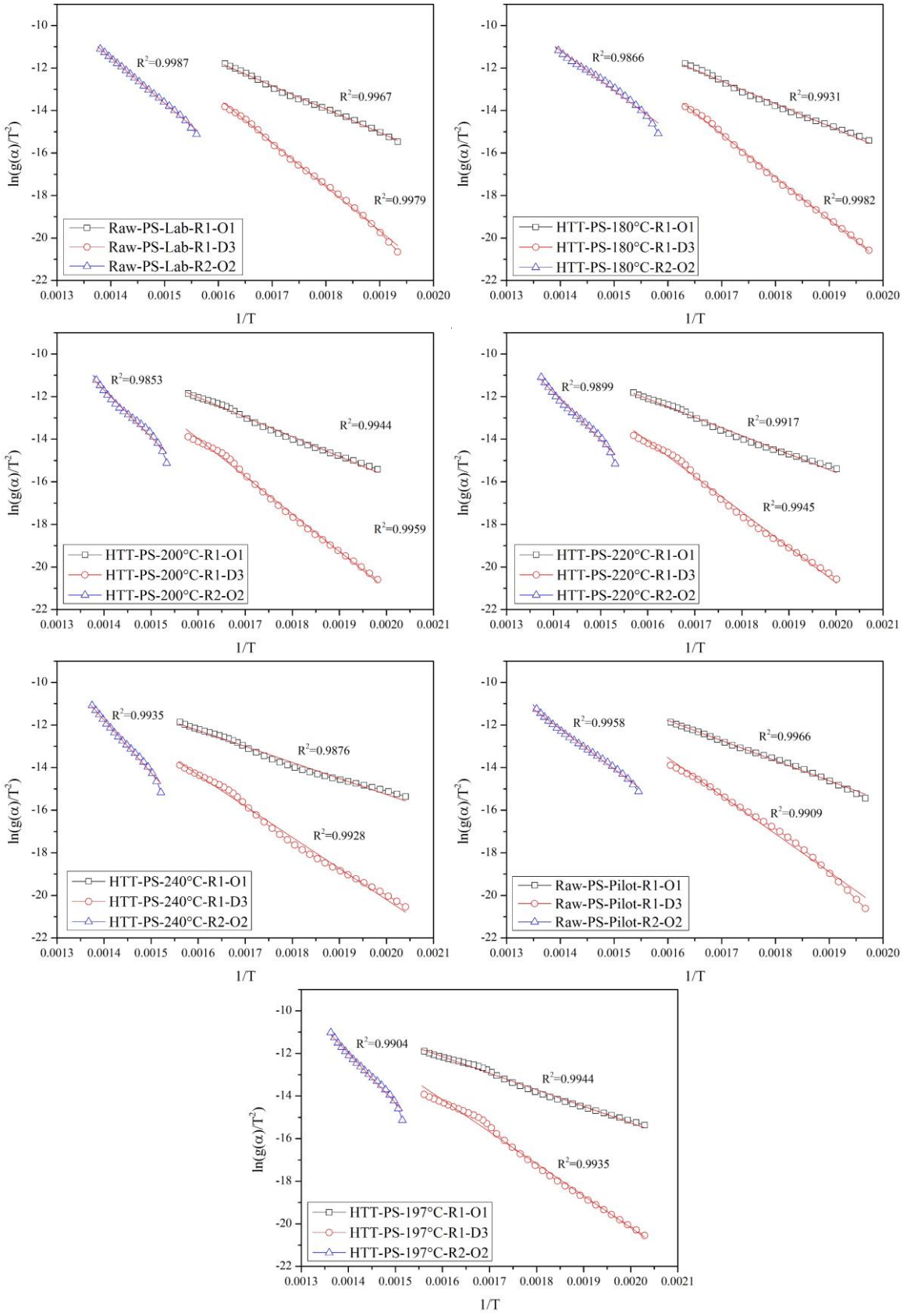

Figure 3-6 Plot of $\ln(g(\alpha)/T^2)$ against 1/T that yielded the highest r-squared values for all samples.

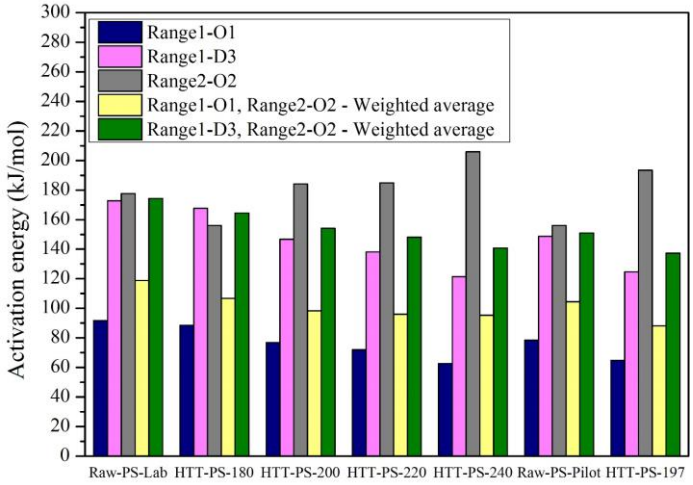

Figure 3-7 The activation energy of raw and hydrothermally treated paper sludge.

3.3.2.2 Activation energy calculated by the isoconversion method

Figure 3-8 shows the plots of the $\ln(\beta/T^2)$ against 1/T obtained at three different heating rates for Raw-PS and HTT-PS from both lab-scale and pilot-scale. Three different heating rate profiles were connected by a straight-line whose slope is used for the activation energy (E) calculation for each conversion. It should be noted that the conversion was chosen from 10% to 90% with appropriate intervals to assure reliability of the calculation [20]. In the isoconversional method, the E value is determined as a function of the conversion. Therefore, the value of E derived from those lines and its average as a function of the conversion have been calculated and plotted in Figure 3-9.

From Figure 3-9 (left), it could be observed that the profile of the E as a function of the conversion of HTT-PS was lower than that from Raw-PS in almost all of the conversion. This, therefore, leads to lower average E values of HTT-PS compared to Raw-PS from both lab-scale and pilot-scale samples as illustrated in Figure 3-9 (right). As mentioned above, the lower E value of HTT-PS implies that HTT-PS would use lower amount of energy to engage in the combustion compared to Raw-PS. In other words, the reactivity of paper sludge was higher after HTT. For example, it can be observed that the E value of HTT-PS was significantly lower than that of Raw-PS at 10–30% conversion. This implies that HTT-PS needs lower amount of energy to reach that conversion. This finding was in agreement with the result on characteristic temperatures (Table 3-3) discussed earlier as the volatile release temperature of HTT-PS was lower than the original value. More importantly, ones can be observed that the average E value from the KAS isoconversional method was similar to the weighted average E value from the model-fitting method (O1 and O2 for first and second range, respectively). The average E value of Raw-PS and HTT-PS from both methods (model fitting O1/O2 and isoconversional) was around 100–130 kJ/mol. Thus, it can be concluded that E value from model-fitting (O1/O2) and model-free or the isoconversional method are consistent and able to show the effect of HTT on the activation energy of paper sludge combustion.

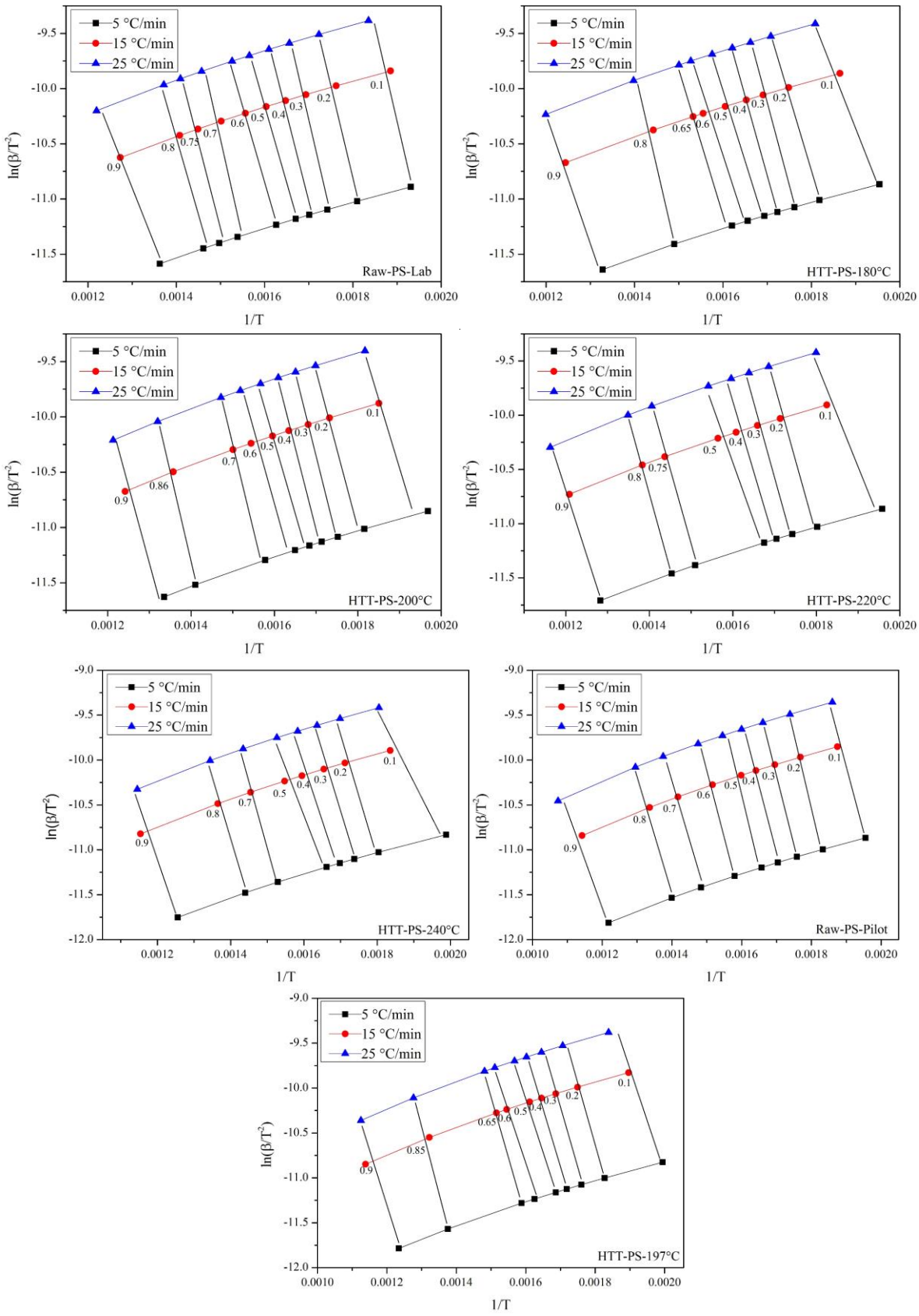

Figure 3-8 Plot of $\ln(\beta/T^2)$ against 1/T at three different heating rates.

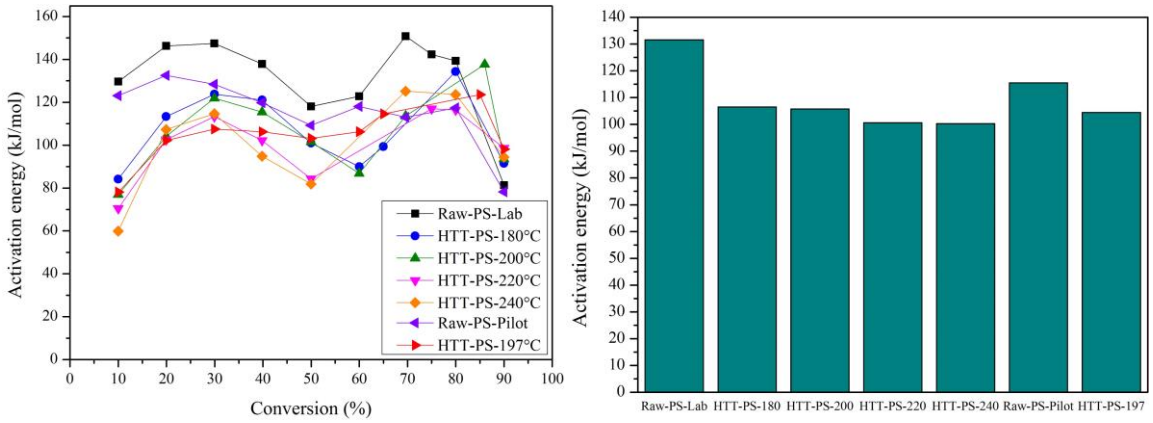

Figure 3-9 The activation energy of raw and hydrothermally treated paper sludge as a function of the conversion calculated from the KAS isoconversional method.

3.3.2.3 Combustion mechanism

From literatures, burning of char particle can generally be defined by three regimes [41-44]. In the regime I, it takes place at a low temperature or when burning small char particle where the combustion occurs throughout particle leading to the decrease in the density or the internal pore rather than the surface chemical reaction that reduces the diameter; therefore, the diffusion rate, the transport of gas molecules, is much faster than the chemical reaction rate [41]. Thus, the reaction rate is kinetics-controlled. When the external surface temperature of a char particle increases as the reaction between carbon and oxygen is so fast, the penetration of oxygen into the char particle becomes limited and zero in the center of the particle; thus, the reaction rate in this state, namely the regime II, is controlled by both the chemical reaction and the pore diffusion [43]. At a high temperature or burning large particle where the mass transfer is difficult, the reaction at the particle surface is very fast so that all of oxygen is consumed at the external surface and the particle shrinks at the constant density [42]. This is categorized as the regime III whose reaction rate is controlled by the mass transfer rate of oxygen molecules (the boundary-layer diffusion control) from the surroundings gas to the external surface of a particle [44].

From model-fitting kinetics analysis, the evaluation temperature was divided into two ranges; therefore, the mechanism based on the mathematical model utilized in the kinetics calculation would be responsible for each range. At the first range, since both of O1 and D3 exhibited high r-squared value (even though the weighted average E value of O1/O2 gave similar result with the isoconversional method) , those two models could be possible play roles in the combustion mechanism. This could be because of high VM characteristic of the paper sludge, the devolatilization could be very fast leading to the reduction in the density. At the same time, oxygen may be consumed as the combustion progressed by either the surface combustion or the secondary combustion of the volatilized substances far from the surface of the paper sludge particle and this could be said that the penetration of oxygen

might be limited inside the particle. Therefore, the first range should have a similar mechanism as the regime II in char combustion whose reaction rate is controlled by both the chemical reaction and the pore diffusion according to the literature mentioned earlier. As the devolatilization advanced and VM has been driven off in the second range, it would be a point that consumed oxygen immediately replaced by the stream of bulk gas from outside the boundary layer. Thus, the mass transfer rate would become very fast; as a result, the reaction rate in this range was, thus, kinetically controlled as the regime I.

3.4 Conclusion

After solid fuel production from paper sludge by HTT, this study provided information on its combustion characteristics and kinetic parameters of both lab-scale and pilot-scale samples. The thermogravimetric analysis was applied to raw and hydrothermally treated paper sludge and the two-stage kinetics study was performed. The results could be summarized as follows:

1. From the DTG profiles, the paper sludge showed three main decomposition characteristics that belonged to: (1) low stability organic compounds and inherent moisture, (2) lignocellulosic and non-lignocellulosic materials that attributed to majority of the weight loss, and (3) calcium carbonate and other minerals. After the hydrothermal treatment, the non-lignocellulosic materials that could be microorganism, dead bacteria, or biopolymer, was eliminated.

2. Based on the comparison of the paper sludge and the reference materials from the thermogravimetric analysis, the paper sludge combustion was triggered by the decomposition of hemicellulose and lignin while the major weight loss was attributed to cellulose

3. The ignition temperature of both raw and hydrothermally treated paper sludge was low, 257–271 ˚C. After the lab-scale hydrothermal treatment, the ignition temperature was decreased while it was slightly increased in the case of the pilot-scale sample.

4. The burnout temperature was around 501–523 ˚C regardless of minerals decomposition.

5. From the two-stage kinetics study, the hydrothermally treated paper sludge became more favor to the reaction since the activation energy was reduced. The activation energy calculated by the isoconversional method shows consistency with the two-stage model-fitting kinetics study and, from both methods, the activation energy was approximately 100–130 kJ/mol.

References

[1] Yanfen L, Xiaoqian M. Thermogravimetric analysis of the co-combustion of coal and paper mill sludge. Appl Energy. 2010;87:3526-32.

[2] Lu L, Namioka T, Yoshikawa K. Effects of hydrothermal treatment on characteristics and combustion behaviors of municipal solid wastes. Appl Energy. 2011;88:3659-64.

[3] Xu M, Sheng C. Influences of the Heat-Treatment Temperature and Inorganic Matter on Combustion Characteristics of Cornstalk Biochars. Energ Fuel. 2012;26:209-18.

[4] Kastanaki E, Vamvuka D. A comparative reactivity and kinetic study on the combustion of coal–biomass char blends. Fuel. 2006;85:1186-93.

[5] Deng N, Zhang YF, Wang Y. Thermogravimetric analysis and kinetic study on pyrolysis of representative medical waste composition. Waste Manag. 2008;28:1572-80.

[6] Fang MX, Shen DK, Li YX, Yu CJ, Luo ZY, Cen KF. Kinetic study on pyrolysis and combustion of wood under different oxygen concentrations by using TG-FTIR analysis. J Anal Appl Pyrol. 2006;77:22-7.

[7] Guo X, Wang Z, Li H, Huang H, Wu C, Chen Y. A study on combustion characteristics and kinetic model of municipal solid wastes. Energ Fuel. 2001;15:1441-6.

[8] Lin Y, Wang D, Wang T. Ethanol production from pulp & paper sludge and monosodium glutamate waste liquor by simultaneous saccharification and fermentation in batch condition. Chem Eng J. 2012;191:31-7.

[9] Yamashita Y, Kurosumi A, Sasaki C, Nakamura Y. Ethanol production from paper sludge by immobilized Zymomonas mobilis. Biochem Eng J. 2008;42:314-9.

[10] Hamzeh Y, Ashori A, Mirzaei B. Effects of Waste Paper Sludge on the Physico-Mechanical Properties of High Density Polyethylene/Wood Flour Composites. J Polym Environ. 2010;19:120-4.

[11] Li X-g, Ma B-g, Xu L, Hu Z-w, Wang X-g. Thermogravimetric analysis of the co-combustion of the blends with high ash coal and waste tyres. Thermochim Acta. 2006;441:79-83.

[12] Skodras G, Grammelis P, Basinas P. Pyrolysis and combustion behaviour of coal–MBM blends. Bioresour Technol. 2007;98:1-8.

[13] Bilbao R, Mastral J, Aldea M, Ceamanos J. Kinetic study for the thermal decomposition of cellulose and pine sawdust in an air atmosphere. J Anal Appl Pyrol. 1997;39:53-64.

[14] Khawam A, Flanagan DR. Role of isoconversional methods in varying activation energies of solid-state kinetics. Thermochim Acta. 2005;436:101-12.

[15] Vyazovkin S, Wight CA. Model-free and model-fitting approaches to kinetic analysis of isothermal and nonisothermal data. Thermochim Acta. 1999;340-341:53-68.

[16] Khawan A, Flanagan DR. Solid-State Kinetic Models: Basics and Mathematical Fundamentals. J Phys Chem B. 2006;110:17315-28.

[17] Yorulmaz SY, Atimtay AT. Investigation of combustion kinetics of treated and untreated waste wood samples with thermogravimetric analysis. Fuel Process Technol. 2009;90:939-46.

[18] Alshehri SM, Monshi MAS, El-Salam NMA, Mahfouz RM. Kinetics of the thermal decomposition of γ-irradiated cobaltous acetate. Thermochim Acta. 2000;363:61-70.

[19] Coats AW, Redfern JP. Kinetic Parameters from Thermogravimetric Data. Nature. 1964;201:68.

[20] Vyazovkin S, Burnham AK, Criado JM, Pérez-Maqueda LA, Popescu C, Sbirrazzuoli N. ICTAC Kinetics Committee recommendations for performing kinetic computations on thermal analysis data. Thermochim Acta. 2011;520:1-19.

[21] Idris SS, Rahman NA, Ismail K. Combustion characteristics of Malaysian oil palm biomass, sub-bituminous coal and their respective blends via thermogravimetric analysis (TGA). Bioresour Technol. 2012;123:581-91.

[22] Barneto AG, Carmona JA, Alfonso JEM, Blanco JD. Kinetic models based in biomass components for the combustion and pyrolysis of sewage sludge and its compost. J Anal Appl Pyrol. 2009;86:108-14.

[23] Vamvuka D, Salpigidou N, Kastanaki E, Sfakiotakis S. Possibility of using paper sludge in co-firing applications. Fuel. 2009;88:637-43.

[24] Méndez A, Fidalgo JM, Guerrero F, Gascó G. Characterization and pyrolysis behaviour of different paper mill waste materials. J Anal Appl Pyrol. 2009;86:66-73.

[25] Yang H, Yan R, Chen H, Lee DH, Zheng C. Characteristics of hemicellulose, cellulose and lignin pyrolysis. Fuel. 2007;86:1781-8.

[26] Gani A, Naruse I. Effect of cellulose and lignin content on pyrolysis and combustion characteristics for several types of biomass. Renew Energ. 2007;32:649-61.

[27] Alda Od, Jesús AG. Feasibility of recycling pulp and paper mill sludge in the paper and board industries. Resour Conserv Recy. 2008;52:965-72.

[28] Font R, Fullana A, Conesa J, Llavador F. Analysis of the pyrolysis and combustion of different sewage sludges by TG. J Anal Appl Pyrol. 2001;58:927-41.

[29] Font R, Fullana A, Conesa J. Kinetic models for the pyrolysis and combustion of two types of sewage sludge. J Anal Appl Pyrol. 2005;74:429-38.

[30] Nakhshiniev B, Gonzales HB, Yoshikawa K. Hydrothermal treatment of date palm lignocellulose residue for organic fertilizer conversion: effect on cell wall and aerobic degradation rate. Compost Sci Util. 2012;20:245-53.

[31] Faúndez J, Arenillas A, Rubiera F, García X, Gordon AL, Pis JJ. Ignition behaviour of different rank coals in an entrained flow reactor. Fuel. 2005;84:2172-7.

[32] Muthuraman M, Namioka T, Yoshikawa K. Characteristics of co-combustion and kinetic study on hydrothermally treated municipal solid waste with different rank coals: A thermogravimetric analysis. Appl Energy. 2010;87:141-8.

[33] He C, Giannis A, Wang J-Y. Conversion of sewage sludge to clean solid fuel using hydrothermal carbonization: Hydrochar fuel characteristics and combustion behavior. Appl Energy. 2013;111:257-66.

[34] Sakaguchi M, Laursen K, Nakagawa H, Miura K. Hydrothermal upgrading of Loy Yang Brown coal — Effect of upgrading conditions on the characteristics of the products. Fuel Process Technol. 2008;89:391-6.

[35] Oniyama E, Wahlbeck PG. Application of transpiration theory to TGA data calcium carbonate and zinc chloride. Thermochim Acta. 1995;250:41-53.

[36] Gil MV, Casal D, Pevida C, Pis JJ, Rubiera F. Thermal behaviour and kinetics of coal/biomass blends during co-combustion. Bioresour Technol. 2010;101:5601-8.

[37] Várhegyi G, Szabó P, Jakab E, Till F. Mathematical Modeling of Char Reactivity in Ar-O_2 and CO_2-O_2 mixtures. Energ Fuel. 1996;10:1208-14.

[38] Sullivan A, Ball R. Thermal decomposition and combustion chemistry of cellulosic biomass. Atmospheric Environment. 2012;47:133-41.

[39] Areeprasert C, Zhao P, Ma D, Shen Y, Yoshikawa K. Alternative Solid Fuel Production from Paper Sludge Employing Hydrothermal Treatment. Energ Fuel. 2014;28:1198-206.

[40] Cumming JW. Reactivity assessment of coals via a weighted mean activation energy. Fuel. 1984;63:1436-40.

[41] Di Blasi C. Combustion and gasification rates of lignocellulosic chars. Prog Energ Combust. 2009;35:121-40.

[42] Dennis JS, Lambert RJ, Milne AJ, Scott SA, Hayhurst AN. The kinetics of combustion of chars derived from sewage sludge. Fuel. 2005;84:117-26.

[43] Williams A, Pourkashanian M, Jones JM. Combustion of pulverised coal and biomass. Prog Energ Combust. 2001;27:587-610.

[44] Hurt RH. Structure, Properties, and Reactivity of Solid Fuels. Symp (Int) Combust. 1998;27:2887-904.

Chapter 4

Co-combustion of hydrothermally treated paper sludge with subbituminous coal in a fixed bed combustor

Abstract: After the fundamental combustion study in Chapter 3, the basic co-combustion test was conducted in this chapter. In this study, the co-combustion of the hydrothermally treated paper sludge with subbituminous coal was investigated. The solid fuel was produced from paper sludge by the hydrothermal pilot plant at the temperature of 197 °C and the pressure of 1.9 MPa for 30 minutes. NO emissions were tested by a batch-type fixed bed combustor. The result showed that the NO emissions could be reduced around 26–31% and, therefore, the mixture of coal and hydrothermally treated paper sludge (HTT-PS) yielded lower NO emission compared to the mixture of coal and raw paper sludge. NO conversion of the HTT-PS was lower than the original paper sludge. Finally, the slagging and fouling indices were calculated. The fouling and slagging tendencies of HTT-PS were improved.

4.1 Background

In practical utilization of biomass in a solid fuel firing system, co-combustion with coal needs minimal modification of boiler operating conditions when compared to burning pure biomass. In the case of paper sludge, recycling through the energy recovery process within the production plant, i.e., a paper production factory, could reduce transportation and disposal costs. At the same time, the volume reduction of waste is satisfied. As the main obstacle of raw paper sludge (Raw-PS), i.e., high moisture content, has been alleviated by using the self-sustained hydrothermal pretreatment, utilizing the hydrothermally treated paper sludge (HTT-PS) in co-combustion application with coal would be possible. In the previous chapter, the combustion characteristics and kinetics study of HTT-PS has been comparatively studied with Raw-PS to obtain fundamental information. Then, in this chapter, a basic co-combustion test with subbituminous coal was carried out in a small-scale combustor. The focus was firstly on the NO_x emission, which is very important regarding solid fuel combustion system. To reach a practical utilization of HTT-PS, a general problematic issue regarding ash of biomass/waste was also studied by evaluating slagging and fouling indices.

Three types of nitrogen oxides namely thermal NO, prompt NO, and fuel NO, have their origins from different formation pathways [1-4]. Thermal NO is formed by an oxidation of atmospheric nitrogen in air at a relatively high combustion temperature [1]. When the nitrogen from air is attacked by hydrocarbon radicals, prompt NO is generated [1]. The prompt NO generally occurs in a fuel-rich combustion scheme because the presence of hydrocarbons is required [5]. In this research, the effect of the hydrothermal pretreatment on NO generated by nitrogen bounded in fuel, fuel-N, was focused. Therefore, the carrier gas was a mixture of Ar and O_2 to avoid the presence of N_2 in the air that could

lead to thermal and prompt NO formation. In general, the combustion of biomass could be divided mainly into two processes: devolatilization and char oxidation. The distribution of fuel-N, nitrogen in the volatile (volatile-N) and nitrogen left in the char matrix (char-N), depends not only on fuel property both physically and chemically but also the heating rate, the combustion temperature, and the residence time [3-5]. During the devolatilization, the biomass is undergone pyrolysis process where nitrogen in tar (tar-N) and volatile substances are released along with the volatile-N, namely ammonia (NH_3), hydrogen cyanide (HCN), and cyanuric acid (HCNO) [4,6,7]. Through the thermal cracking of tar and volatile combustion, NH_3 and HCN, are additionally produced. Finally, these volatile-N species further takes part in formation of NO [8]. Leftover char is combusted heterogeneously and nitrogen in char (char-N) is then oxidized to NO.

Slagging refers to the deposition into furnace of the boiler where radiant heat transfer dominates while fouling is the deposition that occurs on the surface of convective tube bundles [9]. The deposition of ash through slagging and fouling phenomena affects the thermal performance of boilers in many ways such as reduction of the heat transfer rate for steam production, impede steam temperature controlling, and increase fuel consumption to meet a desired load. The problem of slagging and fouling is generally found in combustion of some agricultural residues due to its high potassium and sodium content. These substances can lower melting temperature of ash that causes ash deposition, fouling of boiler tubes, and bed agglomeration (in fluidized bed boiler) [9,10]. Even though higher ash content can increase the deposition tendency, this phenomenon is not only dependent solely on the amount of ash. Many factors have to be considered such as the chemical composition, the mineral composition, the thermal conductivity, the emissivity, and the morphology of each fuel [11,12]. Since ash deposition is the critical issue for co-combustion application, the study on ash composition and slagging and fouling indices of HTT-PS have to be comparatively investigated with Raw-PS.

4.2 Materials and methods

4.2.1 Raw material

Raw paper sludge (Raw-PS) and subbituminous coal (Sub-C) were provided by the Siam Kraft Industry Co., Ltd., Thailand. Raw-PS was subjected to a subcritical hydrothermal treatment (HTT) by a 1-m^3 cylindrical batch-type hydrothermal reactor. The treatment condition was 197 °C and 1.9 MPa with the holding time of 30 minutes. After the treatment was finished, the product was dewatered by a centrifugal decanter and naturally dried. The proximate analysis, the ultimate analysis, and the higher heating value (HHV) of Raw-PS and the hydrothermally treated paper sludge (HTT-PS) were analyzed on a dry basis as shown in Table 4-1.

4.2.2 X-ray photoelectron spectroscopy

In this study, X-ray photoelectron spectroscopy (XPS), which is the effective method to provide qualitative and quantitative surface chemical information, was utilized. The XPS analysis was performed in an ULVAC-PHI's ESCA1700R system equipped with a dual Mg/Al X-ray source and a hemispherical analyzer operating in the fixed analyzer transmission mode. Before the analysis, the sample was degased for 3 h and the working pressure in the analyzing chamber was less than 10^{-7} Pa. The monochromatic Al Kα X-ray source was operated at 350 W and 14 kV ($h\nu$ = 1486.8 eV). Excess charges on the samples were neutralized by the argon ion sputtering. The spectra were obtained with the pass energy of 58.7 eV with the energy step of 0.05 eV and the analysis area was 0.8 x 2 mm. The spectra were acquired in the N1s and C1s regions. The C1s at the binding energy (BE) of 285.0 eV was taken as an internal reference. The surface measurement were done automatically 20 times at the different positions for each sample to ensure the reproducibility of the results. Prior to the spectra analysis, the data was treated by the Shirley background subtraction. Then, the spectra were deconvoluted by the Gaussian-Lorentzian function. The full width at the half maximum (FWHM) of all species were fixed at 1.8–1.9 eV.

Table 4-1 Fuel analysis.

Items	Sub-C	Raw-PS	HTT-PS
	Proximate analysis (%)		
FC	38.6	10.9	10.1
VM	59.3	62.1	59.4
Ash	2.1	27.0	30.5
	Ultimate analysis (%)		
C	63.2	34.8	35.2
H	4.2	4.3	4.2
N	0.8	4.0	3.1
S	0.1	0.6	0.6
O	29.6	29.3	26.5
	Heating value (MJ/kg)		
HHV	16.8	14.1	14.7
	Ash composition (%)		
CaO	19.3	50.0	39.1
SiO_2	27.4	18.4	23.6
Al_2O_3	13.8	12.0	14.1
Fe_2O_3	16.6	4.2	5.4
MgO	2.5	2.7	3.2
Na_2O	3.7	0.9	0.0
K_2O	5.9	1.3	1.3
TiO_2	2.1	2.3	2.8
SO_3	4.3	3.7	5.1
P_2O_5	0.0	2.0	3.4

FC: fixed carbon; VM: volatile matter; C: carbon; H: hydrogen; N: nitrogen; S: sulfur; O: oxygen calculated by difference; HHV: higher heating value.

4.2.3 Fixed bed combustor

A fixed bed combustor shown in Figure 4-1 made from quartz was utilized in this research. Its main structure consists of a top cover with air injection port, an outer tube with the outlet at the bottom for the exhaust gas (50 mm in diameter, 1,130 mm in height), and an inner tube with a single sample bed (40 mm in diameter, 470 mm in height) [13,14]. The sample bed made from a sintered quartz was made porously enough to distribute the exhaust gas as well as to support the sample during the combustion test. Three electric heaters were assembled to the combustor to assure that the target combustion temperature was achieved. In each experiment, 0.3 g of sample was mixed with 10 g of silica sand for preventing the agglomeration and maintaining the height of the sample. Ar gas was mixed with O_2 with the ratio of 79:21 to avoid the formation of the thermal NO and it was supplied from the upper port leaving the lower port as an outlet.

To investigate the effect of the combustion temperature, the combustor was heated to 800, 850, 900, and 950 °C. For the co-combustion experiment, the blending ratios of the paper sludge were 10%, 20%, 30%, 40%, 50%, and 80% and the combustion temperature was fixed at 900 °C. The flow rate of all tests were controlled at 1.4 L/min measured by the flow meter at the outlet of the water scrubber. Then, the exhaust gas was analyzed by the online flue gas analyzer (TESTO 350XL, Japan) and the data was collected by the PC. The oxygen concentration at the outlet was also observed. It can confirm complete combustion of all the samples since the lowest oxygen concentration at the outlet for Sub-C, Raw-PS, and HTT-PS were excessive (12–16%) as shown in Figure 4-2.

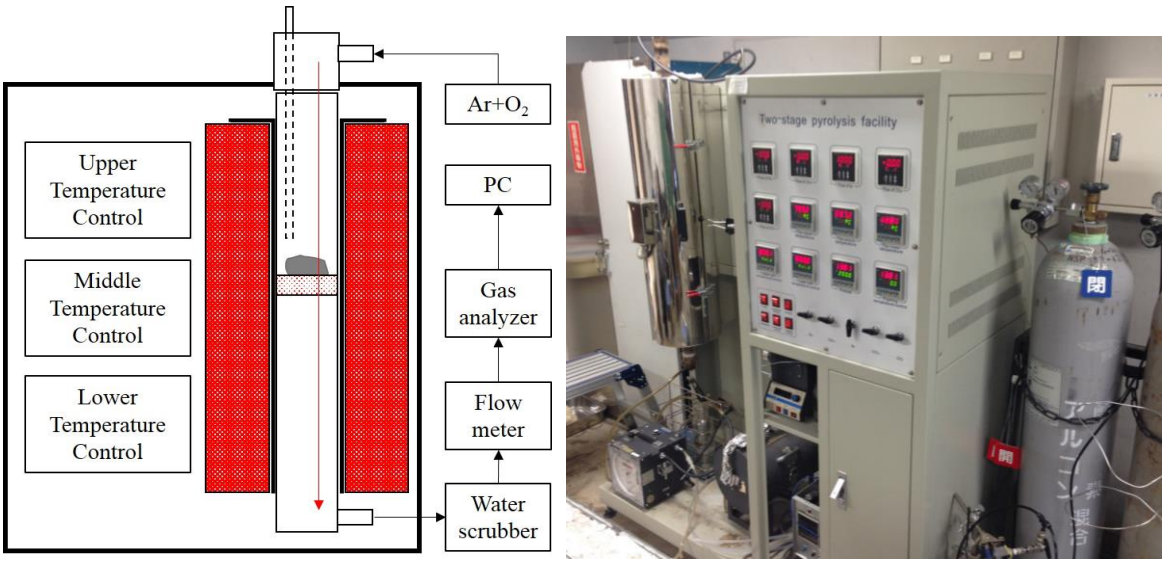

Figure 4-1 Fixed bed combustor and flow diagram

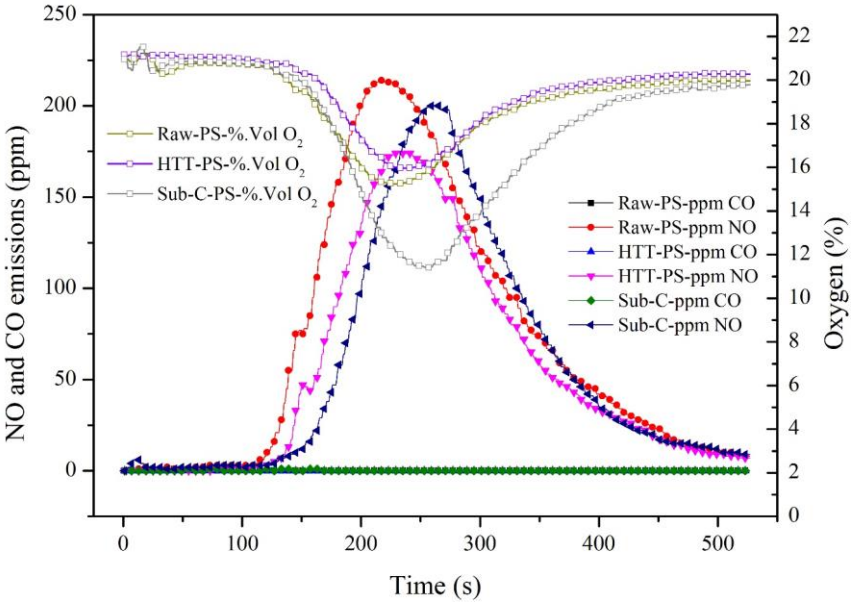

Figure 4-2 Example of oxygen and emission profile from combustio test

The data obtained from the sampling through the gas analyzer was monitored in a unit of concentration (ppm/second), the amount of the NO emission per unit mass basis would be more appropriate to compare the NO produced from different samples. Hence, the NO emission was calculated by Equation 4-1 [14] and, additionally, the NO conversion from the nitrogen in fuel was determined by Equation 4-2 [13] In this study, it should be noted that the nitrous oxide (N_2O) was negligible.

$$[NO] = \left[\frac{M_{NO}}{V_m \times m}\right] \times \left[\int_{t_0}^{t} qc_{NO}\,dt\right] \quad (4\text{-}1)$$

where M_{NO} is the molar mass (g/mol); V_m is the molar volume of an ideal gas at 1 atmospheric pressure which equals to 22.4 (L/mol) at 0 °C; m is the sample mass (g); c_{NO} is the concentration of NO emission continuously recorded by the gas analyzer (ppm/second); t is the sample burning period (s); [NO] is the amount of the NO emission per unit sample (mg/g).

$$[NO]_{conv} = \frac{[NO]_{mol}}{[Fuel-N]_{mol}} \times 100 \quad (4\text{-}2)$$

where $[NO]_{mol}$ is the mole of NO when burning 1 g of the sample (mol/g); $[Fuel - N]_{mol}$ is the mole of nitrogen in 1 g of sample (mol/g) and $[NO]_{conv}$ is the nitrogen conversion (%).

4.2.4 Slagging and fouling indices

To utilize HTT-PS as the alternative solid fuel, one of the concerning issues is the slagging and fouling of ash. In this study, the effect of HTT on the deposition tendency of ash from paper sludge combustion was investigated by the slagging and fouling indices listed in Table 4-2. To calculate the slagging and fouling indices, the ash composition, i.e., metal oxides, of Raw-PS, HTT-PS, and Sub-C, were

determined by the X-ray fluorescence analysis (XRF) as shown in Table 4-1. From Table 4-2, the base-to-acid ratio, generally used for coal, was modified for biomass fuel by adding P_2O_3 to the basic ash side as reported by several researchers [15,16] while the others were calculated based on the empirical indices for low rank coals [17,18]. It should be noted that the slagging and fouling indices of the mixture was derived from the data of the metal oxides of the mixture obtain from XRF (shown later), not the weighted average from each sample.

Table 4-2 Slagging and fouling indices

Indices	Formula	Criteria
Base to acid ratio (B/A)	$\frac{B}{A} = \frac{\%(Fe_2O_3 + CaO + MgO + K_2O + Na_2O + P_2O_3)}{\%(SiO_2 + TiO_2 + Al_2O_3)}$	B/A < 0.5, deposition tendency is low; 0.5 < B/A < 1, deposition tendency is medium; B/A > 1, deposition tendency is high.
Silica-alumina ratio (S/A)	$\frac{S}{A} = \frac{SiO_2}{Al_2O_3}$	S/A < 0.31 or > 3, deposition tendency is low; 0.3 < S/A < 3, deposition tendency is high.
Iron-calcium ratio (I/C)	$\frac{I}{C} = \frac{Fe_2O_3}{CaO}$	I/C < 0.31 or > 3, deposition tendency is low; 0.3 < I/C < 3, deposition tendency is high.
Slagging index (S)	$S = \left(\frac{B}{A}\right) \times \text{Sulfur (\% dry basis)}$	S < 0.6, deposition tendency is low 0.6 < S < 2, deposition tendency is medium; S > 2, deposition tendency is high.
Total alkalis (TA)	$TA = Na_2O + K_2O$	TA < 0.3, fouling tendency is low 0.3 < TA < 0.4, fouling tendency is medium; TA > 0.4, fouling tendency is high.

4.3 Results and discussion

4.3.1 NO emission from individual combustion

Figure 4-3 illustrates the NO emission from Raw-PS and HTT-PS combustion in the unit of mg of NO per g of burned fuel. The NO emission of Raw-PS was 3.6, 3.8, 4.2, and 4.5 mg/g at the combustion temperature of 800, 850, 900, and 950 °C, respectively. Compared to the non-treated material, HTT-PS showed lower amount of NO that was 2.5, 2.8, 3.1, and 3.3 mg/g accounting 30.8%, 26.3%, 27.2%, and 26.9% reduction. Figure 4-2 also shows the NO conversion rate. For Raw-PS, the NO conversion rate was 4.2%, 4.5%, 5.0% and 5.2% when burning at the temperature of 800, 850, 900, and 950 °C, respectively. With the same increment of the combustion temperature, HTT-PS's NO conversion rate was 3.8%, 4.3%, 4.6% and 4.9%. The NO conversion rate of HTT-PS showed 10.7%, 4.9%, 6.1% and

5.7% lower than that of Raw-PS for the combustion temperature of 800, 850, 900 and 950 °C, respectively. As combustion temperature increases, the NO emission and the NO conversion rate of both Raw-PS and HTT-PS were enhanced. From the combustion test of Raw-PS and HTT-PS, it could be stated that HTT lowered the NO conversion rate leading to the reduction of NO emission.

4.3.2 NO emission from co-combustion

Figure 4-3 shows the NO emission during Raw-PS and HTT-PS co-combustion with Sub-C at 900 °C. It was observed that the NO emission from Sub-C was 3.6 mg/g. The NO conversion rate is also illustrated in Figure 4-3. The Sub-C showed significantly high NO conversion rate when compared to Raw-PS and HTT-PS. The NO conversion dropped proportionally when increasing the amount of Raw-PS and HTT-PS.

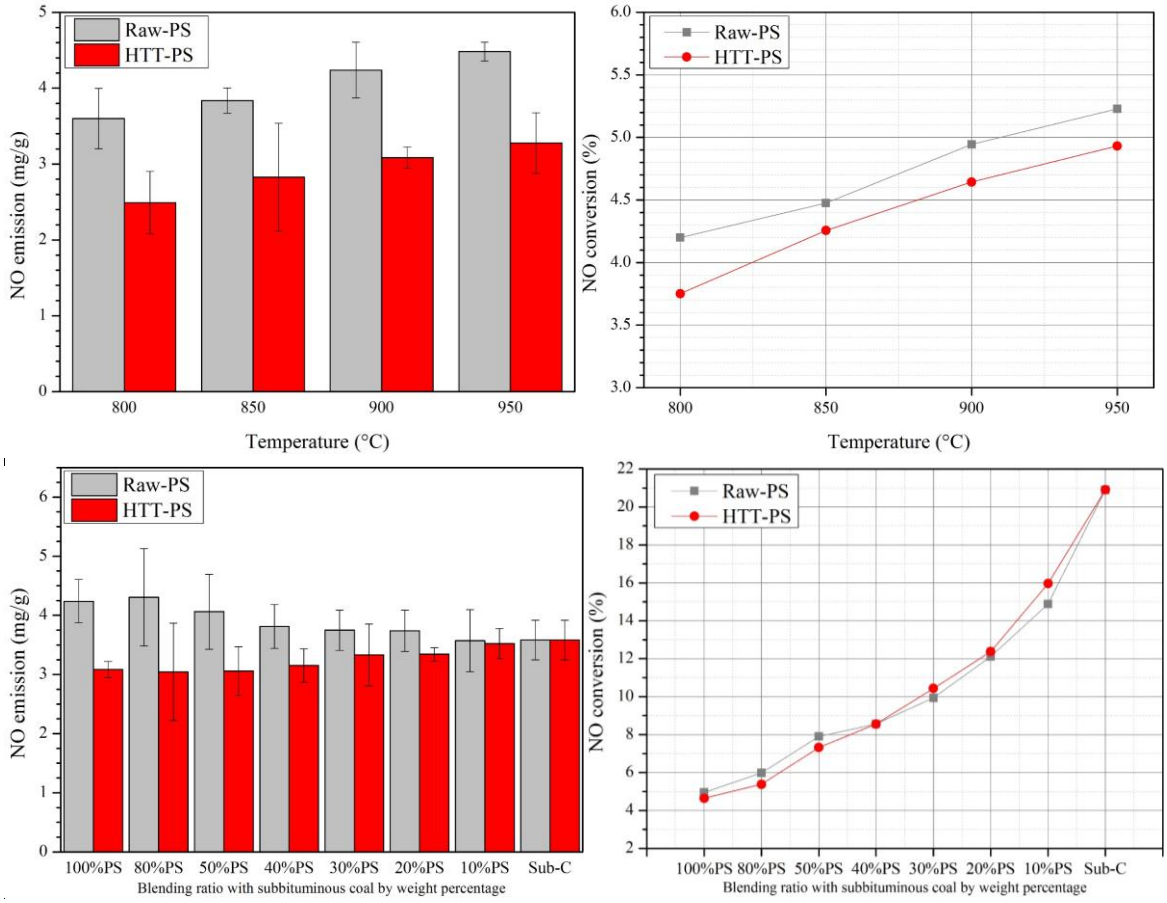

Figure 4-3 NO emission from combustion of raw paper sludge (Raw-PS), hydrothermally treated paper sludge (HTT-PS), subbituminous coal (Sub-C), and co-combustion of blended fuels. (10%PS: 10 wt% of Raw-PS or HTT-PS blended with 90 wt% of Sub-C)

From Figure 4-3, it can be observed that, at the low mixing ratio, 10–30%, the mixture of HTT-PS had a slightly higher NO conversion rate while the mixture of Raw-PS showed a higher NO conversion rate at the high mixing ratio, 50–80%. This is because Sub-C having a high NO conversion rate dominated

the NO conversion characteristic when the mixing ratio of the paper sludge is low. Conversely, when the ratio of the paper sludge was high, they exhibited their characteristics by showing a lower NO conversion rate. Moreover, the effect of HTT that lowered the NO conversion rate was realized when the mixing ratio was higher. For the viewpoint of the NO emission, it was clearly shown that blending of 10% HTT-PS was not effective enough to show the NO reduction, as the amount of NO emission of these two mixtures were almost the same. This could be explained by the NO conversion rate shown in Figure 4-2. The NO conversion rates of HTT-PS-10% and Raw-PS-10% were still high due to the majority of the mixture was Sub-C. Consequently, the NO emission reduction was limited to some extent. However, when increasing the mixing ratio to 20%, the NO from the co-combustion of HTT-PS mixture was much lower than that of the mixture of Raw-PS and Sub-C. The NO reduction was increased from 1.4% to 10.6% when changing the blending ratio from 10% to 20%, which is approximately 7.5 times better. Additionally, the NO reduction was 11.1%, 17.3%, 24.7% and 29.3% for 30%, 40%, 50% and 80% blending ratio, respectively. It was observed that the NO emission could be further reduced with the increase of the blending ratio of HTT-PS; however, there would be some problematic issues that have to be concerned. Even though the heating value was slightly improved after HTT, it was still low when compared to coal. Hence, it would reduce the heat release from the combustion process resulting in the poor boiler performance. Furthermore, the volatile matter of HTT-PS was relatively high. This would be problematic to the post-combustion facility such as the gas cleaning system due to a higher amount of flue gas needs to be treated. Furthermore, the well-known characteristic of sludge is high ash content. HTT-PS has higher ash content and this might bother the gas cleaning system as well as the ash disposal facilities. Therefore, the compromise on the ratio of HTT-PS blending with coal has to be further discussed depending on each system since all aspects of limitation has to be concerned.

4.3.3 XPS study

To understand the mechanism that contributed to the NO reduction, the X-ray photoelectron spectroscopy (XPS) was performed to characterize the nitrogen functionality on the surface of the samples. From the literatures, the nitrogen functionality in the coal contains 50–80% of pyrrolic (five rings), 20–40% pyridinic (six rings), and 0–20% quaternary nitrogen while less than 10% of nitrogen from amino group is found [1,2]. However, the nitrogen functionality in the biomass is different [19,20]. As explained by Williams et al., the fuel-N in biomass is devoted to inorganic nitrate and ammonium ion, amino compound, heterocyclic purine, pyrimidine and pyrrole [20-22]. Additionally, it was reported that protein, which comprises of nitrogen containing amide bond, exists in microorganisms in sewage sludge [23,24]. Thus, these nitrogen compounds would contribute to the fuel-N in the paper sludge since it is a mixture of fibrous materials and sewage sludge.

Figure 4-4 illustrates the XPS spectra of C1s and N1s of Raw-PS and HTT-PS. For C1s, there were four peaks noted C1, C2, C3, and C4 which were located at the binding energy of 285.0, 286.4, 288.1, and 289.7 eV for Raw-PS and 285.4, 286.8, 288.1 and 289.3 eV for HTT-PS, respectively. The peaks of C1, C2, C3 and C4 were assigned to C–C/C–H/C=C, C–O (e.g., ether, alcohol, amine, and amide), C=O (e.g., amide, carbonyl, carboxylate, and ester) and O–C=O (carboxylic group), respectively [25,26]. From Figure 4-4, three peaks were well fitted to the N1s XPS spectra. N1, N2, and N3 were placed at the binding energy of 398.6, 400.3 and 401.8 eV for Raw-PS and 398.9, 400.5 and 401.9 eV for HTT-PS, respectively. The lowest binding energy peak, N1, was assigned to the C=N in pyridine or imine [27,28]. The other peaks, N2 and N3, were given to the N–O/C–N in amide or amine and N–H in ammonia or protonated amine, respectively [26,29].

The effect of HTT on the nitrogen functionality was investigated by comparing the C1s and N1s XPS spectra of Raw-PS and HTT-PS. The area under each deconvoluted curve was calculated. The C1 peak was the major component and its area was increased from 52.8% to 59.1% after HTT. As this peak was belonged to aliphatic/aromatic carbon groups, it could be said that after the treatment, the fraction of the hydrocarbon became slightly higher and this might be used to explain why the heating value was marginally improved. When focusing on C2 and C3 peaks, the area was decreased from 31.9% to 27.2% and 11.1% to 7.8%, respectively. Those two peaks that was assigned to amine and amide showed 14.7% and 29.7% reduction; therefore, this evidence illustrated that the nitrogen functional group was changed after HTT. Finally, the area of C4 that belonged to the carboxylic group was considered as a minor composition and it increased from 4.2% to 5.9%.

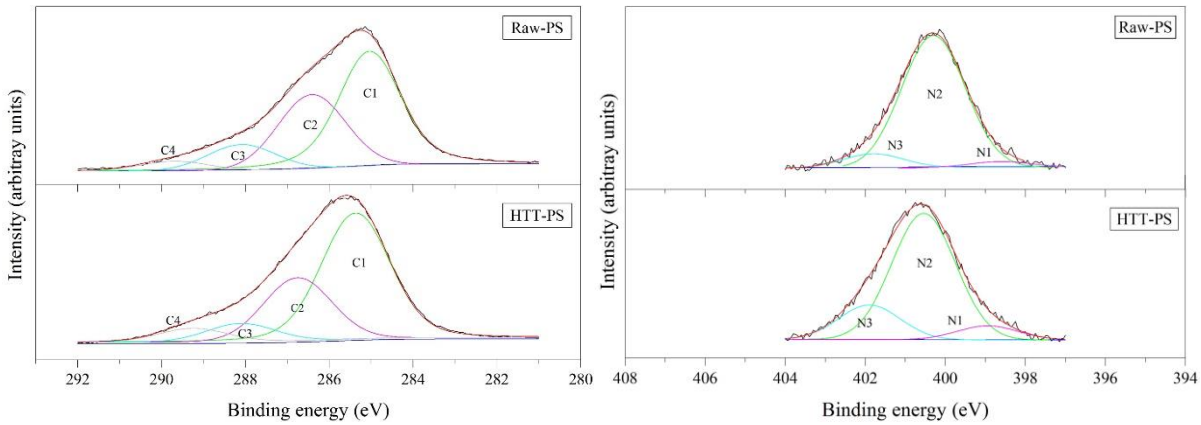

Figure 4-4 XPS spectra (C: carbon C1s and N: nitrogen N1s) of raw paper sludge (Raw-PS) and hydrothermally treated paper sludge (HTT-PS)

For the N1s spectra, the majority constituent was belonged to N2 devoted to the amide or amine peak, which belonged to the nitrogen in protein. After HTT, the area of this peak was decreased from 87% to 72.8% accounting 16.3% reduction whereas the ammonium or protonated amine, the N3 peak, was

increased from 9.3% to 19.3%. This could be explained by HTT condition that is using the subcritical water or hot compressed water in which the ionic product, hydronium (H_3O^+) and hydroxide (OH^-) is higher than ambient water condition leading to the protonation of amine [30]. In addition to the hydrolysis reaction that occurred during HTT, this condition would be suitable for protein degradation resulting in the decrease of amide and other nitrogen compounds [24]. When comparing the area of N1 peak that assigned to pyridine of Raw-PS and HTT-PS, it was increased from 3.7% to 7.9%. As the area of the N1 peak was enhanced, it might be suggested that the unstable nitrogen functionality could be converted into a larger compound i.e., heteroaromatic ring as the pyridine after HTT [31,32]. Therefore, from the XPS spectra of C1s and N1s, it could be stated that HTT protonated or dissolved and simultaneously condensed the nitrogen functional compounds (mainly amine and amide) diverting the fuel-N characteristic of the paper sludge.

4.3.4 Slagging and fouling indices

4.3.4.1 Individual fuel

Table 4-3 presents the result of the slagging and fouling indices: the Base to Acid ratio (B/A), the Silica Alumina ratio (S/A), the Iron Calcium ratio (I/C), the Slagging index (S), and the Total Alkalis (TA) of individual and blended fuels. The indices that have been used to predict the slagging tendency were B/A, S/A, I/C, and S while the fouling tendency is estimated by TA. The slagging phenomena refers to the deposition occurring in the boiler where the radiant heat transfer is dominant, i.e., in a furnace, while the deposition on the section subjected to the convective heat transfer, i.e., a convective backpass, is called fouling [33]. It should be noted that the S index was calculated by the weighted average of sulfur percentage.

The B/A ratio of the paper sludge was reduced from 1.9 to 1.3 after HTT, but the B/A was still in the range of high deposition tendency. As presented in Table 4-2, the B/A was calculated by dividing the basic ash which has a low melting temperature by the acidic ash that has a comparatively higher melting temperature. With HTT, the alkalis metals that have low melting temperatures were reduced; thus, the B/A of HTT-PS was decreased. When silica or alumina reacts with basic compounds, they are able to form silicate or aluminate. Since the melting point of silicate and aluminate are lower than their original substances, the S/A ratio is used to predict the possibility of the low melting temperature compound formation. From Figure 4-5, it was observed that Sub-C had the highest deposition tendency and HTT slightly increased the risk of the silicate and aluminate formation since the value was increased from 1.5 to 1.7 as shown in Table 4-3. When iron and calcium are found in the ash, the eutectic composition that has a low melting temperature is formed through the fluxing action. Raw-PS and HTT-PS had low deposition tendency based on the I/C ratio while Sub-C exhibited high risk. From Figure 4-5, it can be observed that the I/C ratio of the paper sludge was slightly increased after HTT. For the S index, the value of Sub-C was 0.1 showing low deposition tendency due to a low sulfur content. For Raw-PS and

HTT-PS, it was observed from Table 4-3 that the deposition tendency was located in the medium range. HTT-PS showed a lower S index, 0.7, which was lower than the original value of Raw-PS, 1.1. For the fouling tendency, the TA of Sub-C was 9.6, which was significantly high compared to other samples. The TA of the paper sludge was reduced from 2.1 to 1.3 after HTT. This related to the B/A ratio where the alkalis metal were eliminated during HTT. From the slagging and fouling indices of the individual fuel, it could be concluded that the slagging and fouling tendency of the paper sludge was initially high and this risk was substantially alleviated after HTT, except for the S/A ratio; however, they still exhibited a high deposition tendency.

Table 4-3 Slagging and fouling indices of individual and blended fuels (Sub-C: subbituminous coal; Raw-PS: raw paper sludge; HTT-PS: hydrothermally treated paper sludge; Raw-PS-10%: 10 wt% of Raw-PS blended with 90 wt% of Sub-C)

Sample (%)	B/A ratio	S/A ratio	I/C ratio	S index	TA
			Individual fuel		
Sub-C	1.1h	2h	0.9h	0.1l	9.6h
Raw-PS	1.9h	1.5h	0.1l	1.1m	2.1h
HTT-PS	1.3h	1.7h	0.1l	0.7m	1.3h
			Blended fuel		
Raw-PS-10	1.4h	1.6h	0.5h	0.2l	5.1h
Raw-PS-20	1.5h	1.5h	0.4h	0.3l	4.5h
Raw-PS-30	1.6h	1.5h	0.3l	0.4l	3.6h
Raw-PS-40	1.6h	1.4h	0.2l	0.5l	3.5h
Raw-PS-50	1.7h	1.4h	0.2l	0.6l	3.4h
Raw-PS-80	1.9h	1.4h	0.1l	0.9m	2.8h
HTT-PS-10	1.2h	1.6h	0.5h	0.2l	6.9h
HTT-PS-20	1.2h	1.5h	0.4h	0.2l	4.7h
HTT-PS-30	1.2h	1.4h	0.4h	0.3l	3.9h
HTT-PS-40	1.3h	1.5h	0.3l	0.4l	3.7h
HTT-PS-50	1.2h	1.5h	0.2l	0.4l	3.3h
HTT-PS-80	1.3h	1.6h	0.2l	0.6l	1.4h

B/A: Base to Acid ratio; S/A: Silica Alumina ratio; I/C: Iron Calcium ratio; S index: Slagging index; TA: Total Alkalis; h: high deposition tendency; m: medium deposition tendency; l: low deposition tendency

4.3.4.2 Blended fuel

Table 4-4 shows the ash composition of Raw-PS and HTT-PS mixture. Figure 4-5 also illustrates the trend of the slagging and fouling indices of Sub-C added with Raw-PS and HTT-PS. For the B/A ratio, it was clearly shown that the mixture of Sub-C and Raw-PS showed higher deposition tendency when compared to the mixture of Sub-C and HTT-PS whose B/A ratio was limited to 1.2–1.3. For the S/A, the difference was not significant and all of the mixtures exhibited the high deposition tendency similar to their original materials. For the I/C ratio, the low mixture of Raw-PS and HTT-PS attributed to the

high I/C ratio since Sub-C had a high I/C ratio and would dominate the characteristic of the blended fuel. However, when increasing the mixture to around 30–40%, the deposition tendency became low since the I/C ratios of Raw-PS and HTT-PS were initially low. For the S index, Raw-PS and HTT-PS showed the medium deposition tendency while it was low in the case of Sub-C. Thus, when mixing Sub-C with Raw-PS and HTT-PS, it yielded low deposition tendency. TA was significantly reduced when adding Raw-PS and HTT-PS. The mixture showed the decreasing trend of TA; however, the fouling deposition tendency was still high. From Figure 4-5, it can be concluded that mixing HTT-PS to Sub-C would significantly decease S/A, I/C, and TA while B/A was comparable to the original value of Sub-C. It should be noted that the subbituminous coal (Sub-C) in this research had a very low sulfur content leading to the increasing of the S index when blending with HTT-PS. However, the effect of mixing HTT-PS would be noticed when other types of coal that generally has a high sulfur content is used.

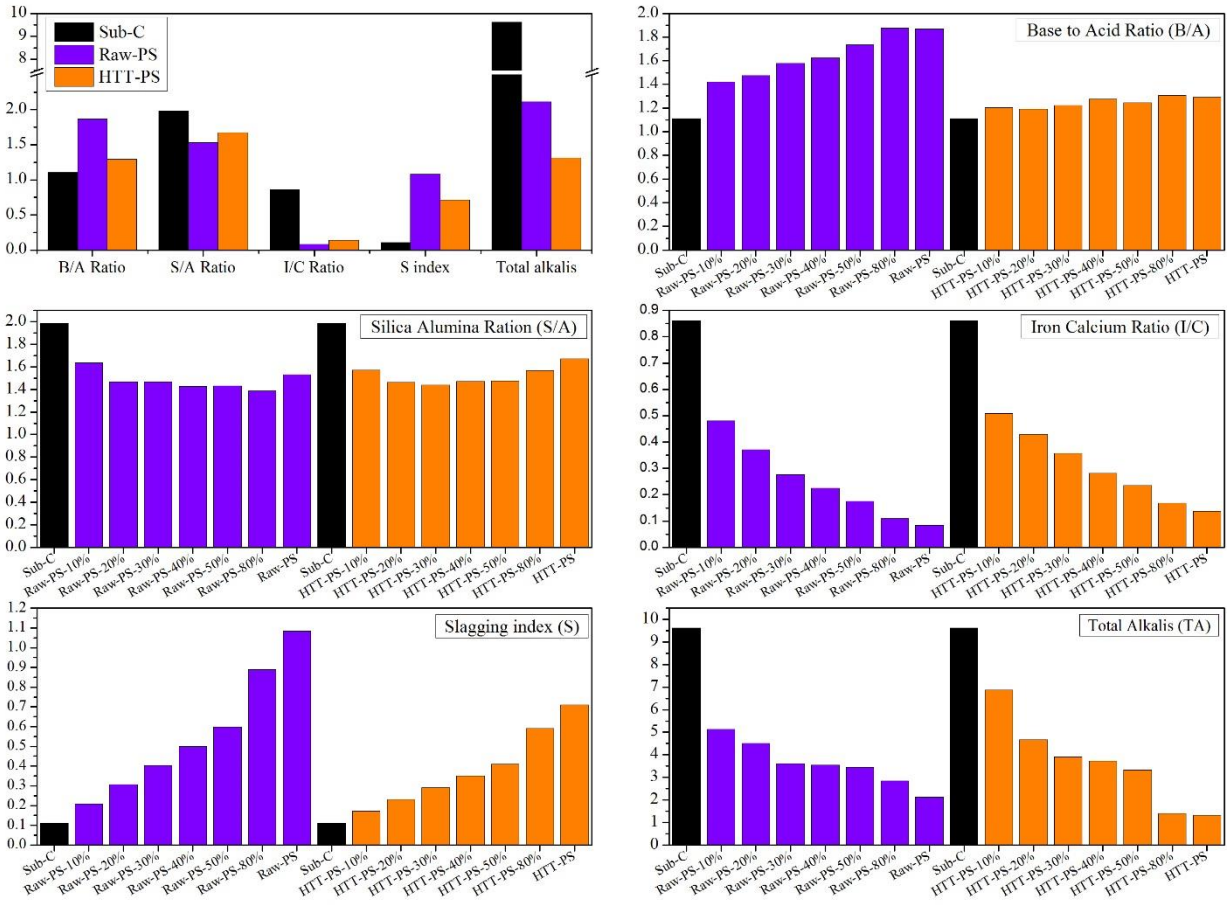

Figure 4-5 Slagging and fouling indices of individual and blended fuels. (Sub-C: subbituminous coal; Raw-PS: raw paper sludge; HTT-PS: hydrothermally treated paper sludge; Raw-PS-10%: 10 wt% of Raw-PS blended with 90 wt% of Sub-C)

Table 4.4 Ash composition of the mixture

Item	Share of Raw-PS (%)						Share of HTT-PS (%)					
(%)	10	20	30	40	50	80	10	20	30	40	50	80
CaO	29.9	33.4	37.6	40.1	43.1	47.9	25.4	27.7	30.3	32.5	33.6	38.8
SiO_2	21.9	20.7	19.8	19.4	18.6	17.5	23.9	23.4	23	22.5	23	22.9
Al_2O_3	13.4	14.1	13.5	13.6	13	12.6	15.2	16	16	15.3	15.6	14.6
Fe_2O_3	14.4	12.4	10.4	9.0	7.5	5.2	12.9	11.9	10.8	9.1	7.9	6.6
MgO	2.8	3.2	3.02	3.0	3.0	3.0	3.2	3.4	3.2	3.4	3.4	2.8
Na_2O	2.3	2.2	1.7	1.7	1.7	1.3	3.1	2.3	1.8	1.8	1.5	0
K_2O	2.8	2.3	1.9	1.8	1.8	1.6	3.8	2.4	2.1	1.9	1.9	1.4
TiO_2	2.2	2.3	2.4	2.2	2.2	2.3	2.3	2.4	2.4	2.6	2.4	2.9
SO_3	4.7	4.7	4.6	4.3	4.1	3.8	4.8	4.9	5.0	5.0	4.9	4.9
P_2O_5	1.0	1.2	1.7	1.6	1.7	1.8	1.4	2.1	2.3	2.8	2.8	3.1

4.4 Conclusion

The solid fuel produced from Raw-PS using the hydrothermal treatment (HTT) was subjected to co-combustion test with subbituminous coal by the batch-type fixed bed combustor. The NO emission and the effect of HTT on NO was further investigated by the X-ray photoelectron spectroscopy (XPS). The oxide of metal obtained from the X-ray fluorescence (XRF) was used to calculate the slagging and fouling indices to clarify the deposition tendency of both individual and blended fuels. The results of these experiments can be summarized as follows:

1. HTT showed the positive effect on the NO emission suppression as the NO emission and the NO conversion rate of HTT-PS were decreased. It was approximately 26–31% lower and when it was blended with Sub-C, the NO was reduced. The effective blending ratio of HTT-PS that illustrated the difference from Raw-PS could be 20% or higher.

2. From the XPS study, it could be suggested that HTT diverted the fuel-N characteristic in the paper sludge, i.e., dissolved or protonated amide and simultaneously condensed the nitrogen functional compounds, and the lower amount of fuel-N observed in the ultimate analysis. These evidences might be the reasons why the NO emission and the NO conversion rate of HTT-PS were lower than Raw-PS.

3. The Base to Acid ratio (B/A), the slagging index (S), and the total alkalis (TA) were improved after HTT while the silica-alumna ratio (S/A) and the iron-calcium ratio (I/C) were slightly higher. When mixing HTT-PS with Sub-C, the significant improvement was also observed in the B/A, S, and TA indices. However, it still exhibited high possibilities of ash deposition problems.

In conclusion, HTT also exhibited the positive outcomes as it lowered the NO emission and improved the slagging and fouling indices. Therefore, the co-combustion of the hydrothermally treated paper sludge could be promising solution to reutilize the waste within the pulp and paper industry effectively.

References

[1] Glarborg P. Fuel nitrogen conversion in solid fuel fired systems. Prog Energ Combust. 2003;29:89-113.

[2] Molina A, Eddings EG, Pershing DW, Sarofim AF. Char nitrogen conversion: implications to emissions from coal-fired utility boilers. Prog Energ Combust. 2000;26:507-31.

[3] Miller JA, Bowman CT. Mechanism and modeling of nitrogen chemistry in combustion. Prog Energ Combust. 1989;15:287-338.

[4] Stubenberger G, Scharler R, Zahirović S, Obernberger I. Experimental investigation of nitrogen species release from different solid biomass fuels as a basis for release models. Fuel. 2008;87:793-806.

[5] Hill SC, Smoot LD. Modeling of nitrogen oxides formation and destruction in combustion systems. Prog Energ Combust. 2000;26:417-58.

[6] Ren Q, Zhao C. NOx and N2O precursors from biomass pyrolysis: nitrogen transformation from amino acid. Environ Sci Technol. 2012;46:4236-40.

[7] Dejong W, Dinola G, Venneker B, Spliethoff H, Wojtowicz M. TG-FTIR pyrolysis of coal and secondary biomass fuels: Determination of pyrolysis kinetic parameters for main species and NOx precursors. Fuel. 2007;86:2367-76.

[8] Yuan S, Zhou Z-j, Li J, Chen X-l, Wang F-c. HCN and NH3Released from Biomass and Soybean Cake under Rapid Pyrolysis. Energ Fuel. 2010;24:6166-71.

[9] Valero A, Cortes C. Ash fouling in coal-fired utility boilers. Monitoring and optimization of on-load cleaning. Prog Energ Combust. 1996;22:189-200.

[10] Vamvuka D, Zografos D. Predicting the behaviour of ash from agricultural wastes during combustion. Fuel. 2004;83:2051-7.

[11] Demirbas A. Potential applications of renewable energy sources, biomass combustion problems in boiler power systems and combustion related environmental issues. Prog Energ Combust. 2005;31:171-92.

[12] Vassilev SV, Baxter D, Vassileva CG. An overview of the behaviour of biomass during combustion: Part II. Ash fusion and ash formation mechanisms of biomass types. Fuel. 2014;117:152-83.

[13] Hongfang C, Peitao Z, Yin W, Guangwen X, Kunio Y. NO Emission Control during the Decoupling Combustion of Industrial Biomass Wastes with a High Nitrogen Content. Energ Fuel. 2013;27:3186-93.

[14] Zhao P, Chen H, Ge S, Yoshikawa K. Effect of the hydrothermal pretreatment for the reduction of NO emission from sewage sludge combustion. Appl Energy. 2013;111:199-205.

[15] Pronobis M. Evaluation of the influence of biomass co-combustion on boiler furnace slagging by means of fusibility correlations. Biomass Bioenerg. 2005;28:375-83.

[16] Pronobis M. The influence of biomass co-combustion on boiler fouling and efficiency. Fuel. 2006;85:474-80.

[17] Carpenter AM. Switching to cheaper coals for power generation. London: IEA Coal Research; 1998.

[18] Vamvuka D, Kakaras E. Ash properties and environmental impact of various biomass and coal fuels and their blends. Fuel Process Technol. 2011;92:570-81.

[19] Tian F-J, Yu J, McKenzie LJ, Hayashi J-i, Li C-Z. Conversion of Fuel-N into HCN and NH3 During the Pyrolysis and Gasification in Steam: A Comparative Study of Coal and Biomass. Energ Fuel. 2007;21:517-21.

[20] Ren Q, Zhao C, Wu X, Liang C, Chen X, Shen J, et al. Effect of mineral matter on the formation of NO_x precursors during biomass pyrolysis. J Anal Appl Pyrol. 2009;85:447-53.

[21] Williams A, Jones JM, Ma L, Pourkashanian M. Pollutants from the combustion of solid biomass fuels. Prog Energ Combust. 2012;38:113-37.

[22] Hansson K-M, Samuelsson J, Tullin C, Åmand L-E. Formation of HNCO, HCN, and NH3 from the pyrolysis of bark and nitrogen-containing model compounds. Combust Flame. 2004;137:265-77.

[23] Zita A, Hermansson M. Effects of Bacterial Cell Surface Structures and Hydrophobicity on Attachment to Activated Sludge Flocs. Appl Environ Microbiol. 1997;63:1168-70.

[24] Liu H, Luo GQ, Hu HY, Zhang Q, Yang JK, Yao H. Emission characteristics of nitrogen- and sulfur-containing odorous compounds during different sewage sludge chemical conditioning processes. J Hazard Mater. 2012;235:298-306.

[25] Lin Y, Munroe P, Joseph S, Kimber S, Zwieten L. Nanoscale organo-mineral reactions of biochars in ferrosol: an investigation using microscopy. Plant Soil. 2012;357:369-80.

[26] Badireddy AR, Korpol BR, Chellam S, Gassman PL, Engelhard MH, Lea AS, et al. Spectroscopic Characterization of Extracellular Polymeric Substances from Escherichia coli and Serratia marcescens: Suppression Using Sub-Ihibitory Concentrations of Bismuth Thiols. Biomacromolecules. 2008;9:3079-89.

[27] Meesuk S, Cao J-P, Sato K, Hoshino A, Utsumi K, Takarada T. Nitrogen Conversion of Pig Compost during Pyrolysis. J Chem Eng Jpn. 2013;46:556-61.

[28] Braghiroli FL, Fierro V, Izquierdo MT, Parmentier J, Pizzi A, Celzard A. Nitrogen-doped carbon materials produced from hydrothermally treated tannin. Carbon. 2012;50:5411-20.

[29] Liao BQ, Lin HJ, Langevin SP, Gao WJ, Leppard GG. Effects of temperature and dissolved oxygen on sludge properties and their role in bioflocculation and settling. Water Res. 2011;45:509-20.

[30] Kruse A, Dinjus E. Hot compressed water as reaction medium and reactant. J Supercrit Fluids. 2007;39:362-80.

[31] Tian Y, Zhang J, Zuo W, Chen L, Cui Y, Tan T. Nitrogen conversion in relation to NH3 and HCN during microwave pyrolysis of sewage sludge. Environ Sci Technol. 2013;47:3498-505.

[32] Zhao L, Baccile N, Gross S, Zhang Y, Wei W, Sun Y, et al. Sustainable nitrogen-doped carbonaceous materials from biomass derivatives. Carbon. 2010;48:3778-87.

[33] Valero A, Cortes C. Ash fouling in coal-fired utility boilers. Monitoring and optimization of on-load cleaning. Prog Energ Combust. 1996;22:198-200.

Chapter 5

Fluidized bed co-combustion of hydrothermally treated paper sludge with two coals of different rank

Abstract: In this chapter, the practical co-combustion test was conducted. Fluidized bed co-combustion of raw paper sludge (Raw-PS) and hydrothermally treated paper sludge (HTT-PS) with either low (Lo-Coal) or high reactivity coal (Hi-Coal) was investigated. The paper sludge was treated in a pilot-scale hydrothermal reactor at 197 °C and 1.9 MPa for 30 minutes. The procedure is the same as in Chapter 2. South African bituminous and Thai subbituminous coals were selected as representative of Lo-Coal and Hi-Coal, respectively. A 110-mm bubbling fluidized bed combustor was used in this study. During the steady combustion tests, the nominal temperature was 850 °C, the fluidization velocity was 0.5 m/s, and the excess air was varied as 20%, 40%, and 60%. Co-combustion tests were conducted by feeding the sludge at the mixing ratio of 30% and 50% (mass basis) with coal. The focus of this study was on NO_x emission and unburned carbon performance. Results showed that at 30% mixing ratio using HTT-PS instead of Raw-PS could reduce NO_x emission by 3–6% and 9–17% in the case of Lo-Coal and Hi-Coal, respectively, and the loss of unburned carbon could be decreased by 15–18% and 36–53% for Lo-Coal and Hi-Coal, respectively. On the whole, the hydrothermally treated paper sludge showed better performance and would be a better choice compared to the original raw paper sludge.

5.1 Background

In our research objective, it has been stated that the hydrothermally treated paper sludge will be co-fired with coals in conventional coal-fired boiler since a large modification is not necessary. To realize this strategy, the fluidized bed combustion (FBC) technology is one of the most suitable combustion technologies [1]. It is well-known that FBC is characterized by excellent fuel flexibility and combustion stability. Thus, a wide range of fuels, including biomass and waste, can be burned in fluidized boilers with a high efficiency. In particular, coal can be partially and conveniently substituted by waste biomass or sludge in the FBC systems. The FBC has uniform temperature distribution and operating at relatively lower temperature; therefore, the problems on slagging and fouling tendency of paper sludge could be alleviated. Moreover, paper sludge originally has low quantities of volatile ash species, such as sulfur, chlorine (no chlorine in the sample in this study) and alkali metals. The onset of bed agglomeration is mostly attributed to the presence of alkali species in the ash of biomass fuels (Na and K). Therefore, it would be no significant vaporization of ash-forming species is suspected to occur. Moreover, from ash composition analysis, the HTT-PS had almost zero percent NaO and very low K_2O that could further reduce the bed agglomeration tendency.

The gas-solid fluidization has variety of application, for example, energy conversion, petrochemical processing, mineral processing, chemical and pharmaceutical, and physical processing [2]. In the field of energy conversion, the FBC technology has been applied to produce steam in fluidized bed boilers. In the boiler, the steam is generated by heat exchanger where heat is generated from burning fuels in gas-solid mixing scheme. The regimes of the FBC is dependent on the physical features and hydrodynamics of the bed material and fuel during the operation. The bubbling fluidized bed (BFB) boiler could be the largest application of fluidized bed. Recently, the first generation fixed bed (stoker-fired) boiler has been replaced by the BFB boiler. The BFB is operating under the bubbling regime [3] and it consists of a furnace, freeboard, and convective heat exchanger. The fuel is mixed and combusted with bed material in the furnace. The open space above the bed is called freeboard and the convective heat exchanger where water in the economizer, superheater, and evaporator is heated is similar to the conventional boiler system. Another type of fluidized bed boiler is circulated fluidized bed (CFB) boiler. In the CFB, fuel is burned under a fast-fluidized bed regime where gas velocity is high enough to blow all the solids out of the furnace [3]. Almost all of the solids are captured and recirculated back to the furnace by gas-solid separator known as a cyclone. Owing to this hydrodynamics regime, the CFB boiler has two sections: the CFB loop and the convective heat exchanger similar to the BFB and other boilers. Since the solids are recirculated back to the furnace, the CFB boilers generally have lower amount of unburned carbon loss leading to a higher combustion efficiency. According to the International Energy Agency, the FBC plant capacities have increased ten times between 1985 and 2010. Now, more than 70 circulating fluidized bed boilers above 300 MWe have been operating all over the world [4].

Recently, the variety of alternative fuels such as biomass and waste have been used as the FBC's additional fuels in co-firing application or even burning individually. Extensive studies on the FBC of biomass and waste such as rice husk [5,6], wood [7,8], sludge [9,10] and others [11,12] have been done. The alternative fuels for FBC generally have high volatile matter (VM) and different characteristics of ash constituents. These distinctions differentiate the combustion process from burning conventional fossil fuels in the FBC such as a solid fuel and VM segregation along and across the furnace, particle fragmentation and attrition associated to a loss of carbon, and different combustion behavior and rate [13]. In this study, the FBC of raw paper sludge (Raw-PS) and hydrothermally treated paper sludge (HTT-PS) and their co-combustion performances with two different types of coals was investigated. The two coals had a different rank, being representative of low and high reactivity coals, respectively. The focus was on the effect of HTT on the NO_x emission, unburned carbon performance in both combustion and co-combustion tests was studied. The combustion efficiency was also evaluated. The combustion/co-combustion conditions in this study are realistic as the excess air is controlled and varied at 20%, 40%, and 60%, which are a common range for solid fuel burning system (20–40%). Moreover,

the feeding system is continuous and the emission sampling is done during the steady state combustion. Therefore, it could be said that this study is relatively practical compared to our previous chapters.

5.2 Materials and methods

5.2.1 Fuel samples

Raw paper sludge (Raw-PS) was provided by the Siam Kraft Industry Co., Ltd., Thailand. A 1-m^3 cylindrical batch-type hydrothermal reactor was utilized to treat Raw-PS at the condition of 197 °C and 1.9 MPa with the holding time of 30 minutes. After the treatment was finished, the residual steam was discharged. Then, the hydrothermally treated paper sludge (HTT-PS) was extracted through drain valves and it was further dewatered by a 1.5 kW centrifugal decanter and naturally dried. The details of the pilot-scale HTT is presented in Chapter 2. The samples were fluffy and this characteristic was problematic for the feeding system of the FBC apparatus, leading to the difficulty to obtain the desired and stable combustion conditions. Therefore, both Raw-PS and HTT-PS were densified by a 5.5 kW pelletizer. The pelletized Raw-PS and HTT-PS were crushed by a lab-scale ball-milling machine. Then, the sludge was sieved at the nominal particle size of 0.3–4 mm. Solid fuel properties of the prepared Raw-PS and HTT-PS, including the proximate and ultimate analysis and the heating value, was analyzed based on standard ASTM procedures and reported in Table 5-1.

Table 5-1 Fuel analysis (dry basis)

	Raw paper sludge (Raw-PS)	Hydrothermally treated paper sludge (HTT-PS)	South African Coal (Lo-Coal)	Thai Coal (Hi-Coal)
		Proximate analysis (%)		
Fixed carbon	8.6	8.3	58.7	41.7
Volatile matter	59.5	55.6	30.2	51.9
Ash	31.9	36.1	11.1	6.4
		Ultimate analysis (%)		
Carbon	33.4	33.2	68.9	64.0
Hydrogen	4.3	4.1	4.0	4.6
Nitrogen	2.9	1.9	1.3	0.6
Sulfur	0.7	0.6	0.6	0.0
Oxygen*	26.9	24.1	14.1	24.4
		Heating value (MJ/kg)		
HHV	12.0	12.3	26.7	25.3
LHV	11.1	11.4	25.8	24.3

*calculated by difference; Lo-Coal: low reactivity coal; Hi-Coal: high reactivity coal

In this study, two different types of coals were utilized. The South African bituminous coal (Lo-Coal) that contains a low amount of volatile matter (30%) is considered as a low reactivity coal whereas the high volatile matter (50%) subbituminous coal (Hi-Coal) provided by the Siam Kraft Industry Co., Ltd., Thailand is representative of high reactivity coals. The coal properties are also presented in Table 5-1. The nominal particle size of coal was 1.18–4 mm.

5.2.2 Bubbling fluidized bed combustor

An atmospheric stainless-steel bubbling fluidized bed combustor was used in this study (Figure 5-1). The internal diameter of the reactor is 110 mm with the height of 2.7 m. It is electrically heated by eight semi-cylindrical ovens with an approximate total power of 20 kW. Air was preheated to the temperature of 600 °C and utilized as the fluidizing gas. Four chromel-alumel thermocouples placed 1 cm protruding from the inner column wall were used to measure the temperature at different heights inside the column. The same type of the thermocouple was also placed 3 cm above the distributor to measure the bed temperature. The temperature set point was kept constant by four PID controllers. The air distributor has a conical shape and it is assembled with a port and a valve at its bottom to rapidly discharge the bed material and bottom ash. The distributor bears 12 cylindrical diffusers with four nozzles each at right angle. Fine particles generated during combustion and elutriated in the outlet gas were collected by using a high efficiency cyclone. Fuel was continuously fed under-bed through a feeding system consisting of a charge hopper, a measurement hopper, and a screw. The screw is used as the fuel feeder as well as a metering device. It is coupled with a cylindrical chamber where the particles, fed by the screw, are pneumatically injected into the bed by a secondary air stream. The fuel feed rate is varied by increasing the rotational velocity of the screw. The fuel feeding rate was evaluated by measuring the emptying time of the measurement hopper with a weighed batch of fuel. On-line gas sampling at the cyclone exit was performed to analyze the flue gas composition. The measurement system consisted of a portable Madur Photon gas analyzer which monitored the outlet concentration of O_2 (0–25%v), CO (0–2%v), CO_2 (0–25%v), NO (0–5000 ppmv) and NO_2 (0–1000 ppmv). A data acquisition unit was used to process signals from the pressure transducers, from the thermocouples and from the on line gas analyzers. Further details of the apparatus can be found in [14].

The reactor was charged with 5 kg of 400–600 μm quartzite (sand) as bed material, corresponding to a bed height of about 0.4 m at minimum fluidization conditions (U_{mf} = 0.085 m/s @ 850 °C). The fluidizing air was fed to the column via high-precision digital mass flow meters. The experiments were carried out at the fluidization velocity of 0.5 m/s. After the bed temperature reached 850 °C, all the heaters were switched off and the bed temperature was controlled by means of an internal water-cooled coil. Each batch of prepared fuel was charged to the hopper and fed to the reactor by the screw feeder. For co-combustion tests, the fuels were thoroughly mixed according to the scheduled mass percentage

before supplying to the hopper. The excess air of combustion/co-combustion tests was varied as 20, 40, and 60%. The experimental conditions are summarized in Table 5-2.

5.2.3 Fly ash collection

Once steady state combustion was reached, for each excess air level, the fly ash collecting process started. The steady state combustion was maintained long enough to collect sufficient amount of fly ash for further analysis. After the test was finished, the elutriated fines were weighed and the particle size distribution was measured by a laser light scattering granulometer, Malvern Instruments Mastersizer 2000. Unburned carbon (UC) in fly ash was also measured by a Leco (CHN) analyzer.

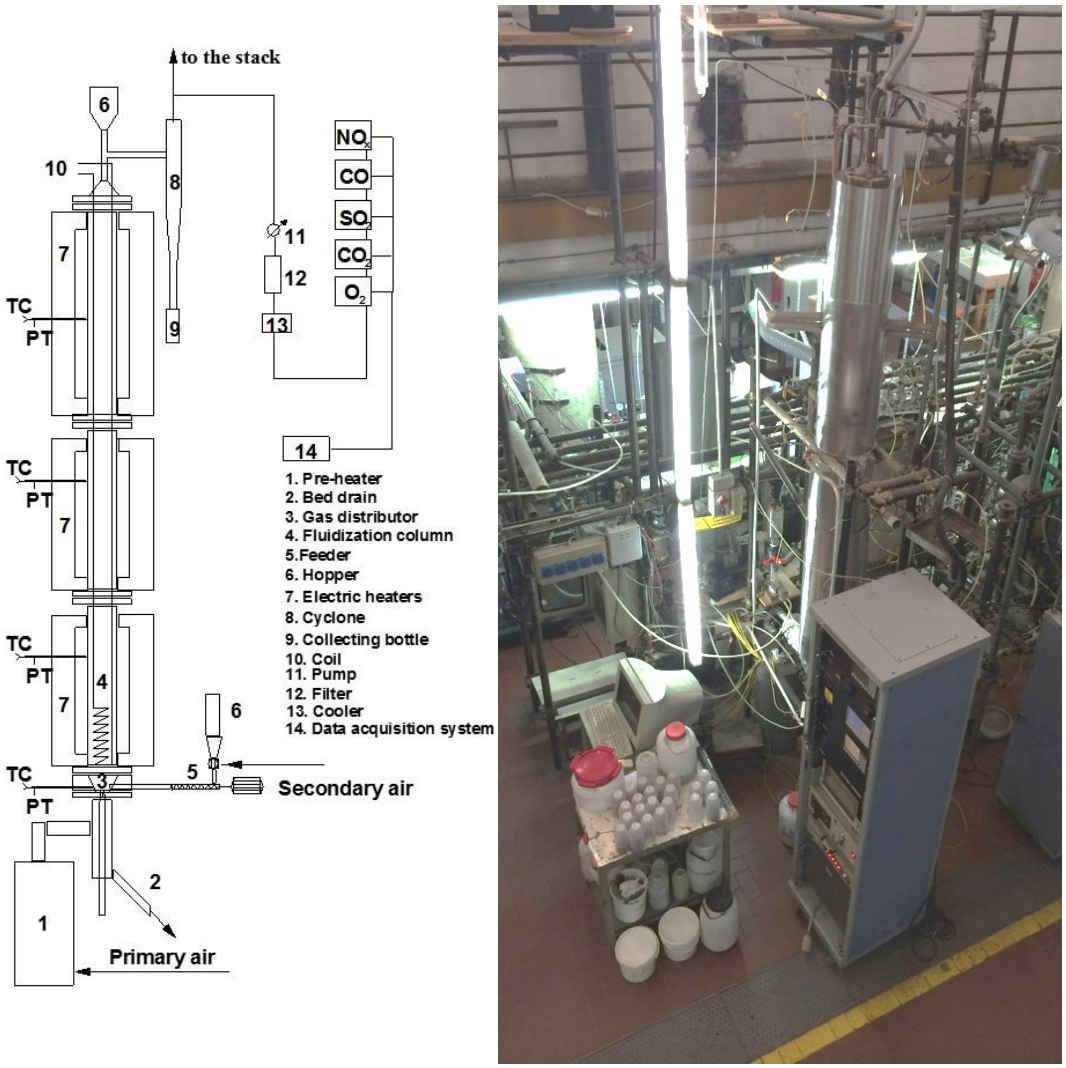

Figure 5-1 The 110 mm ID stainless steel fluidized bed combustor

Table 5-2 Summary of experimental conditions

Experimental condition	
fuel	
Raw paper sludge (Raw-PS)	pelletized and crushed; average size: 0.3–4 mm.
Hydrothermally treated paper sludge (HTT-PS)	pelletized and crushed; average size: 0.3–4 mm.
Low reactivity coal (Lo-Coal)	crushed; average size: 1.18–4 mm.
High reactivity coal (Hi-Coal)	crushed; average size: 1.18–4 mm.
Apparatus	
Combustor	atmospheric bubbling bed
Internal diameter	110 mm.
Height	2700 mm.
Feeding system	continuous under-bed
Fluidizing gas	preheated air
Bed material	5 kg of sand, 400–600 μm.
Fluidization velocity	0.5 (±0.2) m/s
Combustion temperature	850–880 ˚C
Excess air	20, 40, 60 (±0.2)%
Measured emissions	NO_x (NO, NO_2), CO, CO_2

5.3 Results and discussion

5.3.1 Feeding stability

Figure 5-2 shows the O_2 profiles from typical combustion tests of non-pelletized and pelletized Raw-PS, for comparison. Similar profiles were obtained with HTT-PS. It was clearly observed that the profile for non-pelletized Raw-PS was very unsteady and very high peaks of O_2 (and CO) were usually detected due to the unstable combustion process. The improper sludge feeding led to a difficulty to maintain the desired combustion conditions as well as an unacceptable fluctuation of the emission profiles. Very similar feeding problems were reported by Boavida et al. [15] for non-recyclable paper and plastic waste during fluidized bed co-combustion tests with coal. These authors found that the form in which the fuel was fed to the combustor made a significant contribution to achieve desirable combustion performance. They reported that fuel densification was able to solve their combustion instability problem.

Therefore, in this work, the original fluffy Raw-PS and HTT-PS were pelletized before testing. Feeding of the pelletized (and crushed) sludge was much more stable and the combustion process was much smoother, as can be observed in Figure 5-2. So, only pelletized sludge was used in the tests performed in this work and reported hereinafter.

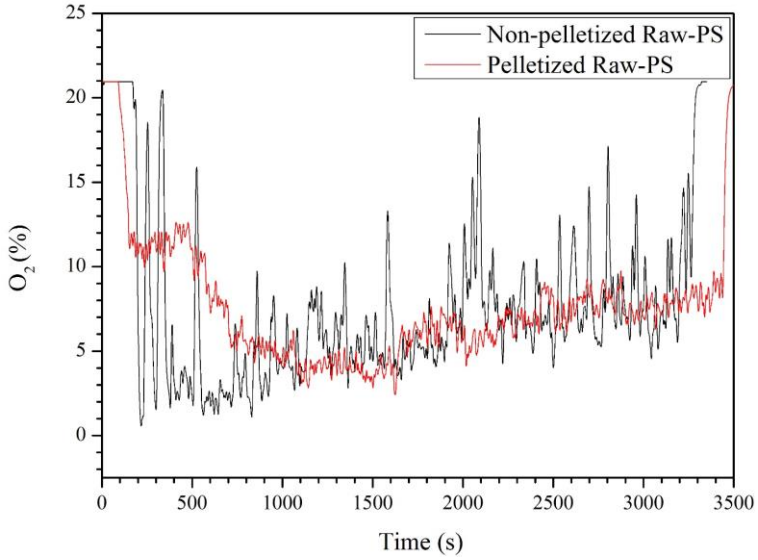

Figure 5-2 Comparison of O_2 profiles from non-pelletized and pelletized Raw-PS feeding during combustion test.

5.3.2 NO_x emission

Table 5-3 reports a summary of the operating variables and emissions from the combustion and co-combustion tests as a function of the excess air. To control the excess air, the feeding rate was adjusted until the desired condition was stably reached. At each steady state condition, CO, CO_2 and unburned carbon were measured and the total combustion efficiency was calculated (accounting for both CO emission and unburned carbon in fly ash). Both NO and NO_2 were measured, but NO_2 was always much lower than NO and almost zero in most cases. In the following, only the total NO_x (= NO + NO_2) emission will be reported. To better clarify the effect of the fuel mixture feeding on the NO_x emission, the reported NO_x values were all collected in the same range of CO concentrations in the flue gas (30–60 ppm). In fact, it was noted that the CO concentration, as representative of the effective oxidizing/reducing conditions in the fluidized bed, had a non-negligible effect on the NO_x level. This effect was most likely due to the catalytic reduction of NO_x by reaction with CO and/or char surface, especially at the low excess air conditions where several high peaks of CO were occasionally observed [16,17].

5.3.2.1 Individual fuel combustion

Figure 5-3a reports the average NO_x emission from the individual fuel combustion tests as a function of the excess air. The NO_x emission increased with the amount of excess air in the case of both Raw-PS and HTT-PS. This result suggests that a higher concentration of oxygen in this case leads to a better combustion environment for volatile matter and char in the fluidized bed, thus leading to the increase of NO_x. On the other hand, the NO_x emission from Lo-Coal and Hi-Coal combustion tests were found to be strongly dependent on the type of coal, not so much on the excess air. It is likely that the larger

fuel-N content in Lo-Coal, compared to Hi-Coal, contributes to the higher NO_x emission. Since the fuel-N conversion to NO_x depends on the nitrogen structure in coals, the characterization of the nitrogen functional groups in various types of coal was investigated by Kambara et al. [18]. The source of nitrogen in coal consists mainly in pyrrolic (five rings), pyridinic (six rings), and quaternary functionalities [18,19].

Obviously, the origin of the fuel-N in biomass and sludge is different from that of coals. The major source of nitrogen in biomass comes from proteins and amino acids and this difference could affect the conversion of the fuel-N during devolatilization and combustion [20,21]. After HTT, the fuel-N in HTT-PS was found to be significantly lower than that of Raw-PS.

Based on our previous investigation, it could be said that HTT is able to decompose or to dissolve the nitrogen-containing compound in paper sludge, which is mainly protein [22]. However, the observable NO_x reduction was limited, especially at 20% excess air condition. The NO_x decrease was enhanced at 40% and 60% excess air presenting approximately 4–7% reduction. Therefore, the correlation between the NO_x emission and nitrogen in fuel cannot be interpreted solely from the ultimate analysis.

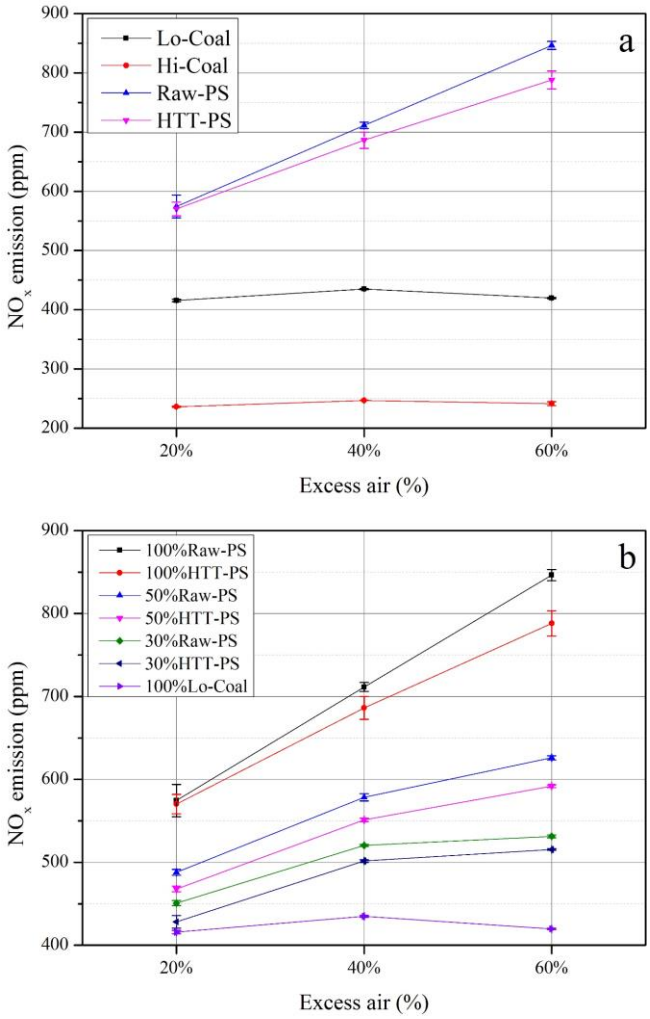

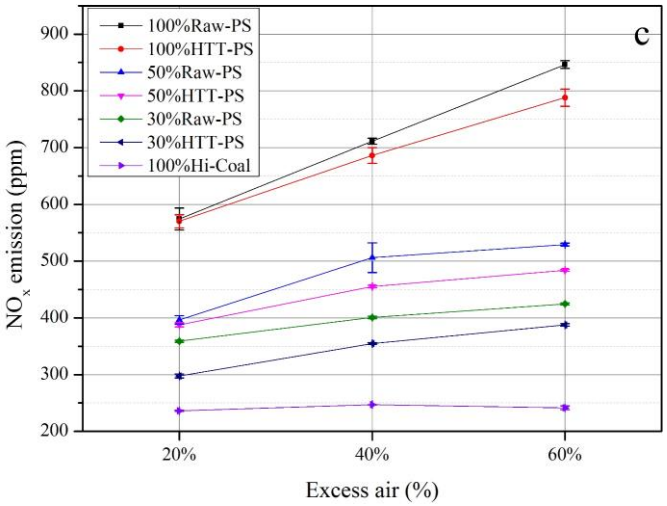

Figure 5-3 Average NO_x emission (ppm): (a) combustion; (b) co-combustion with low reactivity coal; (c) co-combustion with high reactivity coal. (Raw-PS: raw paper sludge; HTT-PS: hydrothermally treated paper sludge; Lo-Coal: low reactivity coal; Hi-Coal: high reactivity coal)

5.3.2.2 Co-combustion tests

Figure 5-3b illustrates the average NO_x emission from the co-combustion tests of Raw-PS and HTT-PS with Lo-Coal. Also in this case, the NO_x emission from the mixture increased as the amount of the excess air was higher. When mixing HTT-PS instead of Raw-PS, the NO_x could be reduced by 3–6%.

In general, the excess air of a fluidized bed coal combustor is controlled at around 20–25% [23,24]. Thus, we analyzed into more detail on the results obtained at these excess air conditions. From Table 5-3, at 20% excess air, the average NO_x from 30% HTT-PS was 428 ppm while burning pure Lo-Coal generated slightly lower amount of NO_x (416 ppm). It can be seen that the NO_x produced from 30% HTT-PS was comparable to the 100% Lo-Coal at 20% excess air. Therefore, adding HTT-PS at a share ≤ 30% to the Lo-Coal burning system could save the amount of fossil fuels without any aggressive drawback on the NO_x emission performance.

The average NO_x emission from co-combustion of Raw-PS and HTT-PS with Hi-Coal are shown in Figure 5-3c. It was clearly observed that the NO_x produced from Raw-PS and HTT-PS was significantly higher than from the Hi-Coal. However, the mixture of HTT-PS and Hi-Coal presented lower NO_x emission. At the mixing ratio of 30%, the NO_x from HTT-PS mixture was lower than that from Raw-PS mixture by 17.1%, 11.4% and 8.7% at 20%, 40% and 60% excess air, respectively. When increasing the mixing ratio to 50%, approximately the same value of NO_x reduction was obtained at the high excess air levels, 40% and 60%. However, at 20% excess air, the NO_x reduction was only 2.1% showing a limitation on the amount of sludge that can be mixed with Hi-Coal.

Even though adding HTT-PS instead of Raw-PS to the low-rank Hi-Coal firing system would help decreasing the NO_x emission, it still generated significantly higher amounts of NO_x when compared to

pure burning of Hi-Coal. Therefore, considering the NO_x emission performance, a compromise between the amount of HTT-PS addition to the Hi-Coal and the consequences on NO_x emission need to be found.

Finally, it can be observed that in the co-combustion tests, the NO_x emission generally show a linear behavior with the share percentage of the sludge in the fuel mixture. In other word, there was no synergetic effect occurring by mixing Raw-PS or HTT-PS to either Lo-Coal or Hi-Coal in the co-combustion tests. Thus, NO_x emission from the co-combustion of the sludge with these two types of coal at different fuel shares can be safely estimated by linear interpolation of the results reported in Figures 5-3b and 5-3c.

5.3.3 CO emission

Table 5-3 also reports the average CO emission measured in combustion and co-combustion tests. It was observed that Raw-PS and HTT-PS exhibited significantly higher CO emission compared to coals, especially at 20% excess air. It has to be noted that an irregular fuel feeding would strongly affect the measured CO levels because of the difficulty to maintain a constant air/fuel ratio in the combustor [15,25]. These evidences were found during the combustion of Raw-PS and HTT-PS even though they were pelletized before being sieved to the specific size. Moreover, from the feeding rate data, it was observed that the feeding rates of Raw-PS and HTT-PS were higher than that of coal because the carbon content and the heating value of those fuels are lower. It means that larger amounts of Raw-PS and HTT-PS had to be fed to the bed per unit time in order to maintain the desired air/fuel ratio and this would also contribute to the higher levels of CO due to the formation of fuel-rich zones in the fluidized bed (mainly due to the large volumes of volatile matter emitted by these fuels). Additionally, it was suggested that due to the density and size differences between sludge and bed material, the sludge particles would mostly float on the bed surface, so that most of the particle drying and devolatilization would occur there [9]. Thus, the presence of fuel-rich zones might contribute to the higher CO concentrations of Raw-PS and HTT-PS during combustion at low excess air conditions. The value of the average CO emission from Raw-PS and HTT-PS were around 703–753 ppm at 20% excess air. The amount of CO was substantially affected by the excess air as its concentration significantly decreased to approximately 139–246 ppm and 35–48 ppm at 40% and 60% excess air, respectively. The average CO emission from Lo-Coal and Hi-Coal were 79 and 196 ppm at 20% excess air, respectively. At the higher excess air, the CO emission of Lo-Coal was slightly reduced to 43–46 ppm while a drastic influence of the excess air was observed in the case of Hi-Coal since the CO emission was reduced to 4–6 ppm. At 20% excess air, it is likely that high volatile matter fuels would generate higher amounts of CO as observed in Raw-PS, HTT-PS, and Hi-Coal regardless of the feeding rate variation. This might be due to mixing limitations in the fluidized bed since high volatile matter fuels often produce high concentrations of unburned gases [26].

Table 5-3 Operating variables and emissions from combustion/co-combustion of raw (Raw-PS) and hydrothermally treated paper sludge (HTT-PS) with low (Lo-Coal) and high (Hi-Coal) reactivity coals.

Excess air (%)	Samples	Feeding rate (g/h)	NO_x (ppm)	CO (ppm)	Unburned carbon (g/h)	Combustion efficiency (%)
Individual combustion						
20	Raw-PS	1311	575	753	0.94	99.3
	HTT-PS	1168	570	703	0.26	99.5
	Lo-Coal	543	416	79	3.00	99.1
	Hi-Coal	748	236	196	0.23	99.8
40	Raw-PS	1125	711	139	0.89	99.6
	HTT-PS	1004	686	246	0.22	99.7
	Lo-Coal	463	435	46	1.90	99.3
	Hi-Coal	640	247	4	0.20	99.9
60	Raw-PS	992	846	48	0.77	99.7
	HTT-PS	883	788	35	0.21	99.9
	Lo-Coal	406	420	43	1.34	99.5
	Hi-Coal	555	242	6	0.16	99.9
Co-combustion of 30% paper sludge with 70% low reactivity coal by mass						
20	Raw-PS	645	451	92	3.57	98.9
	HTT-PS	623	428	116	2.87	99.1
40	Raw-PS	552	520	46	1.74	99.4
	HTT-PS	536	502	47	1.56	99.4
60	Raw-PS	481	531	40	1.21	99.5
	HTT-PS	464	515	43	1.22	99.5
Co-combustion of 50% paper sludge with 50% low reactivity coal by mass						
20	Raw-PS	763	488	392	2.93	98.9
	HTT-PS	729	468	34	2.84	99.2
40	Raw-PS	654	578	49	1.55	99.4
	HTT-PS	629	551	40	1.87	99.3
60	Raw-PS	568	626	43	1.26	99.5
	HTT-PS	547	592	36	1.12	99.5
Co-combustion of 30% paper sludge with 70% high reactivity coal by mass						
20	Raw-PS	947	359	173	0.54	99.8
	HTT-PS	902	298	212	0.34	99.8
40	Raw-PS	816	401	20	0.50	99.8
	HTT-PS	769	355	33	0.23	99.9
60	Raw-PS	714	425	21	0.20	99.9
	HTT-PS	674	388	14	0.11	99.9
Co-combustion of 50% paper sludge with 50% high reactivity coal by mass						
20	Raw-PS	975	396	511	1.01	99.4
	HTT-PS	895	388	51	0.29	99.9
40	Raw-PS	839	506	18	0.46	99.9
	HTT-PS	773	455	24	0.26	99.9
60	Raw-PS	741	529	19	0.48	99.8
	HTT-PS	679	484	22	0.25	99.9

From 30% share co-combustion tests of sludge and coal at 20% excess air, the CO emission of HTT-PS mixture were not significantly different from those of Raw-PS since most of the mixture was composed by coal. However, when increasing the share of Raw-PS and HTT-PS to 50%, it was observed that HTT-PS showed better combustion performance than Raw-PS, as the CO emission were significantly lower.

5.3.4 Unburned carbon

5.3.4.1 Individual fuel combustion

Figure 5-5a reports the unburned carbon (UC) measured in the fly ash from individual fuel combustion tests. UC was normalized with the carbon feeding rate, i.e. it is reported as g of UC per g of carbon fed. This way of reporting UC is considered to be more appropriate to compare the effect of HTT on UC regardless of the feeding characteristics. For completeness, the results of unburned carbon (UC) in fly ash were also calculated in terms of g/h flow rate at the exhaust as summarized in Table 5-3. It can be clearly observed in Figure 5-5a that Lo-Coal exhibited the highest amount of UC due to its low reactivity while Hi-Coal showed the lowest amount of UC. With the increase of excess air, UC significantly reduced in case of Lo-Coal. Generally, adding more air to the combustion system would enhance the char combustion rate since more oxygen is supplied and more vigorous motion of the bed is generated. Therefore, the UC reduction can be easily explained. A similar finding was also reported in a circulating FBC experimental campaign [24]. On the other hand, the influence of the excess air on UC for Raw-PS, HTT-PS and Hi-Coal tests was less significant. The most likely reason for this result is that these three fuels are much more reactive than Lo-Coal, so that the excess air should have a lower effect on the combustion rate. When comparing UC from burning pure HTT-PS and Raw-PS, the UC from the former was significantly lower and it was also very similar to the UC from combustion of Hi-Coal. Figure 5-5a clearly illustrates this result. HTT-PS presented 72%, 76%, and 73% reduction in UC compared to the raw sludge at 20%, 40%, and 60% excess air, respectively. The effect of HTT on the improvement of UC performance was dramatic. In order to explain this result, both physical and chemical aspects of HTT-PS have to be taken to account. Regarding the physical characteristic, it was clearly observed that the structure of HTT-PS is more uniform than that of Raw-PS, as shown in the appearance and SEM analysis from our previous study [27]. On the other hand, a kinetic study of combustion of the two fuels showed that the apparent activation energy of HTT-PS was lower than that of Raw-PS [28]. This evidence suggests that HTT-PS is likely to be more reactive than Raw-PS.

5.3.4.2 Co-combustion tests

Figure 5-5b shows the UC generated from the co-combustion tests of Raw-PS and HTT-PS with Lo-Coal. It was clearly observed that the characteristics of the UC from the mixtures were controlled by Lo-Coal. For example, UC was significantly affected by the excess air since the mixture became less reactive. Then, when the excess air increased, UC was reduced. This was not observed during the

individual fuel combustion of Raw-PS and HTT-PS. Burning 30% Raw-PS with 70% Lo-Coal at 20% excess air showed that UC increased possibly due to the poor physical properties of Raw-PS. Once switching from Raw-PS to HTT-PS, results showed a better UC performance. The reduction of UC by adding HTT-PS was limited due to the low amount of excess air. However, when increasing the excess air to 40%, it was observed that the UC from the 30% mixture of HTT-PS showed 15.4% and 18.4% reduction with respect to the UC from 100% Lo-Coal combustion and 30% Raw-PS mixture, respectively. For 60% excess air, UC was further reduced and HTT-PS mixture showed better UC performance than for Raw-PS. Therefore, mixing portions of HTT-PS to Lo-Coal firing system or changing the mixture from Raw-PS to HTT-PS would significantly help reducing the loss of carbon during the combustion process.

Figure 5-5c shows the UC from co-combustion of Raw-PS and HTT-PS with Hi-Coal. It was clearly observed that HTT-PS and its mixture with Hi-Coal showed similar levels of UC as for Hi-Coal. The variation of the excess air had no significant influence on the UC from these samples since they were originally reactive. The reduction of UC by mixing HTT-PS instead of Raw-PS was substantial. At 30% mixing ratio, the UC reduction was 35.5%, 52.6% and 41.7% at the excess air of 20%, 40% and 60% excess air, respectively. In case of 50% mixing ratio, the decrease in UC was 70%, 40.6% and 45.9 % when burning at the excess air of 20%, 40% and 60%, respectively. A possible synergetic effect of mixing the two highly reactive fuels was observed when burning 30% HTT-PS mixture at 60% excess air. The UC from this mixture was even lower than the UC from burning 100% Hi-Coal.

5.3.5 Combustion efficiency

Table 5-3 shows the combustion efficiency values for all the combustion and co-combustion tests. The combustion efficiency was higher than 99% for most of the tests. In more detail, the combustion efficiency of HTT-PS was slightly higher than that of Raw-PS, especially at 20% excess air. Hi-Coal showed the highest combustion efficiency regardless of the excess air. Generally, the primary source of combustion loss in a fluidized bed is unburned carbon in fly ash. This variable is strongly dependent on the reactor configuration as well as operating conditions such as fuel loading, combustion modes, and excess air conditions [2,11,24]. The present combustor has a high freeboard height (FBH) which is about 2.1 m above the surface of the expanded bed at 850 °C, and it is significantly higher than the transport disengagement height (TDH) which is estimated to be approximately 0.6 m at the operating conditions of the tests, according to the experimental TDH results reported by Fung and Hamdullahpur [29]. In addition, the (empty-tube) gas residence time in the combustion chamber at the present operating conditions is about 5.4 s. Therefore, the amount of unburned carbon was anticipated to be relatively low.

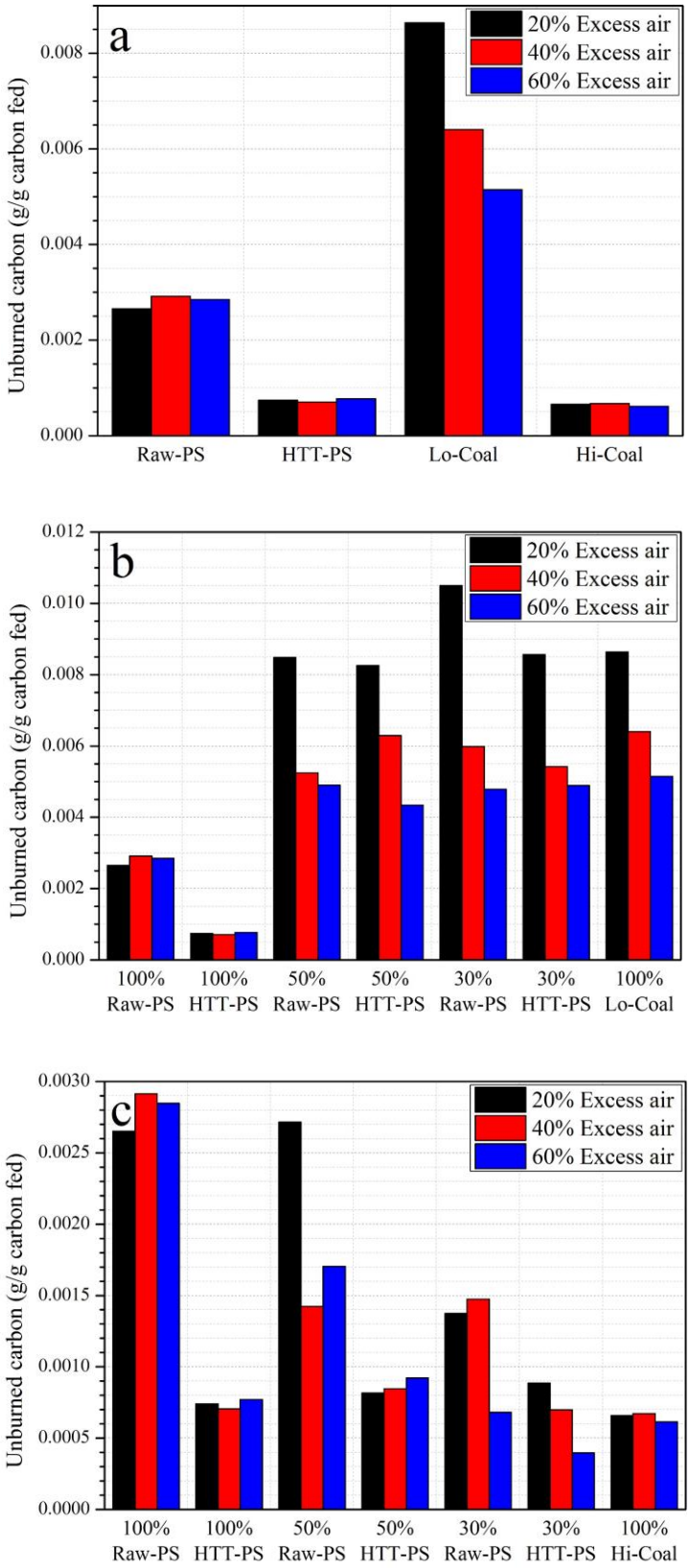

Figure 5-5 Unburned carbon (g per g carbon fed): (a) combustion; (b) co-combustion with low reactivity coal; (c) co-combustion with high reactivity coal. (Raw-PS: raw paper sludge; HTT-PS: hydrothermally treated paper sludge; Lo-Coal: low reactivity coal; Hi-Coal: high reactivity coal)

5.3.6 Ash particle size distribution

In this study, fly ash collection was performed by capturing the elutriated particles in the high efficiency cyclone during steady combustion conditions. Figure 5-6a presents the cumulative particle size distribution (CPSD) results from the single fuel combustion tests for all excess air. The profiles of the CPSD of all the tests were very similar, and the excess air had no particular effect. For example, the mean surface-volume diameter (d_{32}) of Lo-Coal and Hi-Coal averaged from all excess air conditions was 6.4±0.3 and 6.4±0.4 μm, respectively. In the case of Raw-PS and HTT-PS, the average of d_{32} was 7.5±0.3 and 7.9±1.3 μm, respectively. The mean surface-volume diameter of the ash from paper sludge combustion in this study was similar to the results from sewage sludge combustion performed by Cammarota et al [14]. The fly ash particle size distribution in these tests is most likely determined by the interplay of two variables: the gas fluidization velocity (which dictates the maximum elutriable particle size from the bed) and by the cyclone cut-size.

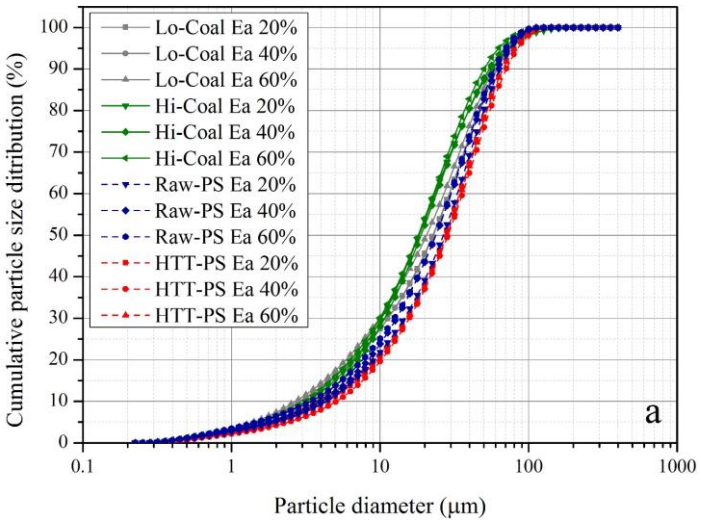

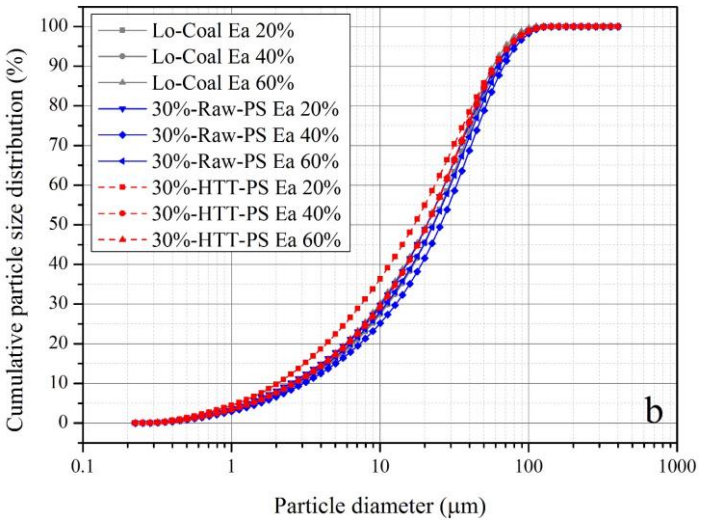

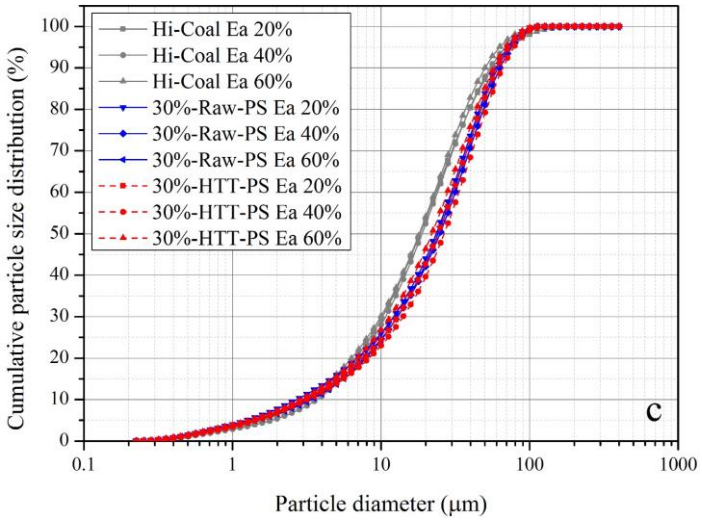

Figure 5-6 Cumulative particle size distribution: (a) combustion; (b) co-combustion with low reactivity coal; (c) co-combustion with high reactivity coal. (Raw-PS: raw paper sludge; HTT-PS: hydrothermally treated paper sludge; Lo-Coal: low reactivity coal; Hi-Coal: high reactivity coal)

Figure 5-6b and 5-6c show CPSD of the paper sludge co-combustion with the two types of coal as a function of the excess air. Similar results were found, as the variation of the excess air did not significantly affect the size of the fly ash. The average d_{32} from all of the co-combustion tests, including 30% and 50% paper sludge mixtures of all excess air conditions, was 6.4±0.2 μm. It is likely that the mean surface-volume diameter of the fly ash from coal dominated the characteristic of the fly ash in the mixture.

5.4 Conclusion

The co-combustion of raw paper sludge (Raw-PS) and hydrothermally treated paper sludge (HTT-PS) with low (Lo-Coal) and high reactivity (Hi-Coal) coals was investigated by using a bubbling fluidized bed combustor. The focus of the work was on NO_x emission and unburned carbon (UC) performance. The NO_x emission could be reduced by using HTT-PS instead of Raw-PS in co-combustion application with both Lo-Coal and Hi-Coal. It can be concluded as follows:

1. Adding HTT-PS at a share lower or equal than 30% to the conventional Lo-Coal combustion system (burning at 20% excess air) could lower the cost of the fossil fuels without any detrimental effect on the NO_x emission.

2. The UC performance of HTT-PS showed 72% reduction at 20% excess air compared to that from Raw-PS. This improvement also helped decreasing the loss of carbon in the fluidized bed

combustion of Lo-Coal and Hi-Coal when switching from the original paper sludge to the treated one.

3. The particle size distribution of fly ash of all fuels and their mixture was similar regardless of the variation of the excess air.

Therefore, HTT-PS could be used in the co-combustion with either Lo-Coal or Hi-Coal without worsening the current performance on the NO_x emission, while the unburned carbon performance would be improved.

References

[1] Scala F. Fluidized bed technologies for near-zero emission combustion and gasification. Cambridge, UK: Woodhead Publishing; 2013.

[2] Basu P. Combustion and gasification in fluidized beds: CRC press; 2006.

[3] Kunii D, Levenspiel O. Fluidization engineering: Elsevier; 2013.

[4] Energy Technology Initiatives 2013 Implementation through Multilateral Co-operation. International Energy Agency; 2013.

[5] Armestoa L, Bahilloa A, Veijonenb K, Cabanillasa A, Oteroa J. Combustion behaviour of rice husk in a bubbling uidised bed. Biomass Bioenerg. 2002;23:171-9.

[6] Fang M, Yang L, Chen G, Shi Z, Luo Z, Cen K. Experimental study on rice husk combustion in a circulating fluidized bed. Fuel Process Technol. 2004;85:1273-82.

[7] Lyngfelt A, Leckner B. Combustion of wood-chips in circulating fluidized bed boilers—NO and CO emissions as functions of temperature and air-staging. Fuel. 1999;78:1065-72.

[8] Leckner B, Karlsson M. Gaseous emissions from circulating fluidized bed combustion of wood. Biomass Bioenerg. 1993;4:379-89.

[9] Ogada T, Werther J. Combustion characteristics of wet sludge in a fluidized bed: release and combustion of the volatile. Fuel. 1996;75:617-26.

[10] Shin D, Jang S, Hwang J. Combustion characteristics of paper mill sludge in a lab-scale combustor with internally cycloned circulating fluidized bed. Waste Manag. 2005;25:680-5.

[11] Permchart W, Kouprianov VI. Emission performance and combustion efficiency of a conical fluidized-bed combustor firing various biomass fuels. Bioresour Technol. 2004;92:83-91.

[12] Suksankraisorn K, Patumsawad S, Fungtammasan B. Combustion studies of high moisture content waste in a fluidised bed. Waste Manag. 2003;23:433-9.

[13] Chirone R, Salatino P, Scala F, Solimene R, Urciuolo M. Fluidized bed combustion of pelletized biomass and waste-derived fuels. Combust Flame. 2008;155:21-36.

[14] Cammarota A, Chirone R, Salatino P, Solimene R, Urciuolo M. Particulate and gaseous emissions during fluidized bed combustion of semi-dried sewage sludge: effect of bed ash accumulation on NO_x formation. Waste Manag. 2013;33:1397-402.

[15] Boavida D, Abelha P, Gulyurtlu I, Cabrita I. Co-combustion of coal and non-recyclable paper and plastic waste in a fluidised bed reactor. Fuel. 2003;82:1931-8.

[16] Werthera J, Saengera M, Hartgea E-U, Ogadab T, Siagib Z. Combustion of agricultural residues. Prog Energ Combust. 2000;26:1-27.

[17] Molina A, Eddings EG, Pershing DW, Sarofim AF. Char nitrogen conversion: implications to emissions from coal-fired utility boilers. Prog Energ Combust. 2000;26:507-31.

[18] Kambara S, Takarada T, Toyoshima M, Kato K. Relation between functional forms of coal nitrogen and NO_x emissions from pulverized coal combustion. Fuel. 1995;74:1247-53.

[19] Glarborg P. Fuel nitrogen conversion in solid fuel fired systems. Prog Energ Combust. 2003;29:89-113.

[20] Ren Q, Zhao C, Wu X, Liang C, Chen X, Shen J, et al. Effect of mineral matter on the formation of NO_x precursors during biomass pyrolysis. J Anal Appl Pyrol. 2009;85:447-53.

[21] Liu H, Luo GQ, Hu HY, Zhang Q, Yang JK, Yao H. Emission characteristics of nitrogen- and sulfur-containing odorous compounds during different sewage sludge chemical conditioning processes. J Hazard Mater. 2012;235:298-306.

[22] Areeprasert C, Chanyavanich P, Ma D, Shen Y, Prabowo B, Yoshikawa K. An investigation on co-combustion of hydrothermally treated paper sludge with coal by thermogravimetric analysis and fixed bed combustor. Appl Energy. 2015:submitted.

[23] Babcock, Company W, Stultz SC, Kitto JB. Steam: its generation and use: Babcock & Wilcox; 1992.

[24] Xiao X, Yang H, Zhang H, Lu J, Yue G. Research on Carbon Content in Fly Ash from Circulating Fluidized Bed Boilers. Energ Fuel. 2005;19:1520-5.

[25] Gulyurtlu I, Abelha P, Boavida D, Lopes H, Cabrita I. Consideration for mixing different biomass fuels and non-toxic waste during fluidised bed combustion. 2nd World Conference on Biomass for Energy, Industry and Climate Protection. Rome, Italy2004. p. 1297-300.

[26] Leckner B, Åmand LE, Lücke K, Werther J. Gaseous emissions from co-combustion of sewage sludge and coal/wood in a fluidized bed. Fuel. 2004;83:477-86.

[27] Areeprasert C, Zhao P, Ma D, Shen Y, Yoshikawa K. Alternative Solid Fuel Production from Paper Sludge Employing Hydrothermal Treatment. Energ Fuel. 2014;28:1198-206.

[28] Areeprasert C, Chanyavanich P, Ma D, Shen Y, Prabowo B, Yoshikawa K. Combustion characteristics and kinetics study of hydrothermally treated paper sludge by thermogravimetric analysis. Biofuels. 2015:in press.

[29] Fung AS, Hamdullahpur F. Effect of bubble coalescence on entrainment in gas fluidized beds. Powder Technol. 1993;77:251-65.

Chapter 6

Effect of hydrothermal treatment on primary fragmentation and attrition phenomena during fluidized bed combustion of paper sludge

Abstract: In Chapter 6, the effect of HTT on fluidized bed combustion of paper sludge focusing on essential particle comminution phenomena, i.e., the primary fragmentation and the char particle attrition, were investigated. This chapter explains the important findings in Chapter 5, i.e., the reduction of unburned carbon by HTT. The systematic combination of experimental techniques were carried out to test raw paper sludge (Raw-PS), hydrothermally treated papers sludge (HTT-PS), and subbituminous coal (Sub-C). The results showed that all three samples extensively underwent the primary fragmentation. From the char particle attrition, the Sub-C intensely experienced particle rounding off and, after that, became very strong against mechanical abrasive attrition followed by HTT-PS and Raw-PS. It was clearly observed from the oxidative attrition test that Sub-C exhibited postcombustion of fines and resulted in significantly lower amount of the elutriation rate whereas Raw-PS and HTT-PS went through a combustion-assisted attrition leading to higher amount of generated fines. In both cases, HTT-PS showed lower amount of fine particles than the original material indicating better combustion performance. Furthermore, CO_2 profile from the oxidative attrition test implied that the combustion of HTT-PS completed significantly earlier than the other fuels showing its superior burnout performance.

6.1 Background

In the previous chapter, the fluidized bed combustion (FBC) which is viable technology and has been using worldwide for energy recovery [1-3] has been successfully implemented to paper sludge in combustion and co-combustion applications. The interesting finding is a significantly better unburned carbon performance for the hydrothermally treated paper sludge (HTT-PS) compared to the raw paper sludge (Raw-PS). This result is substantial when ones consider switching from using Raw-PS to HTT-PS since the loss of carbon can be reduced. The implementation can also be used in both conventional low and high reactivity coal-firing systems. Consequently, an investigation on the essential phenomena during the FBC has to be done.

The particle fragmentation and attrition phenomena is an interactive process occurring during the FBC and plays very important roles. An exploitation of tiny particles by attrition not only affects fuel particle conversion and mass and heat transfer coefficients, but also causes a loss of carbon through elutriation [4]. Moreover, it also has an impact on other combustion aspects [5], e.g., time and temperature history of char particles [6,7] and gaseous emission due to the change of the axial distribution of char along the combustor [8]. Therefore, an investigation on the fragmentation and attrition phenomena are indispensable in the FBC application.

After injection of a fuel particle into the fluidized bed, it will be subjected to a series of particle fragmentation and attrition phenomena known as a particle comminution. This includes the primary fragmentation during devolatilization, the char particle attrition by abrasion and combustion, the secondary fragmentation, and the percolative fragmentation. The studies on the fuel particle comminution have been done on biomass and waste fuels by many researchers [5,9-12]. These alternative fuels contain high VM that affects the particle comminution phenomena in the FBC. Based on the study on combustion and attrition phenomena of different kinds of biomass char during the FBC investigated by Scala et al., they concluded that the primary and secondary fragmentation were dependent on the type of biomass and these phenomena strongly affect the average particle size and particle size distribution of fuel in the fluidized bed [10]. Chirone et al. performed the systematic characterization of fuel properties for three different types of pelletized biogenic fuels during the FBC and found that three fuels exhibited different and distinctive combustion patterns mostly depending on the amount and the property of ash in each fuel [5]. Two different types of sewage sludge have been subjected to the full attrition test in the FBC performed by Cammarota et al., and they found that the different origins and preprocessing that the sludge underwent moderately affected the fragmentation and attrition [11]. These previous studies gave us a conclusion that the fragmentation and attrition phenomena during the FBC was significantly dependent on a type of fuels and their origins.

6.2 Materials and methods

6.2.1 Samples

Raw paper sludge (Raw-PS) was provided by the Siam Kraft Industry Co., Ltd., Thailand. It was treated by the pilot-scale hydrothermal reactor at the temperature of 197 ˚C and pressure of 1.9 MPa as the optimal condition for 30 minutes. Then, the hydrothermally treated paper sludge (HTT-PS) was dewatered and dried. The detail procedures of the pilot-scale hydrothermal treatment (HTT) is explained in Chapter 2. Since the original characteristic of the paper sludge is extremely fluffy, Raw-PS and HTT-PS were pelletized. Then, they were crushed by lab-scale ball milling machine and were sieved at the nominal size between 3 and 4 mm. The Thai subbituminous coal (Sub-C) was also crushed and sieved at the same size. From this point, they were further utilized according to each experiment described later. The fuel properties of the samples are shown in Table 6-1.

Furthermore, scanning electron microscopy (SEM) was performed by the JSM-6610LA scanning electron microscope (JEOL Co., Ltd. Japan) to study the surface morphology of the samples. Additionally, the specific surface area (SSA) of Raw-PS and HTT-PS from both lab- and pilot-scale were determined by N_2 adsorption/desorption measurement via the Microtrac BELSORP-mini II (BEL Japan, Inc.). Under equilibrium conditions, a quantity of gas molecules required to saturate the surface

of a sample is measured by the Brunauer, Emmett and Teller (BET) technique [13]. To prevent the inherent moisture, the samples were dried in the electric oven at 110 ℃ for 12 h and degassed at 200 °C for 3 h prior to the measurement.

Table 6-1 Fuel properties

Sample	Proximate analysis (%)			Ultimate analysis (%)					Heating value(kJ/kg)	
	FC	VM	Ash	C	H	N	S	O	HHV	LHV
Raw-PS	8.6	59.5	31.9	33.4	4.3	2.9	0.7	26.9	12.0	11.1
HTT-PS	8.3	55.6	36.1	33.2	4.1	1.9	0.6	24.1	12.3	11.4
Sub-C	41.7	51.9	6.4	64.0	4.6	0.6	N/A	24.4	25.3	24.3

Raw-PS: raw paper sludge; HTT-PS: hydrothermally treated paper sludge; Sub-C: subbituminous coal; FC: fixed carbon; VM: volatile matter; HHV: higher heating value; LHV: lower heating value.

6.2.2 Particle comminution test

6.2.2.1 Apparatus

An atmospheric bubbling fluidized bed made from stainless steel AISI 312 was utilized in this study. It has 40 mm internal diameter and 1 m height. A 22 mm thick perorated plate with 55 holes with 0.5 mm in diameter disposed in a triangular pitch is used as a gas distributor. Heat is supplied to fluidization column and preheating section by two semicylindical (2.2 kW) electric furnaces. A chromel-alumel thermocouple placed 40 mm above the distributor was used to measure the temperature of the bed and it was controlled at the desired temperature by a PID controller. The freeboard is kept unlagged to minimize post combustion of fine particles. Gases fed into the fluidized bed was controlled by two high-precision digital mass flow meters. The bed material consisted of 180 g of silica sand with the nominal size of 300–400 μm. The minimum fluidization velocity was 0.05 m/s at 850 ˚C.

6.2.2.2 Primary fragmentation

For primary fragmentation experiments, the basket-equipped configuration shown in Figure 6-1A was utilized. The top of the fluidized bed is left open to the atmosphere. The sample were put into the stainless steel circular basket and it was inserted to the fluidized bed column. The gap between the column and the basket is kept minimal to prevent the loss of small fragmented particles during the test. The basket is able to retrieve both fragmented and non-fragmented particles. With the mesh of 0.8 mm, the bed materials can be easily pass through leaving only the products from the fragmentation test for further analysis. The sand bed was fluidized with nitrogen at 0.8 m/s. The experiments were carried out by injecting single fuel particles, nominal diameter of 2–4 mm, into the bed kept at 850 ˚C from the top of the column for about 3 minutes. During the devolatilization, the basket rested on the distributor. Then, after the devolatilization was completed, the resulting char was retrieved from the basket. The number and size of the products including fragmented and non-fragmented were analyzed. In each

batch, five particles were used and the experiments were done six times with the total particles of 30 for the statistical purpose.

6.2.2.3 Char particle attrition

The second configuration shown in Figure 6-1B is used in the attrition test. The top of fluidized bed reactor is assembled by a two-exit brass head equipped with a three-way valve. By switching this valve, it allows flue gases to flow alternately to two sintered brass-made removable filters. Batches of samples can be fed to the reactor by a hopper connected to the upper part of the freeboard. O_2 and CO_2 concentrations in the exhaust gas were measured on-line by a paramagnetic analyzer and two NDIR analyzers.

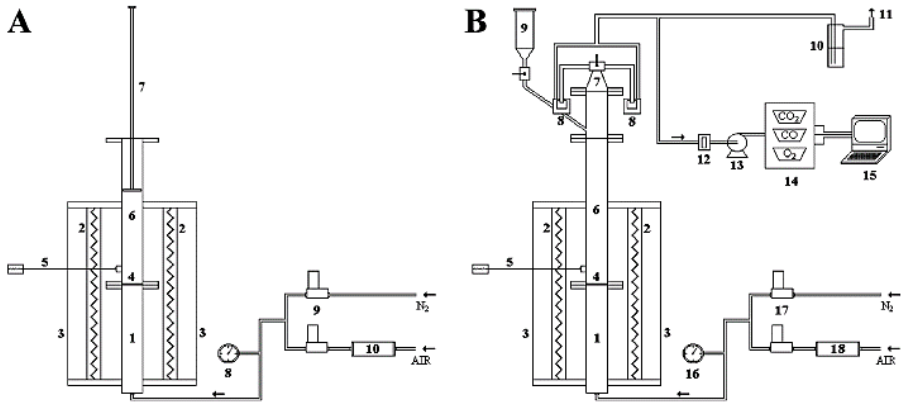

Figure 6-1 Experimental apparatus: (A) basket equipped configuration for primary fragmentation test and (B) two-exit head configuration for attrition test; (A) (1) gas preheating section, (2) electrical furnaces, (3) ceramic insulator, (4) gas distributor, (5) thermocouple, (6) fluidization column, (7) steel basket, (8) manometer, (9) digital mass flow meters, and (10) air dehumidifier (silica gel). (B) (1) gas preheating section, (2) electrical furnaces, (3) ceramic insulator, (4) gas distributor, (5) thermocouple, (6) fluidization column, (7) head with three-way valve, (8) sintered brass filters, (9) hopper, (10) scrubber, (11) stack, (12) cellulose filter, (13) membrane pump, (14) gas analyzers, (15) personal computer, (16) manometer, (17) digital mass flow meters, and (18) air dehumidifier (silica gel).

In the attrition experiment, char has to be prepared from the original prepared samples. The char was obtained by using the method similar to the primary fragmentation test; however, more particles were put into the reactor and the resulting char was sieved at the nominal size between 2–4 mm. For each test, 9 g of char particles were injected into the bed kept at 850 ˚C with the fluidization velocity of 0.8 m/s. Nitrogen and air mixture was adjusted to form the desired condition, which were 0% and 4.5% O_2 for investigating the mechanical abrasive attrition and the oxidative attrition tests, respectively. Elutriated fine particles were collected by the sequences of filters assemble inside the two-exit head. The continuous collecting process can be achieved by switching the flue gas alternately by a three-way

valve and replaced the previously used filter one to another. The test was done for definite period as it was terminated after the elutriation rate was stabilized. After the filter was taken out, it was placed in a drier to prevent hydration. The filter was weighted after cooling down. The mass of the elutriated materials divided by the time interval that the filter was in operation yields the average elutriation rate relative to that interval. This procedure allowed time-resolved measurement of the carbon elutriation rates. After that, the elutriated particles were analyzed its carbon content by a Leco (CHN) elemental analyzer. Results of blank tests, in which only sand was charged in the reactor and fluidized under the same operating conditions, indicated that the generated fine particles from attrition of sand was negligible.

Table 6-2 Summary of experimental condition

Experimental condition	
Condition	Description
Primary fragmentation	
Combustor	Figure 6-1A
Bed material	180 g of sand at 300–400 μm
Fluidizing gas	Nitrogen
Fluidization velocity	0.8 m/s
Reaction temperature	850 ˚C
Devolatilization time	3 min
Fuel size	30 fresh particles at 3–4 mm
Char particle attrition	
Combustor	Figure 6-1B
Bed material	180 g of sand at 300–400 μm
Fluidizing gas	0%, 4.5% oxygen (in nitrogen)
Fluidization velocity	0.8 m/s
Reaction temperature	850 ˚C
Residence time	3 min
Fuel size	9 g of char samples at 2–4 mm
Flue gas measurement	O_2, CO_2

6.3 Results and discussion

6.3.1 Primary fragmentation

The primary fragmentation takes place firstly during the devolatilization due to volatile releasing from pore structures of fuel followed by collapsing of internal bridges of char particles [9]. In this study, the primary fragmentation test was carried out to monitor the amount of the particles and their sizes during the devolatilization. The focus was on the effect of HTT on the fragmentation behavior of the paper sludge and compared to the behavior of Sub-C as representative of fossil fuel. For a comprehensive

study, the results of the primary fragmentation on South African bituminous coal (SA-C), that has relatively lower volatile matter (30%wt), studied by Chirone et al. is reported [9].

The key parameters that have been used to evaluate the primary fragmentation behavior are the Sauter mean diameter (d), the primary fragmentation probability (S) which is defined by a number of the particles that undergo the fragmentation during the devolatilization divided by the total number of fed particles, the primary fragmentation multiplication factor (n) given by a number of generated fragments (neglect particle that has the average diameter less than 0.275 mm) per unit of fuel particle that is fed to the reactor, and shrinkage factor which provides an information on size reduction of un-fragmented particles [10].

6.3.1.1 Primary fragmentation behavior

Table 6-3 reports the results from the primary fragmentation experiments. The initial Sauter mean diameters (d_0) of Raw-PS, HTT-PS, and Sub-C were approximately the same before the test as being controlled. After the primary fragmentation, the Sauter mean diameters (d_1) was reduced 34.0%, 29.4% and 30.6% for Raw-PS, HTT-PS and Sub-C, respectively, indicating that all the samples extensively underwent fragmentation due to their high volatile content. On the other hand, d_1 of SA-C showed 3.5% reduction from the original value. This might be attributed to a comparatively low amount of volatile released during the devolatilization. However, it should be noted that the extensive fragmentation characteristic cannot solely be claimed by the amount of volatile matter [10].

The probability of the samples that could undergo fragmentation (S) was moderate in the case of HTT-PS and Sub-C and it was slightly lower for Raw-PS. Approximately half of HTT-PS and Sub-C particles were fragmented after the devolatilization. In the case of SA-C, the S value was 50% lower than Sub-C and this indicated that SA-C infrequently experienced the fragmentation. When the value of S approaches zero, it implies that the fragmentation probability becomes very limited and this means that the particle is very resistant to the fragmentation. By this definition, the probability of the samples that could undergoes the primary fragmentation are listed as HTT-PS > Sub-C > Raw-PS > SA-Coal, respectively.

The primary fragmentation multiplication (n) was very high in the case of Raw-PS. It was approximately 48% higher than that of HTT-PS. For instance, once a particle of Raw-PS breaks down, as eight small particles would be generated whereas it would be approximately five fragments in the case of HTT-PS. For Sub-C, generated fragments per unit fed fuel particle was higher than that from SA-C whose n value was very low. Feeding one particle of SA-C might generate approximately three pieces of fragments. Even though the probability of Sub-C to undergo the fragmentation (S) was high and was comparable to HTT-PS, it might generate relatively small amount of fragments during the devolatilization.

6.3.1.2 Particle size evolution upon devolatilization

Cumulative particle size distribution before and after the primary fragmentation test of Raw-PS, HTT-PS and Sub-C are illustrated in Figure 6-3. It was clearly observed the difference of the particle size distribution (PSD) profiles before and after the tests in all three samples, especially the generation of small particles (lower than 3 cm). The amount of these fines after the primary fragmentation from three fuels was similar. In more detail, the particle lower than 2 cm was higher in the case of Raw-PS. HTT-PS was likely to preserve PSD for larger particles since the profile after the fragmentation was relatively closer to the one before. However, in the case of Raw-PS and Sub-C, the reduction in the size of the larger particle was obvious. This could be articulated by the shrinkage factor presented in Table 6-3. The shrinkage factor illustrated that only one-fifth of the size of HTT-PS would be reduced whereas more than one-third of the size of Raw-PS and Sub-C would be diminished due to shrinking. Sub-C also exhibited large particle shrinkage similar to Raw-PS. It should be noted that the moisture content of Raw-PS and HTT-PS were approximately 10% while that of Sub-C was around 20%. The evaporation of the moisture in the samples could also have an impact on the particle shrinkage.

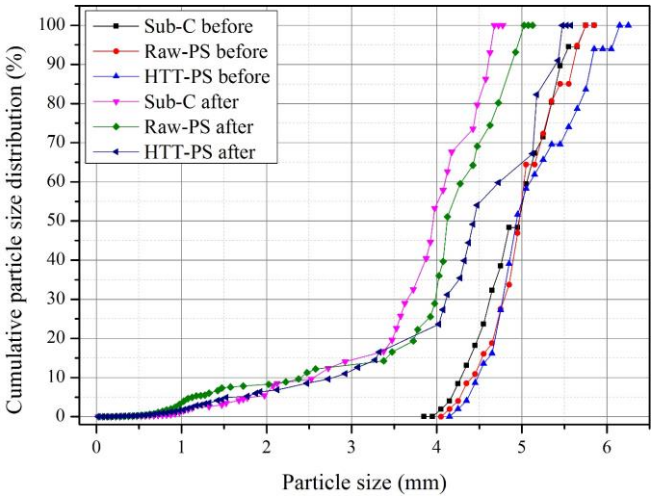

Figure 6-3 Cumulative particle size distribution before and after the primary fragmentation

Table 6-3 Result from primary fragmentation experiments

	d_0 (mm)	d_1 (mm)	S	n	shrinkage factor
Raw-PS	5.0	3.3	0.37	8.0	0.65
HTT-PS	5.1	3.6	0.53	5.4	0.80
Sub-C	4.9	3.4	0.50	3.3	0.62
SA-C*	4.0–4.7	4.2	0.25	2.8	–

Raw-PS: raw paper sludge; HTT-PS: hydrothermally treated paper sludge; Sub-C: subbituminous coal; SA-C: South African bituminous coal (*results are from reference [9]); d_0: Sauter mean diameter before the test; d_1: Sauter mean diameter after the test; S: primary fragmentation probability; n: primary

fragmentation multiplication (taken into account only fragmented particle neglected very tiny particles (average diameter lower than 0.275 mm) that might undergoes attrition instead of fragmentation.

6.3.1.3 Effect of HTT on the primary fragmentation

As shown in Table 6-3, the average particle size of Raw-PS and HTT-PS was similar both before and after the primary fragmentation. This implies that HTT had no significant effect on the average particle size. Therefore, when switching the fuel from Raw-PS to HTT-PS, the average fuel size in the fluidized bed would not be altered from the original combustion condition. Even though HTT-PS showed slightly higher primary fragmentation probability, once it undergoes fragmentation, HTT-PS tends to generate significantly less amount of fragments when compared to Raw-PS. From the result on PSD, the primary fragmentation influences the fuel PSD after devolatilization for both Raw-PS and HTT-PS. PSD of Raw-PS was significantly changed after the primary fragmentation due to both particle breaking and shrinking while HTT-PS tends to retain PSD for large particle after the devolatilization better than Raw-PS. The factors regarding the primary fragmentation should be taken care of in order to minimize errors of the actual fuel particle distribution in the fluidized bed during the operation.

6.3.2 Char particle attrition

6.3.2.1 Mechanical attrition

Figure 6-4 illustrates the elutriation rate (E) from the attrition test. Pure mechanical attrition and the oxidative attrition tests have been conducted by operating the fluidized bed in two conditions: pure nitrogen and 4.5% oxygen in nitrogen mixture, respectively. For the mechanical attrition, Sub-C showed a large elutriation rate at the very beginning. It was significantly higher than that from Raw-PS and HTT-PS. Then, it was sharply reduced and became lower than that from Raw-PS and HTT-PS after several minutes. The first large elutriation rate was due to a particle rounding off in the fluidized bed. The E profiles of Raw-PS and HTT-PS had the same characteristic; however, the elutriation rate of HTT-PS was always lower. After Sub-C underwent the particle round off at the very beginning of the test, it became very strong against the mechanical abrasive in the fluidized bed. From this point, Sub-C has the highest mechanical resistance followed by HTT-PS and Raw-PS until the E values were stabilized.

6.3.2.2 Oxidative attrition

Figure 6-4 also presents the attrition under an oxidative condition. In an oxidizing atmosphere, two different phenomena can occur and affect the elutriation rate namely, combustion-assisted attrition and postcombustion of fines. The combustion-assisted attrition contributes to higher elutriation rate since the structure of the fuel particle is weakened by an internal combustion. On the other hand, the postcombustion of the generated fines decreases elutriated particles. This occurs in the case of the char particle that has a very high intrinsic reactivity. It was clearly observed that when Sub-C was subjected

to the oxidative attrition test, the elutriated rate was very low throughout the profiles. It is likely that the generated fines from Sub-C underwent the postcombustion. However, Raw-PS and HTT-PS showed the different mechanism. The elutriation rate from the oxidative attrition of these two samples were higher than that from the inert condition mainly because of the combustion-assisted attrition.

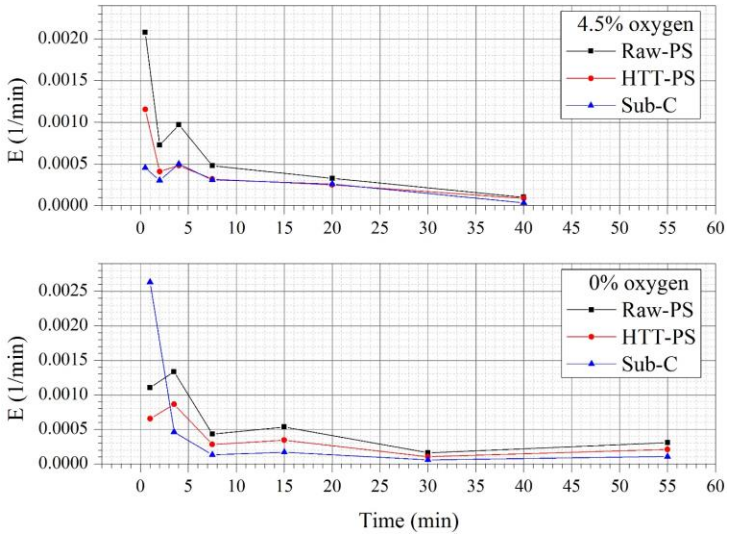

Figure 6-4 Elutriation rate (E) during char particle attrition tests (Raw-PS: raw paper sludge; HTT-PS: hydrothermally treated paper sludge; Sub-C: subbituminous coal).

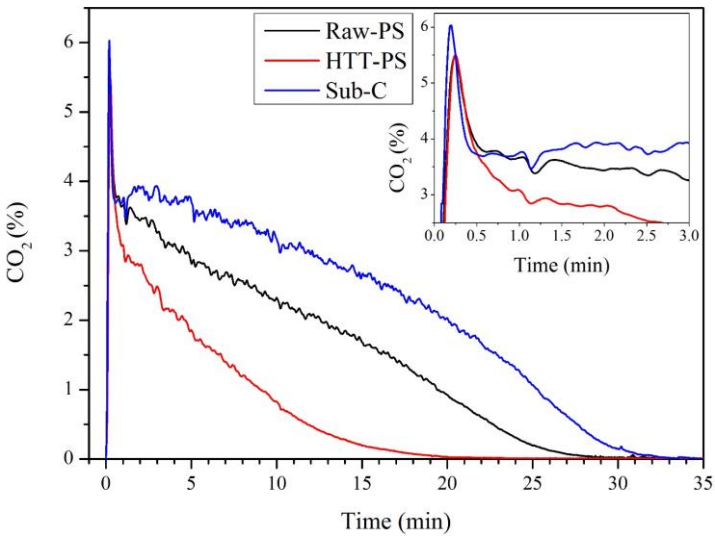

Figure 6-5 CO_2 (%) from 4.5% O_2 char particle attrition test (Raw-PS: raw paper sludge; HTT-PS: hydrothermally treated paper sludge; Sub-C: subbituminous coal)

Figure 6-5 and 6-6 shows the CO_2 profiles and the carbon conversion measured during the oxidative attrition tests. As char particles were fed into the reactor, the initial small CO_2 peak was due to the O_2 adsorbed in the pores of the char structure at ambient conditions. The release of CO_2 in the case of Sub-C was slightly higher than that of Raw-PS and HTT-PS. The difference of the CO_2 peaks between Raw-

PS and HTT-PS was not observable. However, CO_2 profile of HTT-PS was sharply decreased after 0.5 min and approached zero within 20 min. It was significantly different compared to the CO_2 profile of Raw-PS, which took approximately 30 min to decrease to zero. As the CO_2 becomes zero, it implies that the combustion of the sample is finished. Thus, the burnout time of the sample in this test can be noted. The char burnout time of HTT-PS was the shortest followed by Raw-PS and Sub-C. It should be noted that the mass of the char samples used in this test were controlled by the total weight of the sample, not by the weight of fixed carbon. Therefore, Sub-C that contains a significantly higher amount of fixed carbon obviously had a longer burnout time. The behavior of the two sludges, on the contrary, which have approximately the same fixed carbon content, is directly comparable. Carbon conversion results clearly show that combustion of HTT-PS was completed earlier than for the other fuels.

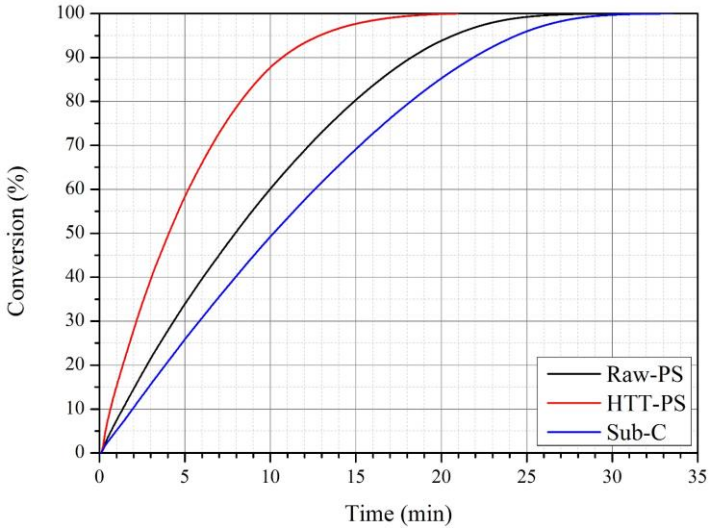

Figure 6-6 carbon conversion (%) from 4.5% O_2 char particle attrition test (Raw-PS: raw paper sludge; HTT-PS: hydrothermally treated paper sludge; Sub-C: subbituminous coal).

6.3.2.3 SEM and BET surface area

Figure 6-7 shows the scanning electron micrograph (SEM) analysis of Raw-PS and HTT-PS. It can be observed that Raw-PS from Figure 6-7a contained many large fibrous particles and they had had flat surfaces as illustrated in Figure 6-7a'. In general, these kinds of surfaces can be commonly found in the large particles of Raw-PS. On the other hand, Figure 6-7b presents the SEM image of HTT-PS and shows that several small size fibrous materials can be observed. Figure 6-7b' clearly illustrates the destructive effect of HTT on the surface of the fibrous particle. To obtain more detail, Raw-PS and HTT-PS were subjected to the BET surface area measurement. Raw-PS sample in this study cannot be analyzed by the BET test and this might be due to the limitation of porosity in the samples. Thus, the BET value of the raw paper sludge was reported from the literature, which was about 4.8 m^2/g [14]. HTT-PS had a BET surface area around 10.2 m^2/g, which was significantly higher than that of Raw-PS.

The BET surface area was consistent with the result from the SEM image. These could be the reason why HTT-PS had better combustion performance compared to Raw-PS.

6.3.2.4 Effect of HTT on char particle attrition

From previous discussion of the results on both the mechanical and the oxidative attrition tests, the influence of HTT on the attrition phenomena was obvious. From the elutriation rate data, both cases showed that HTT-PS tends to generate less amount of elutriated fines even though the characteristic of the profile was approximately the same. This means that HTT-PS has a higher mechanical resistance on the particle surface than Raw-PS. These behaviors are essential since HTT-PS will produce less fine particles that could generally leave the fluidized bed unburned. The particles of HTT-PS would spend more time in the bed; as a result, the loss of carbon would be lessened. From the CO_2 profiles and the carbon conversion during the oxidative attrition, HTT-PS has a superior burnout performance than Raw-PS since it took significantly less time to complete the combustion. Therefore, HTT-PS could enhance the combustion performance via reducing the loss of carbon and time to finish the combustion in the fluidized bed.

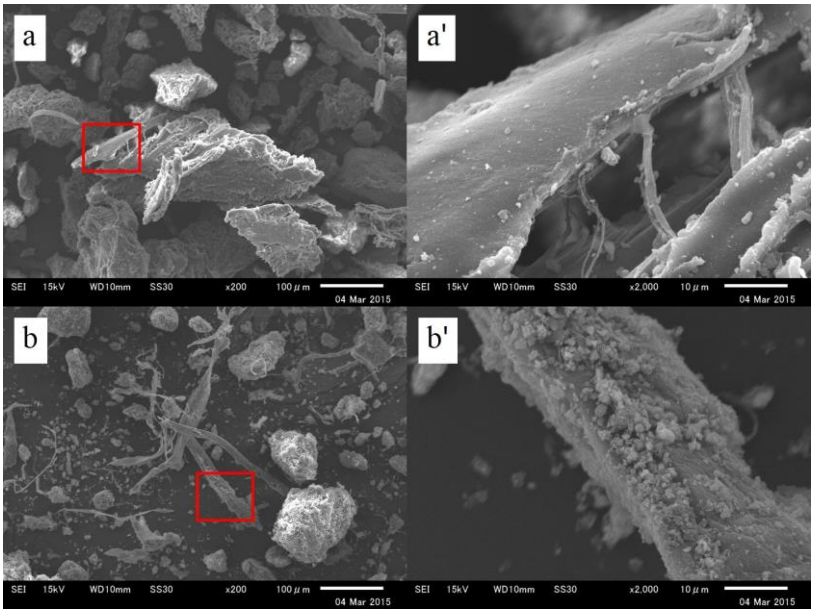

Figure 6-7 SEM images (a: Raw-PS at low magnificent; a': Raw-PS at high magnificent; b: HTT-PS at low magnificent; b': HTT-PS at high magnificent)

6.4 Conclusion

The primary fragmentation and the char particle attrition during fluidized bed combustion of raw paper sludge (Raw-PS), hydrothermally treated papers sludge (HTT-PS) and subbituminous coal (Sub-C) were investigated. The conclusion can be summarized as follows:

1. The Sauter mean diameter after the primary fragmentation of all the samples were reduced approximately one-third. This indicates that they extensively underwent the primary fragmentation. The probability of HTT-PS and Sub-C that could undergo the primary fragmentation is moderate whereas Raw-PS was slightly lower. However, the results on the primary fragmentation multiplication shows that once the samples fragmented, Raw-PS would generate significantly larger amount of fines compared to HTT-PS and Sub-C.

2. From the inert atmosphere attrition test, Sub-C intensely experienced particle rounding off at the beginning then it became very strong against the mechanical abrasive attrition followed by HTT-PS and Raw-PS, respectively. The oxidative attrition test showed that Sub-C had a significantly lower amount of elutriation rate because of the postcombustion of fines whereas Raw-PS and HTT-PS underwent a combustion-assisted attrition leading to higher amount of generated fines compared to the inert condition.

3. The CO_2 profiles from the oxidative attrition test indicate that the combustion of HTT-PS completed significantly before Raw-PS and Sub-C showing the superior burnout performance. In both cases, HTT-PS had lower amount of fines than Raw-PS and this indicates better combustion performance as well as lower unburned carbon emission in the fluidized bed.

4. SEM images and BET surface area showed physical evidences on the destructive effect of HTT on the structure that led to a better combustion performance of HTT-PS.

References

[1] Basu P, Butler J, Leon MA. Biomass co-firing options on the emission reduction and electricity generation costs in coal-fired power plants. Renew Energ. 2011;36:282-8.

[2] Khan AA, de Jong W, Jansens PJ, Spliethoff H. Biomass combustion in fluidized bed boilers: Potential problems and remedies. Fuel Process Technol. 2009;90:21-50.

[3] Yan R, Liang DT, Tsen L. Case studies—Problem solving in fluidized bed waste fuel incineration. Energ Convers Manage. 2005;46:1165-78.

[4] Ammendola P, Chirone R, Miccio F, Ruoppolo G, Scala F. Devolatilization and Attrition Behavior of Fuel Pellets during Fluidized-Bed Gasification. Energ Fuel. 2011;25:1260-6.

[5] Chirone R, Salatino P, Scala F, Solimene R, Urciuolo M. Fluidized bed combustion of pelletized biomass and waste-derived fuels. Combust Flame. 2008;155:21-36.

[6] Scala F, Chirone R, Salatino P. The influence of fine char particles burnout on bed agglomeration during the fluidized bed combustion of a biomass fuel. Fuel Process Technol. 2003;84:229-41.

[7] Chirone R, Salatino P, Scala F. The relevance of attrition to the fate of ashes during fluidized-bed combustion of a biomass. P Combust Inst. 2000;28:2279-86.

[8] Liu H, Gibbs BM. Modelling of NO and N 2 O emissions from biomass-fired circulating fluidized bed combustors. Fuel. 2002;81:271-80.

[9] Chirone R, Massimilla L, Salatino P. Comminution of carbon in fluidized bed combustion. Prog Energ Combust. 1991;17:297-326.

[10] Scala F, Chirone R, Salatino P. Combustion and Attrition of Biomass Chars in a Fluidized Bed. Energ Fuel. 2006;20:91-102.

[11] Cammarota A, Chirone R, Salatino P, Scala F, Urciuolo M. Attrition phenomena during fluidized bed combustion of granulated and mechanically dewatered sewage sludges. P Combust Inst. 2005;30:3017-24.

[12] Arena U, Cammarota A, Mastellone ML. The phenomenology of comminution in the fluidized bed combustion of packaging-derived fuels. Fuel. 1998;77:1185-93.

[13] Bai RS, Abraham TE. Studies on enhancement of Cr(VI) biosorption bychemically modified biomass of Rhizopus nigricans. Water Res. 2002;36:1224-36.

[14] Devi P, Saroha AK. Effect of temperature on biochar properties during paper mill sludge pyrolysis. International Journal of Chem Tech Research. 2013;5:682-7.

Chapter 7

Conclusions and recommendations

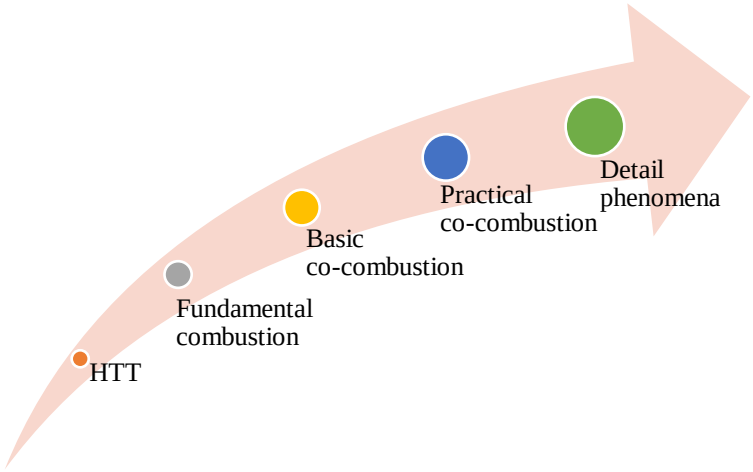

Figure 7-1 Outline of this research

Outline of this research in Figure 7-1 shows the way to promote Waste-to-Energy technology in pulp and paper industry by using the hydrothermal treatment (HTT) to upgrade the paper sludge followed by the co-combustion of the hydrothermally treated paper sludge with coal. The general conclusion both in and in-between each study can be summarized as follows:

1. Chapter 2, *Lab-scale and pilot-scale investigation on hydrothermal treatment of paper sludge for solid fuel production*, shows that HTT was able to produce alternative solid fuel from paper sludge (Raw-PS). The hydrothermally treated paper sludge (HTT-PS) had better dewatering and drying performance and comparable or even better solid fuel properties such as heating value. The feasibility of HTT has been proved at the pilot-scale level.

2. Chapter 3, *Combustion characteristics and kinetics study of hydrothermally treated paper sludge by thermogravimetric analysis*, explains that the major decomposition of paper sludge was devoted to cellulose. The ignition temperature was originally low. The activation energy of HTT-PS was lower than Raw-PS indicating higher reactivity.

3. Chapter 4, *Co-combustion of hydrothermally treated paper sludge with subbituminous coal in a fixed bed combustor*, shows possibility of NO emission reduction of HTT-PS as well as alleviation of slagging and fouling tendency.

4. Chapter 5, *Fluidized bed co-combustion of hydrothermally treated paper sludge with two coals of different rank*, shows that switching from Raw-PS to HTT-PS in the fluidized bed co-combustion with either low or high reactivity coals can improve NO_x and unburned carbon emission performance.

5. Chapter 6, *Effect of hydrothermal treatment on primary fragmentation and attrition phenomena during fluidized bed combustion of paper sludge*, shows that HTT-PS had lower amount of fines particle than the original material during the fluidized bed combustion indicating better combustion performance. The combustion of HTT-PS completed significantly earlier than Raw-PS showing the superior burnout performance as well.

6. The finding from Chapter 3, i.e., HTT-PS had higher reactivity, can be articulated by the results from the Chapter 6 which found that HTT-PS had more surface area than Raw-PS. These findings suitably explains the reason why HTT-PS had low amount of unburned carbon during the bubbling fluidized bed combustion test in Chapter 5 as well as superior combustion and burnout performance in the attrition test in Chapter 6.

Finally, the integrated solution of using hydrothermal treatment to upgrade paper sludge and co-combusting the hydrothermally treated paper sludge will give many positive effects and will be more appropriate than the conventional way of dealing with paper sludge such as landfilling or co-firing the original high water sludge.

For the recommendation on future work, large-scale (commercialization) of hydrothermal treatment technology should be implemented on paper sludge or other similar type of sludge using in pulp and paper industries. Detail feasibility and engineering work should be adopted based on raw materials, process condition, and other important factors. Energy efficiency of the hydrothermal plant could be significantly improved by reusing the steam between two reactors. Moreover, process steam or waste steam from pulp making factory could be used for the treatment instead of producing new steam from a boiler.